QATAR UNIVERSITY

COLLEGE OF ENGINEERING

POLYURETHANE-BASE MULTIFUNCTIONAL COATING FOR CORROSION PROTECTION OF STEEL IN THE OIL & GAS INDUSTRY

BY

SAMRA ZAFAR

A Thesis Submitted to

the College of Engineering

in Partial Fulfillment of the Requirements for the Degree of

Masters of Science in Environmental Engineering

January 2025

COMMITTEE PAGE

The members of the Committee approve the Thesis of
Samra Zafar defended on 05/12/2024.

Prof. Ramazan Kahraman
Thesis/Dissertation Supervisor

Dr Abdul Shakoor
Co-Supervisor

Dr. Anand Kumar
Committee Member

Dr. Mohamed Korany Ibrahim Hassan
Committee Member

Approved

Dean College of Engineering

ABSTRACT

ZAFAR,SAMRA., Masters : January : [2025], Masters of Science in Environmental Engineering

Title: Polyurethane-Based Multifunctional Coatings for Steel in the Oil & Gas Industry.

Supervisor of Thesis: Prof. Ramazan Kahraman.

The study of polyurethane-based multifunctional coatings for steel protection in the oil and gas sector is the focus of this thesis. Polyurethanes are versatile polymeric materials with excellent wear resistance, superb thermophysical and elastic properties, and exceptional operating capabilities in the oil and gas sectors. Following an overview of the developments in PU coatings, including novel additives and self-healing processes, the study concentrates on two cutting-edge systems. By dispersing TiO_2 nanoparticles uniformly, the first technique improves barrier qualities and corrosion resistance of PU coatings using a graphene oxide-titania (GO-TiO_2) composite. In the second system, PU coatings enhanced with TiO_2 are combined with MS30, a green corrosion inhibitor. Electrochemical and salt spray studies validate that these formulations achieve 99.9% efficiency, a significant improvement in corrosion inhibition. The results show that these innovative PU-based coatings provide steel with outstanding protection, prolonging durability in challenging conditions, especially in oil and gas applications.

DEDICATION

"To my parents, for their endless love and encouragement,

and to my sister, for her constant support whenever needed.

To my husband and children, for their patience, sacrifices,

and unwavering belief in me throughout this journey.

This work would not have been possible without you."

ACKNOWLEDGMENTS

I would like to express my deepest gratitude to my supervisor, Prof. Ramazan Kahraman, and co-supervisor, Dr. Abdul Shakoor, for their invaluable guidance, support, and expertise throughout my MSc journey. I also extend sincere thanks to the committee members for their insightful feedback and contributions to this dissertation. I am immensely grateful to the Center for Advanced Materials, Qatar University, along with all the lab technicians, Central Laboratory Units, and the College of Engineering, Department of Chemical Engineering, for providing the resources and support essential to completing this research.

My special thanks go to my friends Sehrish Habib, Muddasir Nawaz, and Zawar Qureshi for their unwavering support, guidance, and encouragement whenever I needed it.

This research work was supported by Qatar University Graduate Assistant grant number QUGA-2022-ID-140, Qatar National Research Fund (QNRF) (a member of the Qatar Foundation) grant number NPRP13S-0120-200116, Qatar Research Development and Innovation Council (QDRI) grant number ARG01-0516-230189.

Publications

1. **Samra Zafar**, Ramazan Kahraman, R.A. Shakoor, Recent developments and future prospective of polyurethane coatings for corrosion protection − a focused review, Eur Polym J 220 (2024) 113421. https://doi.org/10.1016/J.EURPOLYMJ.2024.113421. (I. F=5.8)
2. **Samra Zafar**, Ramazan Kahraman, R.A. Shakoor, Silane functionalization of titania-graphene oxide nanocomposite for superior anticorrosion polyurethane coatings on steel, Colloids Surf A Physicochem Eng Asp 703 (2024) 135434. https://doi.org/10.1016/J.COLSURFA.2024.135434. (I. F=4.9)
3. **Samra Zafar**, S. Habib, M. Shkoor, R. Kahraman, M. Khaled, I.A. Hussein, A. Dawoud, R.A. Shakoor, Enhanced steel surface protection using TiO2/MS30 modified polyurethane coatings: Synthesis and performance evaluation, J Mol Liq (2024) 126669. https://doi.org/10.1016/J.MOLLIQ.2024.126669. (I.F = 5.3)
4. S. Habib, A. Qureshi, **Samra Zafar**, E.M. Ahmed, R.A. Shakoor, TiO2-Mesoporous Ceria Carrier Modified with Sodium Benzoate: An Innovative Polyurethane Matrix for Enhanced Corrosion Protection of steel, Colloids Surf A Physicochem Eng Asp 697 (2024) 134471. https://doi.org/10.1016/J.COLSURFA.2024.134471. (I.F=4.9)

TABLE OF CONTENTS

LIST OF TABLES

LIST OF FIGURES

Chapter 1: Introduction

Background

The drastic expansion of steel made infrastructures, necessity in many industries, including Oil & Gas has been accompanied by demanding regulations due to concerns about population safety, asset reliability and environmental protection. The compliance with all these regulations, while keeping competitive construction, operations and maintenance costs, imposes significant challenges to a wide array of industrial sectors. It is well known that corrosion of metallic assets is the most important cause of components and equipment failure, resulting in serious economic losses. In fact, in the Middle East region, direct corrosion costs are approximately 5% of the gross domestic product (GDP), a value that represents an enormous expenditure. n industries like Oil & Gas, corrosion has been identified as a significant factor contributing to the degradation and failure of equipment and components. This issue leads to elevated operational and maintenance (O&M) expenses, with these costs often comprising up to 50% of the total expenditure for maintaining infrastructure. A substantial portion of these O&M expenses, approximately 80%, is directly attributed to corrosion-related damage [1,2]. As a result, corrosion poses a considerable challenge to industrial efficiency and profitability, driving up operational expenditures (OPEX) across various sectors. It not only negatively impacts the economic performance of infrastructure owners but also shortens the operational lifespan of industrial assets. One highly effective method for mitigating corrosion and safeguarding both metallic and non-metallic materials is through the use of protective organic coatings. These coatings serve as a critical line of defense, extending the service life of assets while reducing the financial burden associated with corrosion management. Protective coatings, first, must ensure high barrier properties and this is the reason why they are typically multilayered and thick (overall thickness depends on the aggressiveness of the environment), dense

and non-porous. Polyurethane coatings have been proposed as promising solutions to achieve the goal, easy to apply and to maintain [3]. The smart autonomous corrosion protection strategy envisioned by polyurethane based coating grounds in recent advances addressing smart delivery of functional species stored in specially designed smart carriers that can be easily introduced into protective organic matrices commercially available [4][5]. Self-healing coatings for autonomous corrosion protection are at the top of coating research priorities and are, no doubt, considered the next frontier for smart materials. Self-healing coatings designed for corrosion protection generally encompass two primary mechanisms of action [6]: (i) restoring the polymeric structure, which enables the recovery of the coating's barrier properties, and (ii) passivating or inhibiting corroded areas, thereby preventing or repairing corrosion. Polyurethane coatings naturally possess the ability to self-heal, which inherently satisfies the first functionality. However, the second function—active corrosion prevention and repair—remains underdeveloped in polyurethane coatings. Current research highlights an innovative approach to address this gap by utilizing carriers embedded with corrosion inhibitors. These carriers enable the controlled release of inhibitors, facilitating autonomous repair of corrosion damage and offering a promising enhancement to the self-healing capabilities of polyurethane coatings [7–9].

The underlying concept is straightforward[6]: carriers, such as nanostructured porous particles or microcapsules, are filled with corrosion inhibitors and are engineered to respond intelligently. These carriers are designed to detect specific local changes caused by the corrosion process, which serve as stimuli to trigger the release of the stored inhibitor. The release is only activated when these stimuli are present. Once the stimuli subside, the carriers halt the release of the corrosion inhibitors, effectively storing them until another corrosion event occurs. This approach allows the

development of smart inhibitor carriers capable of detecting successive corrosion events, thereby ensuring prolonged corrosion protection. Since the onset of corrosion is typically driven by moisture and aggressive species like chlorides, which also create pH variations, these factors—chloride buildup, water presence, and pH gradients—serve as effective triggers for the release of corrosion inhibitors from these smart carriers. The accumulation of chlorides has been used as trigger to promote the ion-exchange process in layered double hydroxides loaded with corrosion inhibitors. The concept has been proposed for imparting corrosion healing ability in different coatings and substrates (aluminum alloys and galvanized steel). However the high sensitivity to chlorides and the fast exchange kinetics makes these layered double hydroxides more suitable for early corrosion inhibition [7]. Thus, the concept is clearly feasible, and the deliverables are tangible, because the smart carriers will be designed, tailored and functionalized for enhanced compatibility with conventional protective polyurethane matrices as represented in Figure 1.

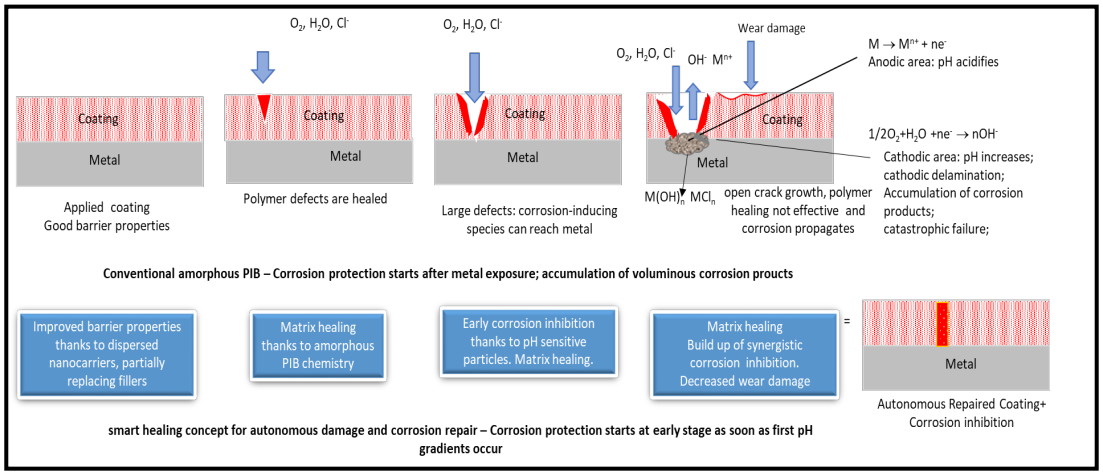

Figure 1: Conventional Polyurethane-based coatings (top) vs. the novel autonomous self-healing corrosion protection concept delivered by multifunctional polyurethane-based smart coatings (bottom).

The strategy addressed in this concept skips the formulation of new organic matrices, which is a long and time-consuming step, and introduces into conventional polyurethane coatings a new concept and a new route for corrosion protection that will drive these coatings into a new era – autonomous corrosion protection based on smart delivery of functional species. Therefore, the scientific premise of this concept challenges the conventional way of using polyurethane-based coatings that presently serve essentially as a preventive physical barrier, and shifts them into the autonomous self-healing era, by introducing novel functional nanostructured carriers with smart properties. Since polyurethane matrices are used in a wide array of industrial applications where the smart delivery of functional species can be used, such as the packaging industry, reinforced concrete industry or rubber industry [10]. The ambitious key outcome of polyurethane-based coating is that corrosion activity starting in defects formed in the coating due to impact, abrasion, mechanical damage, handling, repairs and aggressive environmental conditions will be autonomously prevented and healed, maximizing the component lifetime and reducing the need of human interventions. The novel smart self-healing concept can be applied directly to new steel parts, or to repaired parts, because it is well known that polyurethanes have good surface tolerance and thus can be applied into surfaces that have been previously affected by corrosion after proper surface preparation [3].

Motivation

In the Middle East, corrosion imposes a significant economic burden, with direct costs amounting to nearly 5% of the region's gross domestic product. This represents a substantial financial drain. In the Oil & Gas sector, corrosion has been identified as a major cause of equipment and component failure. As a result, operational and maintenance (O&M) costs can account for up to 50% of the total infrastructure expenses, with approximately 80% of these costs stemming from corrosion-related

damage[1,2]. Consequently, corrosion presents a serious challenge to industrial competitiveness, leading to high operational expenditures (OPEX) across various sectors. It also adversely affects the financial performance of infrastructure owners while significantly reducing the lifespan of industrial assets.

The multifunctional polyurethane-based coating project delivers a smarter protection solution to the oil and gas industry that combines corrosion protection through self-healing and super hydrophobicity. Hence, this project demonstrates its very close alignment with the topmost thematic area Energy and Environment and addresses the most demanding challenges of corrosion persisted in the oil and gas industry natural gas satisfying the goals of attaining self-reliance in technologies related to the processing of oil and gas and in separate natural gas. These multifunctional smart coatings provide autonomous protection in the oil and gas industry, minimizing operation and maintenance costs, increasing output, and thus strengthen the economy of the State of Qatar.

The innovation resides on the synergistic combination of a graded composition and the exploration of the nano additives' full potential in terms of corrosion inhibition. This project combines the most current concepts of engineering and technology (nanotechnology-nanomaterials production and properties) and fundamental concepts of the natural sciences (electrochemistry-corrosion). It proves its strong relevance with research areas of Energy and Environment as outlined by Qatar University (Q.U.) priority thematic areas. The project will deliver a unique, innovative anti-corrosion concept, driving the state-of-art from "damage prevention" towards "damage management," saving on Capital Expenditures (CAPEX) (by decreasing coating thickness and the number of layers) and OPEX (by reducing maintenance/repair needs). Ultimately, this project's impact is expected to increase the lifetime of coated steel parts

by at least for 30%-40%.

Objectives

To deliver this autonomous corrosion protection solution, these coatings must achieve very ambitious objectives, as follows:

i) To design and tailor novel pH sensitive corrosion inhibitor carriers for enhanced compatibility with the Polyurethane matrix using nanostructured materials, which surface will be functionalized with selected silane molecules. These carriers, once loaded with corrosion inhibiting species, are expected to sense local pH gradients, releasing the loaded inhibitor species in a smart way - "*exactly when and where needed*."

ii) To optimize combinations of corrosion inhibitors that will be loaded in the smart carriers to act, in a synergistic manner, on the inhibition of corrosion processes.

iii) To maximize the cooperative effect resulting from the polymer healing ability of polyurethane combined with the presence of pH sensitive smart carriers loaded with corrosion inhibitors that are tailored to heal the corrosion processes from the early to late stage.

iv) To take advantage of the fact that nanostructured carriers may partially replace coating fillers, to optimize mechanical properties of the intended single layer protective coating.

v) To demonstrate a new smart polyurethane-based coating fulfilling the requirements for autonomous corrosion protection ability and improved mechanical properties.

Multifunctional polyurethane-based coatings are of excellent scientific merit and its objectives are clear, measurable, realistic and achievable and will allow to overcome

an important barrier that has been limiting the development of polyurethane coatings to answer existing needs: smarter polyurethane coatings for autonomous corrosion protection.

Chapter 2: Literature Review

Introduction

Corrosion protection is a paramount concern in various industries and fields, and its significance cannot be overstated. The relentless and pervasive impact of corrosion, which is the gradual deterioration of materials due to chemical reactions with their environment, poses a substantial threat to infrastructure, equipment, and public safety. Effective corrosion protection measures are indispensable in a world where metals and alloys are integral to everything from transportation and construction to energy production and healthcare. Beyond the financial burdens, corrosion can lead to structural failures, environmental contamination, and health hazards. Consequently, understanding and implementing corrosion protection strategies are vital for ensuring the longevity, safety, and sustainability of our modern world [1,2].

The corrosion of metals is a widespread issue that significantly affects various aspects of human life, including its economic, environmental, and health safety implications[3,4]. Preserving the integrity of metal surfaces against corrosion holds paramount significance. The safeguarding of these surfaces takes precedence over protecting the inner bulk of the material, given that surface areas are more susceptible to environmental exposure and vulnerable to potential damage from both mechanical forces and chemical agents. Corrosion is a plausible outcome when surface imperfections like cracks or pits exist. To put this into perspective, the economic toll of corrosion is estimated to account for roughly 3.4% of the global GDP as of 2013 [5,6]. This substantial cost primarily arises from expenses related to inspection procedures, repair methods, and environmental and safety protocols. Notably, the oil and gas industry bear a substantial share of this corrosion-related expenditure. Prioritizing corrosion prevention is crucial in the modern world, as it not only mitigates financial burdens but also ensures industrial safety and reliability, reduces waste generation, and

lowers energy consumption.

Many methods are utilized to prevent corrosion, including cathodic and anodic protection, inhibitor inclusion, protective coating application, and so forth. Among these methods, using an appropriate coating is widely embraced to shield metal surfaces from environmental factors. These coatings may contain chemical agents, called inhibitors, in minute quantities to reduce the corrosion rate. The fundamental principle behind coatings is to create a barrier that impedes the penetration of oxygen and moisture into the metal. Additionally, organic coatings offer remarkable impact resistance, aesthetic qualities, and strong adhesion to the substrate [7]. Organic coatings, a time-honored and extensively used protective technology, lead the pack in protective coatings. Including inhibitors in these coatings ensures their durability and effectiveness for the specific metal in use [8]. Polyurethane coatings are highly valued for corrosion protection due to their excellent durability, chemical resistance, and flexibility. They form a robust protective layer that adheres well to various substrates, including metals and composites, shielding them from corrosive agents such as moisture, salts, and industrial chemicals. The versatility of polyurethane coatings allows for customization in terms of hardness, elasticity, and environmental resistance, making them suitable for a wide range of applications from industrial equipment to architectural finishes. Their ability to withstand harsh environmental conditions and mechanical stresses ensures long-lasting protection and reduces maintenance costs, making them a preferred choice for enhancing the lifespan of structures and equipment [9–13] .

This comprehensive thesis aims to delve deep into the multifaceted world of polyurethane coatings for corrosion protection, shedding light on their pivotal role in safeguarding various substrates against the relentless forces of corrosion. The thesis

aims to provide an exhaustive exploration of the diverse types of polyurethane coatings Figure 2(a), their characteristics, and the intricate factors influencing their performance. Beyond a mere catalogue of coating varieties, we aim to investigate the nuanced aspects of container selection, inhibitors, and application techniques, delving into how these elements influence the protective attributes of polyurethane coatings Figure 2(b). Furthermore, this report will conduct a comparative analysis of polyurethane coatings against other prevalent types of protective coatings, offering valuable insights for practitioners and researchers seeking the ideal corrosion protection solution for their specific applications. Additionally, this thesis will consider environmental and sustainability aspects, addressing the growing need for eco-friendly solutions in corrosion protection. With an eye on current challenges and prospects, this report endeavors to serve as an informative resource, guiding professionals and researchers toward optimized corrosion protection strategies and innovations in polyurethane coating technology. In Figure 2(c), a compelling upward trend is evident, showcasing the substantial growth in publications related to polyurethane coatings over the past decade (2014-2024). This surge highlights the increasing interest and research activity in the field, underscoring the current momentum and relevance of polyurethane coating studies.

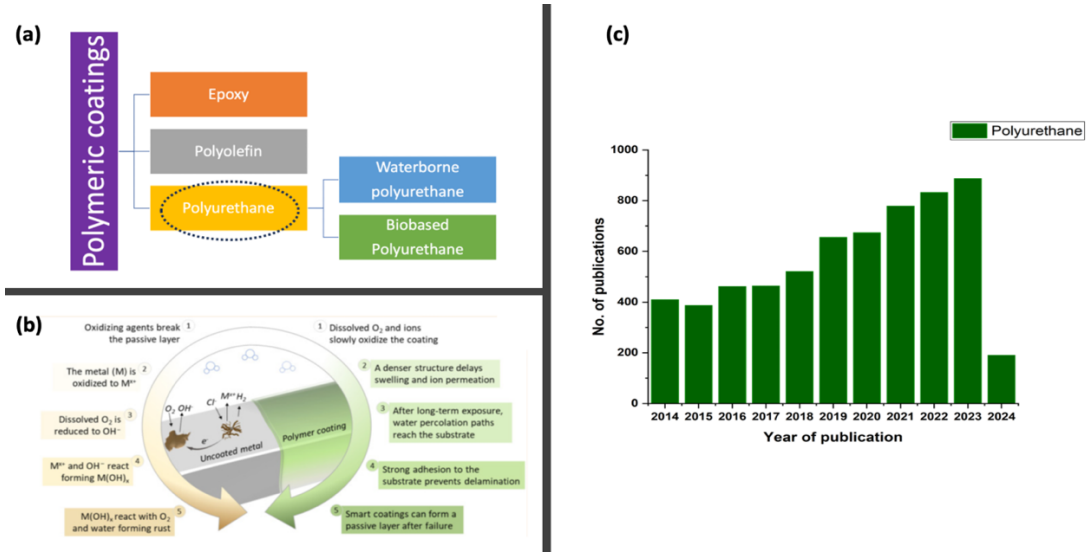

Figure 2: (a) Types of polymeric coatings. (b) A representative cycle of metallic corrosion (left) and protection of typical polymeric coatings (right) immersed in aerated neutral saline solution. Reproduced [14]. (c) Graphical presentation of number of publications on polyurethane coatings in a period of 10 years from SCOPUS (2014 - 2024).

Corrosion Mechanisms

The slow breakdown or disintegration of materials—mostly metals—caused by electrochemical reactions with their environment is known as corrosion. When it comes to metals, this deterioration takes the form of rusting, essentially the oxidation reaction with oxygen, resulting in the formation of iron oxides. The process necessitates the simultaneous presence of both water and oxygen, as without either, corrosion will not take place [15].

The steel corrosion process occurs in multiple stages Figure 3. The initial stage of corrosion occurs when solution contacts metal ions at certain anodic regions of the surface. Electrons released from these anodic interface points travel through the metal structure to nearby cathodic places, where they mix with water and oxygen to form

hydroxyl ions. These ions react with the ferrous ions in the anodic region to form ferrous hydroxide. This hydroxide then oxidises in the presence of oxygen to form hydrated ferric oxide or rust [16]. The following equation can represent this chemical reaction:

$$4Fe + 3O_2 + 2H_2O = 2Fe_2O_3.2H_2O$$

Iron + Oxygen + Water = Rust (Hydrated Ferric Oxide)

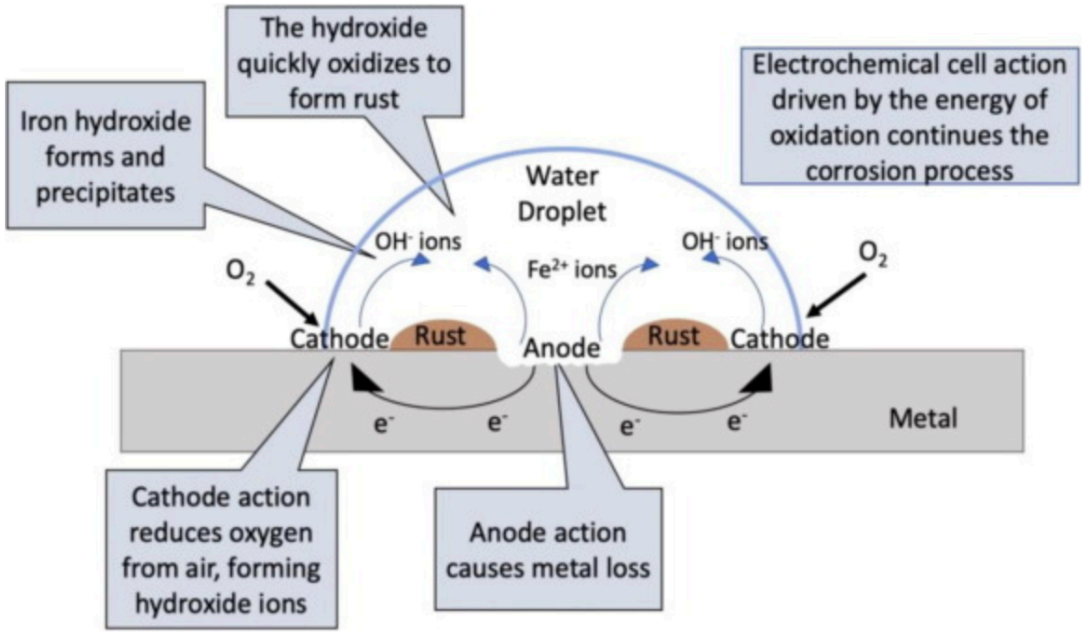

Figure 3: Schematic of corrosion process of steel. Reproduced with permission of Elsevier 2021, [17].

Over the period, the buildup of rust on the surface can inhibit the corrosion process. This suppression of corrosion may lead to fresh anodic sites in nearby areas, facilitating continued corrosion. In overextended durations, this scenario results in a consistent loss of metal across the surface, commonly referred to as general or uniform corrosion. The release of electrons from anodic sites and their reception at cathodic sites establishes the fundamental electrical circuit that propels the corrosion process. Ionic resistance

must be inserted between the anodic or cathodic reaction to restrict or slow down the current passage through the anode and cathode and, as a result, prevent corrosion [18]. There are four fundamental approaches to corrosion management:

(i) Material Choice: Select materials that are compatible with the surrounding environment.

(ii) Corrosion Inhibitors: Modify the immediate surroundings of the metal to passivate and safeguard it.

(iii) Cathodic Protection: Electrochemically modify the metal's surface state to relocate anodic reactions to other areas.

(iv) Coatings: Offer a shield against the electrolyte, safeguarding the metal from harm [19].

Chemistry of polyurethane

The coupling of polyisocyanate or diisocyanate with polyol or diol is the basic chemistry of polyurethane. As seen in Figure 4, this reaction creates recurring urethane connections, usually with the inclusion of a linkage extender and other additives. The essential components of polyurethane can be simplified to just two primary elements: an isocyanate and a polyol. Both the linkages have a significant influence on the final properties of the product. Modifying either the polyol or the isocyanate can lead to significant alterations in the polyurethane's properties. Consequently, the relationship between the structure of polyols and isocyanates is crucial for comprehending and designing polyurethane products [20]. Within the polyurethane, the isocyanate and polyol form distinct regions or domains. These areas are in charge of giving the finished product qualities like hardness, softness or flexibility. Figure 4 illustrates the presence of hard and soft segments. Polyols typically have longer chain lengths, which enhance mobility and thus contribute to the flexibility of the polyurethane; longer-chain diols offer increased flexibility. In contrast, the hard segments are influenced by the

isocyanates and chain extenders used. Isocyanates are generally short-chain molecules, resulting in a higher degree of crystallization and the creation of compact, rigid segments that lack flexibility. Because of its blend of soft and firm parts, polyurethane is incredibly adaptable and appropriate for a variety of uses [21–23].

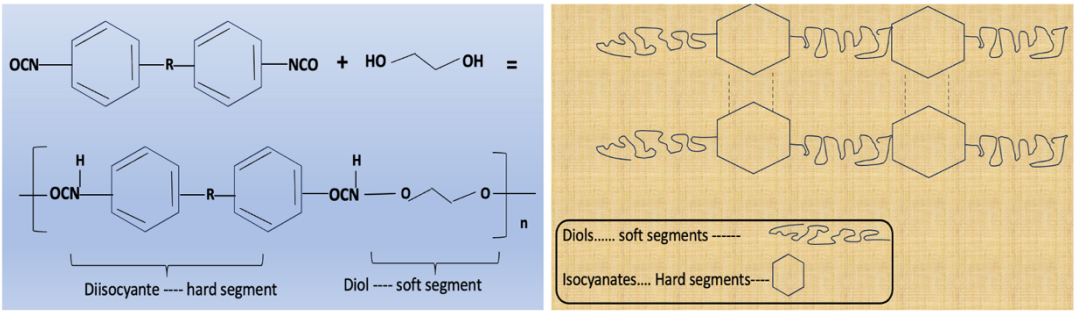

Figure 4: Presentation of polyurethane and its hard and soft segments.

Isocyanates

One of the characteristics of isocyanates is the existence of reactive compounds with the formula (O=C-N). This is the reactive group that is complementary to hydroxyl in the addition reaction that creates polyurethanes. Comparatively speaking, there are far fewer commercial isocyanates than polyols. Because of their strong reactivity towards hydroxyl groups, isocyanates are important because they increase the efficiency of polyurethane manufacturing. The production of isocyanates can be accomplished in part by starting with amine-based compounds and reacting them with phosgene [24].

PU coatings can be made using a polyfunctional isocyanate that has an aromatic, aliphatic, cycloaliphatic, or polycyclic structure. TDI, MDI, 4,4 -dibenzyl diisocyanate (DBDI), H12MDI, XDI, tetramethyl-xylylene diisocyanate (TMXDI),(IPDI), hydrogenated xylene diisocyanate (HXDI), naphthalene 1,5-diisocyanate (NDI), p-phenylene diisocyanate (PPDI), DDDI, hexamethylene diisocyanate (HDI), TMDI etc. [25]. Compared to cycloaliphatic or aliphatic diisocyanates, aromatic isocyanates are

more reactive. The PU characteristics are influenced by various diisocyanates in different ways. For instance, PUs produced by aromatic diisocyanates are stiffer than those produced by aliphatic ones, but they have worse oxidative and UV stabilities.

Diols/Polyols

PUs can contain polyols in the form of polyester, polycarbonate and acrylic polyol, castor oil, polypropylene and polyethene glycol, PTMG, or polycaprolactone diol, or a mixture of these. Due to the ability to modify the functionality of the isocyanate or reactant containing hydroxyl, a broad range of branching or crosslinked polymers can be generated. Glycols, including , 1,4-butane diol BDO, ethylene glycol and 1,6-hexane diol, are the most basic type of polyols. Because of the large concentration of urethane groups in the reactants with low molecular weight, rigid and stiff polymers are produced. Conversely, polymer chains with more flexible alkyl chains and fewer urethane groups are produced when high molecular weight polyols are used as the primary reactants. Soft, elastomeric polyurethane (PU) is produced by long-chain polyols with low functionality, whereas more rigid, crosslinked products are produced by short chain polyols with high functionality. Either propylene oxide or ethylene oxide is added to a polyhydroxy molecule to create polyether polyols. Ethylene glycol, Glycerol, trimethylolpropane are examples of typical starting molecules. Polyfunctional alcohols and polyfunctional carboxylic acids or anhydrides react condensation to form PEPOs. By polymerizing hydroxyethyl acrylate with additional acrylic precursors, ACPOs are created [14]. Generally speaking, the application field has determined the choice of PEPO, polyether polyols, or ACPO. Commercial applications commonly use polyesters formed from a combination of diacids interacting with glycols, which leaves plenty of opportunity for a wide series of incredibly difficult products [15,16]. Even while the ester group's gradual hydrolysis can affect PUs based

on PEPO and ACPO, they are nevertheless sufficiently robust to resist weathering over time. The ester groups undergo hydrolysis, returning the carboxylic acid and alcohol as a result. Furthermore, an autocatalytic effect is caused by the production of carboxylic acid in situ which catalyzes additional hydrolysis of ester [17]. Consequently, the average molar mass experiences a notable reduction, and mechanical characteristics gradually deteriorate during extended interaction to a damp environment. Polycarboimides are acid explorers and auto catalyst inhibitors that may be used to treat poly(ester urethanes) to decrease the breakdown of polyester groups. [17, 18]. Oil resistance, adhesive qualities, and heat stability are all very good in PU coatings made from PEPO. Furthermore, the widespread use of polyester-type PU coatings has been made possible by the decreased cost of manufacturing.

Polyurethane coatings

Epoxy, Polyolefin, and polyurethane are some examples of polymeric coatings based on matrices [26][27]. For about 75 years, polyurethanes (PUs), initially discovered by Otto Bayer and his colleagues, have evolved into an extremely adaptable category of polymers[28]. They are derived from two basic liquid components and are used in many different industrial sectors depending on the production circumstances. Many of these applications exhibit significant sustainability attributes due to their exceptional properties. Some examples include improving the insulation properties of buildings and refrigerators, lowering the weight of construction and transportation materials using PU-based foams and adhesives, and increasing the life of coatings that are used to protect metal, concrete, and wood surfaces [27].

Types of Polyurethane Coatings

Because of its many uses and adaptability, polyurethane coatings have been made in different types of forms to satisfy a range of industry demands. Waterborne and

biobased polyurethane coatings have attracted interest among them because they show improved sustainability and eco-friendliness (

Table 1). To shed light on the special qualities and possible benefits of waterborne and biobased polyurethane coatings for environmentally aware coating technologies, we have examined the features and uses of these coatings in this study.

Waterborne polyurethane

The development of waterborne polyurethane (WPU) is the first step towards creating coatings that are sustainable, free of volatile solvents, and kind to the environment. Moreover, waterborne PU exhibits commendable mechanical, physical, and anti-corrosion properties. They stick to glass and polymeric fibres, among other surfaces, with ease. It's important to remember that polyurethanes don't break down in water and are typically hydrophobic. Therefore, changes must be made to allow for their dispersion in water. These changes might include adding ionized or non-ionized segments to the polymer matrix [29].

In the early 1990s, Waterborne Polyurethanes (WPUs) emerged in response to increasingly stringent environmental regulations in North America and Europe[30]. The major problem of excessive Volatile Organic Compound (VOC) pollution associated with conventional solvent-based coatings was addressed by using water as the principal solvent. Moreover, adding water removes the possibility of hazardous non-reactive isocyanate building up in the system [31]. To maintain the stability of WPU dispersions, it is crucial to introduce hydrophilic groups into the formulation. However, this reduces the final coating's ability to withstand water, limiting the

potential for anticorrosion applications. To address this challenge, manipulating the diverse chemistry of polyurethanes (PUs) offers a means to customize coating characteristics, including resistance to water and non-corrosive efficiency. Studies have found that optimizing the polyether/polyester polyol ratio enhances anticorrosion performance, while the choice of diisocyanate structure also influences protective ability. Chemical modifications of the PU backbone, such as the preparation of fluorinated WPU or the incorporation of polydimethylsiloxane, have been proposed to enhance the coating's wetting behavior. The water resistance of WPU coatings modified with sulfonate polyester diol and HPDMS was improved by 5% [32], and in other work, Bo Zhao and Runping Jia created superhydrophobic films of waterborne fluorinated polyurethanes (WFPUs) with guanidine groups using a one-step spray method. The carbonyl and guanidine groups in the PUs films quickly formed hydrogen bonds, resulting in superhydrophobic films with the right roughness of the surface. When the guanidine salt chain framework enhancer was at 11%, the PU film showed a water contact angle (CA) of 153.82° [33]. These modifications aim to overcome environmental concerns associated with fluorinated compounds. Additionally, the use of nanoparticles presents a promising strategy for achieving hydrophobic WB coatings without altering the PU matrix chemically.

Nanoparticles have proven to be effective not only in altering surface properties, such as wettability but also in enhancing coating barrier properties, which play an important role in retarding the diffusion of harmful substances through the coating to the metal surface [34]. Incorporating nanoparticles to improve the coating's barrier characteristics and extend the metal surface's exposure to surroundings is known as a "passive" protection strategy [9]. The aspect ratio, direction, and level of scattering of nanoparticles are important elements determining the barrier characteristics of the

coating, based on diffusion theory and the tortuosity model [35]. Consequently, layered nanoparticles like $Ti3C_2$ (MXene) [36], boron nitride[37] nanosheets, and especially graphene and its derivatives are often preferred due to their heightened effectiveness in improving barrier properties.

Pan Yi et al. investigate the effect of mixture fillers containing CNTs and graphene on the corrosive behavior of polyurethane coatings. The outcome indicates that the coating containing 2 wt % composite fillers demonstrates outstanding thermal conductivity and corrosion resistance behavior [38]. In another work, Xia Wang et al. studied the behavior of composite-modified nano Titania. They studied the thermogravimetric and corrosion resistance of AKT-modified waterborne polyurethane coatings. The results show that adding 0.7% AKT to the polymeric coating significantly improves corrosion resistance. The resistive modulus for this coating reached 5.05×10^{6} Ω, and the corrosion current density significantly decreased to 5.21×10^{-9} A, over two orders of magnitude lower than that of the pure WPU coating. The improvement in corrosion resistance efficiency reached more than 90%. The effectiveness of the coating in preserving the quality of the steel sample was proven by a 360-hour extended immersion test and scanning electron microscopy examinations [39].

An alternative approach to address potential coating failures involves the use of materials with self-healing properties, seeking to repair affected coatings' stability and insulating qualities. Recent literature suggests both extrinsic and intrinsic self-healing waterborne polyurethane (WPU) coatings[26]. In the extrinsic method, a healing agent is enclosed within hollow carriers like microcapsules or core-shell fibers, which are then incorporated into the PU dispersion. When the coating experiences damage, the healing agent is released, autonomously filling cracks and flaws to preserve protective capabilities. To extend the longevity of both the coating and the steel substrate, a self-

healing hybrid polyurethane anti-corrosion coating was developed. This coating incorporated nanofillers with furan groups (f-PFP), specifically graphene oxide polydopamine/polyaniline. The modified furan additive, constituting 0.5% of maleimide (m-WPU) under optimal conditions, demonstrated outstanding resistance to corrosion and durable protection. Figure 5 illustrates the outcomes highlighted the synergistic effects of the barrier properties of GO, the passivation mechanism of PANI, and the reversibility of DA bonds, contributing to the enhanced corrosion resistance and remarkable self-healing properties of the hybrid coating with the f-PFP additive [40].

Christopher et al. [41] developed a method to create affordable, low-volatile organic content nanocomposite coatings through solution blending. They used waterborne polyurethane dispersion containing ZnO nanoparticles modified with biopolymers like sodium alginate and lignosulfonate, which were applied to mild steel. The nanocomposite coatings with varying levels of nano ZnO loading were produced using ultrasonication. The study evaluated the corrosion resistance of the coated steel after incorporating surface-modified ZnO nanoparticles using potentiodynamic polarization and electrochemical impedance spectroscopy. Additionally, the surface wettability of the composite coating was examined through contact angle measurements, showing that increasing nanomaterial dosages did not affect surface wettability. The results suggested that higher percentages of surface-modified ZnO in waterborne polyurethane led to better dispersion of particles and improved corrosion performance in the nanocomposite coatings. Specifically, corrosion results indicated that a 0.3 wt% loading of ZnO modified with lignosulfonate provided better protection compared to sodium alginate modification.

In other work, Akbarian et al. [42] compared Waterborne Polyurethane (WPU) and

High Solid Polyurethane (HPU) coatings with and without nanoparticulate silver on mild steel using electrochemical impedance spectroscopy (EIS) in NaCl solution. They observed that the presence of nanoparticulate silver caused degradation in the WPU coating, while it had no significant effect on the resistance of the HPU coating. Additionally, morphological analysis showed integrity loss in the WPU coating with nanoparticulate silver, whereas the HPU coating remained largely unaffected. This differential behavior of nanoparticulate silver was attributed to the distinct chemical structures of WPU and HPU.

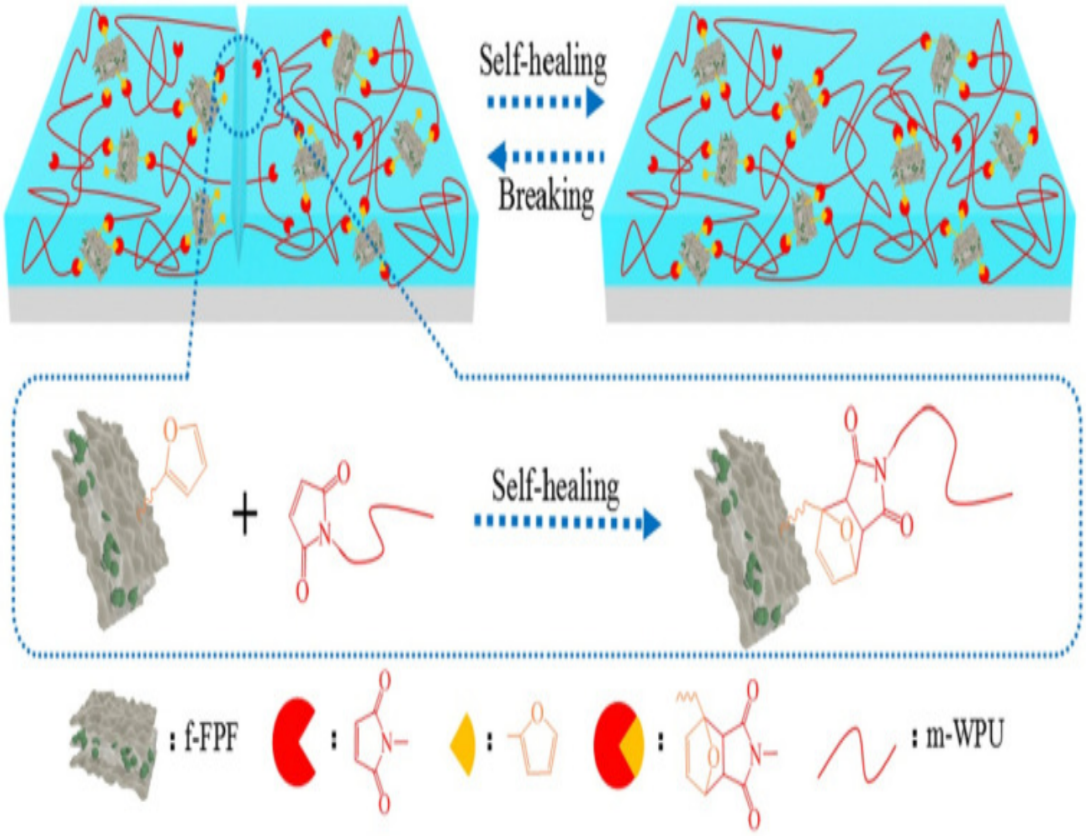

Figure 5: The self-healing phenomena of the WPUx coating [40]. Copyright 2023, Elsevier.

Table 1: The Table Shows the Types of Polyurethane Coatings, Formulations, and Fillers.

Matrix type	Formulation	Filler	Substrate	Ref.
WPU	IPDI-BDO	-	Plastic mold film	[43]
WPU	TDI-PBA	-	cotton	[44]
WPU	DSB-KPS-(COPS-2)	Ti_3C_2(MXene)	Q235 steel	[45]
WPU	As received	Boron nitride (BN)	steel	[46]
WPU	As received	CNTs-Carbon nanohorns, Graphene, ultrafine graphite powder	Q235 steel	[47]
WPU	As received	Nano-TiO_2	steel	[48]
WPU	As received	ZrO_2	steel	[49]
BiO-PU	safflower oil	Modified-GO	steel	[50]
WPU	As received	GO	steel	[51]
WPU	HDI modified PU	TiO_2-GO	steel	[52]
WPU	IPDI- PPG	Furan modified CeO_2	steel	[53]
WPU	As received	Fe_2O_3	steel	[54]
WPU	Polyaniline modified PU	-	steel	[55]
WPU		CeO_2-MXene	steel	[56]
Bio-PU	Jatropha Oil	ZnO	steel	[57]
Bio-PU	Mahua oil fatty amide/ MDI-TDI	-	steel	[58]
WPU	-	ZnO	steel	[59]
WPU	-	Montmorillonite-Ce^{3+}	steel	[60]
Bio-PU	crambe and castor oil	tannin	AA2024-T3	[61]
WPU	-	BN	Steel	[62]
WPU	-	SiO_2	Zn-Al	[63]
Bio-PU	Starch	-	Glass	[64]
Bio-PU	Crambe and castor oil	Zn Flakes	AA7475	[65]
Bio-PU	Citrullus colocynthis Seed Oil	-	Glass	[66]
Bio-PU	soybean oil	-	Steel	[67]
Bio-PU	Nonedible castor oil	-	Steel,	[68]

Matrix type	Formulation	Filler	Substrate	Ref.
Bio-PU	Cardanol	silane-grafted ZnO	glass steel	[69]
Bio-PU	Castor oil	-	steel	[70]
Bio-PU	Jatropha oil.	$BaSO_4$ and TiO_2	Metal, plastic, wood and glass	[71]
Bio-PU	Lignin based PU	-	steel	[72]

Biobased polyurethane

Developing eco-friendly chemical processes to substitute petroleum-derived components like diisocyanates and diols presents a challenging endeavor. Consequently, researchers are exploring alternative sources such as starch, lignin, cellulose and fats to produce polymers from sustainable natural materials. These substances contain esters and carbon double bonds that can be adapted to create polyols, ultimately yielding bio-based polyurethanes.

Vegetable oils serve as the predominant renewable source for producing environmentally friendly polyurethanes (PUs). Primarily composed of triglycerides, these oils exhibit diverse functionalities and active sites, enabling various chemical transformations. In the creation of bio-based polyols, modifications are typically made to vegetable oils to incorporate hydroxyl groups. These groups can do reactions with isocyanates, leading to the formation of polyurethanes. Additionally, a broader range of functional groups can be introduced to polyols derived from vegetable oils, allowing for diverse chemical adjustments to fine-tune the properties of the resulting polyurethane coatings. Alagi et al. address the challenge of replacing petroleum-based polymeric materials in the polymer industry with eco-friendly alternatives. The study

proposes a technology using thiol-ene reactions to create sustainable polyols. Specifically, soybean oil-based polyols with various functionalities are synthesized. Silane-modified polyols, such as SiMSO, are highlighted for their superior performance in polyurethane (PU) coatings. Compared to conventional polyols, SiMSO-based PU coatings exhibit higher hardness, glass transition temperature (Tg), adhesion strength, and improved anticorrosion properties in aqueous NaCl solutions. The study concludes that soybean oil-based functional polyols hold promise as environmentally friendly alternatives, offering desirable properties for PU coatings [73].

Using hexamethylene diisocyanate trimer and bio-based acetylated starch, a new omniphobic PU coating is created. The coating's characteristics are improved by the addition of a significant quantity of polydimethylsiloxane. Adjusting the polydimethylsiloxane content results in high-transparency (>97%) PU coatings with excellent anti-smudge characteristics. The coatings effectively repel various liquid contaminants, providing anti-corrosion properties for metal surfaces. These bio-based coatings show promise for sustainable, environmentally friendly protection against contamination and corrosion [74].

Incorporating corrosion inhibitors into coatings provides sustained protection by releasing inhibitors when microcracks appear – see Figure 6. Bio-based polyurethane sublayer coatings with lignin-corrosion inhibitor (LCI) conjugates were developed by Wang et al., offering robust anti-corrosion performance. These coatings, applied to stainless steel, significantly improved corrosion resistance and formed a protective barrier layer within artificial cracks, demonstrating enhanced durability [72].

Chen et al. developed feasible, non-fossil, and bio-renewable sources in response to the growing need for energy. They were able to effectively create a prepolymer of biomass polyurethane (PU) from Jatropha oil (JO). They added hybrid nanoparticles to the PU

matrix that had different ratios of titanium dioxide (TiO_2) and barium sulphate ($BaSO_4$) to improve its characteristics. The resultant composite coatings showed excellent infrared radiative cooling and UV blocking after UV curing. In the UV zone, the ideal reflectance was 97.30%, with a notable temperature differential of up to 20.8 °C. Even after being submerged in corrosive acids, alkaline and salt solutions for 30 days, the coatings showed outstanding anti-corrosion qualities. It was also discovered that they may be recycled and put to further use by going through many processing steps [71].

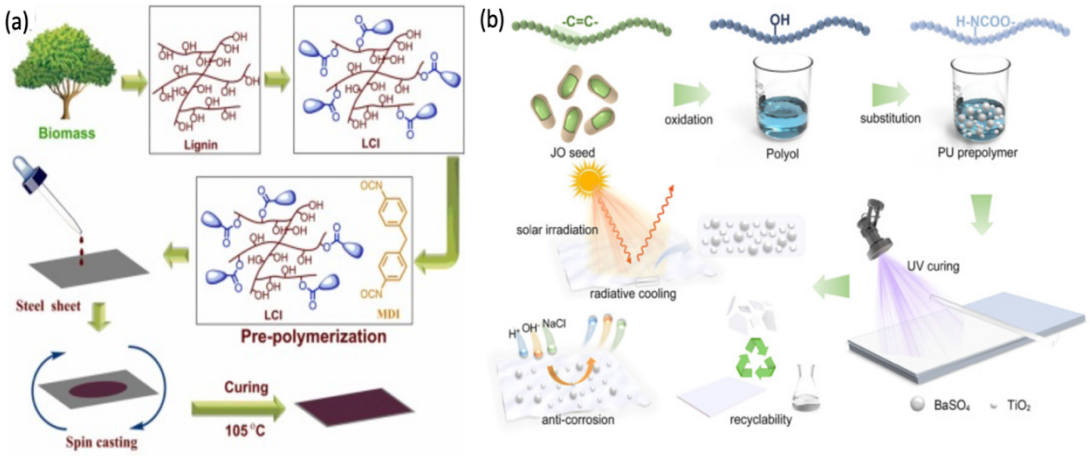

Figure 6: (a) The schematic shows how to conjugate a corrosion inhibitor with lignin and create polyurethane coatings based on lignin [72]. (b) The preparation procedure of bio-PU-based composite coating. Copyright 2022-2023 Elsevier.

Mekonnen et al. integrated cellulose nanocrystals (CNC) modified with epoxy-functionalized silane (ES) to develop waterproof and corrosion-resistant polyurethane (PU) nanocomposite coatings. Varying levels of grafting were achieved by adjusting reaction time and ES concentration, improving the heating properties and wetting behavior of the modified CNC. The incorporation of these modified CNCs into PU

enhanced thermal and mechanical properties, reduced water absorption, and improved dispersion and interfacial adhesion. Mild steel coated with the resulting nanocomposite has superior anticorrosion performance compared to PU alone, as demonstrated in salt spray and electrochemical impedance spectroscopy (EIS) studies. The silanization of CNC proves to be a robust, eco-friendly, and scalable process, making it a promising material for various polymer composite applications [75].

John et al. developed a nano-texture for a heat-stable, superhydrophobic, and anticorrosive coating using a modified CPU polymer matrix and ZnO nanoparticles. The bilayer assembly forms a strong interface, enhancing coating properties. ZnO modification improves compatibility, reducing particle attraction and maintaining surface roughness for super hydrophobicity. The layer-by-layer design provides double protection, slowing corrosion by repelling water and enabling cathodic protection. This sustainable and less-toxic design broadens the applicability of mild steel [69].

Castor oil (CO), modified castor oil, and dimer fatty acid diisocyanate (DDI) were used to create organic polyurethane dispersion mixtures with a high carbon content. The study looked into structure/property connections and how to improve the efficiency of DDI-based PUDs. The Silicon oxygen cross-link network and the molecular structure of MCO were discovered during characterization. Properties were affected by changes in the alkoxysilane and NCO/OH ratio, resulting in higher Young's modulus, glass transition temperature and tensile strength. On the other hand, when the alkoxysilane concentration increased, the starting degradation temperature and the elongation at break dropped. After being submerged in sodium chloride solution for some days, the resultant modified DDI-based PUD showed outstanding corrosion resistance, suggesting the possibility for high-performance, biobased coatings [76].

Self-healing mechanism in polyurethane coatings

Two primary categories may be used to categorize the process behind self-healing

polymeric polyurethane coatings that shield the metal from corrosive media: Self-healing mechanisms that are intrinsic and extrinsic, as exhibited in Figure 7. Extrinsic self-healing mechanisms rely on external stimuli to activate the repair process in materials. These systems require triggers such as heat, light, ultraviolet (UV) radiation, or changes in pH to initiate healing. For example, microcapsules containing healing agents may break open when exposed to heat or UV light, releasing their contents to repair damage. Similarly, thermal-responsive polymers can undergo reversible changes when heated, helping to close cracks or restore material properties. These mechanisms are effective in controlled environments where external activation can be reliably applied. On the other hand, Intrinsic self-healing mechanisms operate autonomously without the need for external stimuli. In these systems, materials contain built-in components that enable self-repair when damage occurs. For instance, polymers with dynamic covalent bonds can reassemble themselves after a crack or fracture, while materials with internal healing agents can spontaneously migrate to and repair damaged areas. Supramolecular polymers, which rely on non-covalent interactions, can also self-heal through their inherent chemical properties. These mechanisms are advantageous in applications requiring continuous self-repair without external intervention [77]. Creating such coatings that protect may be approached from both the extrinsic and internal healing perspectives. To provide surface protection against damage, the extrinsic method incorporates discrete active healing agents into the coating system, such as binders and corrosion inhibitors. Reversible chemicals are included as part of the intrinsic method to facilitate damage repair and sealing [78]. Table 2 shows the intrinsic and extrinsic mechanism approach explained by some of the researchers.

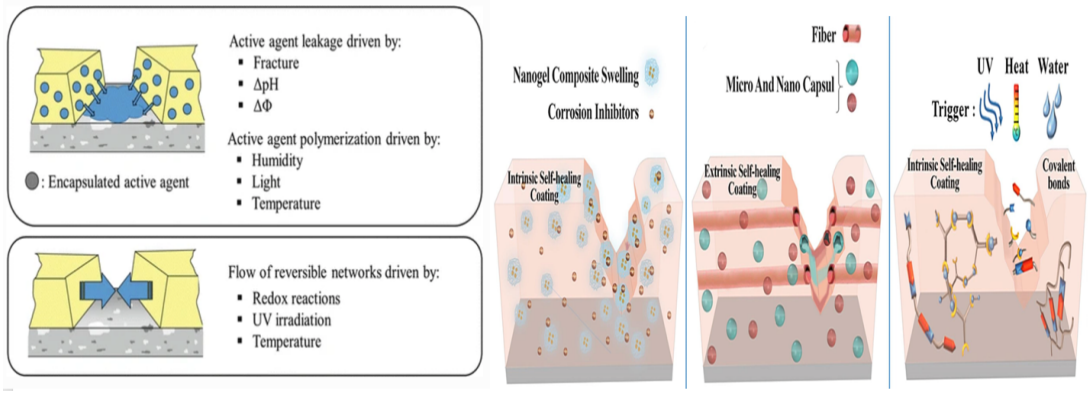

Figure 7: Extrinsic and intrinsic mechanism of self-healing coatings. Reproduced with permission of Springer [79] and Elsevier [80].

Table 2 : Self-healing Mechanism of Polyurethane Coatings.

Matrix formulation	**Self-healing agent**	**Mechanism**	**Substrate**	**Ref.**
PU-Linseed Oil	Sodium dodecyl sulfate (SDS)	Extrinsic	Q235 carbon steel	[81]
PU-Carboxylated GO	Modified Chitosan	Intrinsic	Aluminium	[82]
PU-furan modified HNTs	-	Intrinsic	Steel disc	[83]
PU-LDH	MBT	Extrinsic	HDG steel	[84]
PU	TEMPO	Intrinsic	Aluminum	[85]
PU-modified Linseed oil	Benzotriazole/ potassium ethyl xanthate	Extrinsic	Copper sheets	[86]
PU-SiO_2	MBT	Extrinsic	Steel	[87]
PU-tannin	-	Extrinsic	AA2024-T3 plates	[61]
PU-Zinc flakes	-	Extrinsic	AA7475 Alloy	[65]
PU-MXene	CeO_2	Intrinsic	Steel	[56]
PU	Furan modified Ceria	Intrinsic	Steel	[53]
PU	Starch	Intrinsic	Steel	[88]
PU	MXene- CeO_2	Extrinsic	Steel	[89]
PU	Diisocyanate	Intrinsic	steel	[90]

Importance of Containers and Inhibitors

In the realm of corrosion protection, the effectiveness of polyurethane coatings is not solely determined by the composition of the coating material itself. Instead, the choice of containers and matrices plays an important role in shaping the performance and durability of these coatings. The careful selection of containers encapsulating the polyurethane formulations and the matrices within which these coatings are suspended are fundamental steps in achieving the desired protective attributes.

This section delves into the crucial aspect of containers and matrices within polyurethane coatings. It explores how these components' design, material, and properties can significantly influence the coating's adhesion, mechanical strength, chemical resistance, and overall corrosion protection capabilities. From traditional metal cans to advanced nanocomposite matrices, the choices made in this regard have far-reaching implications for industries relying on polyurethane coatings as a frontline defense against the relentless forces of corrosion.

Throughout this section, we will navigate the multifaceted world of containers and matrices used in polyurethane coatings, shedding light on the intricate interplay between these components and the polyurethane itself. We will also discuss how container and matrix technology innovations are pushing the boundaries of corrosion protection, enabling longer service lifetimes and enhanced performance in various environments. Ultimately, understanding the role of containers and matrices is essential for engineers, researchers, and practitioners seeking to harness the full potential of polyurethane coatings in the battle against corrosion.

Types of containers/nanoparticles used in polyurethane matrices

Coatings that are smart or self-healing offer both passive and active defense. One way

to create these intelligent coatings is by using nanoparticles, or nanocontainers, that have been impregnated with an appropriate inhibitor. By applying stimuli like pH, violent breakage, or electrostatic exchange of the inhibitory species, one can accomplish extended and periodic release of the inhibitor. The following characteristics are presented by using nano containers. In order to prevent premature coating degradation, the inhibitor molecules are first isolated by the nanocontainers, which also remove any contact between the inhibitor molecules and the coating. Second, the inhibitors are kept from leaking too soon by the nanocontainers, reducing concerns about the accumulation of osmotic pressure, which may eventually result in adhesion failure. Lastly, the inhibitors can be released gradually and continuously from the nanocontainers [91].

Alrashid et al. [91] studied a novel approach to enhance the corrosion protection of 2024-T3 aluminum alloy coatings. Traditional inhibitor incorporation causes premature coating deterioration, but the use of polylactic acid (PLA) nanoparticles encapsulating the organic inhibitor MBT overcomes this issue. The study optimizes nanoparticle parameters, evaluates coating properties (impact resistance, adhesion, hardness, solvent resistance), and demonstrates a substantial 200-fold increase in corrosion resistance with the incorporation of MBT-encapsulated PLA particles into a polyurethane hybrid coating.

In a study [92], Waterborne coatings that improved steel's resistance to corrosion and water were made using modified montmorillonites. The problem of poor water resistance while employing Na-montmorillonite was addressed by substituting Ce^{3+} for Na^{+} in montmorillonite. The manufacture of chitosan increased the Ce concentration and improved the dispersion's stability. The coating comprising Ce-CS-Mt particles showed a low level of water absorption, indicating better water resistance. Furthermore,

it demonstrated superior resistance to corrosion, with no apparent corrosive particles after 768 hours of salt spray exposure and high impedance in EIS measurements, highlighting the effectiveness of Ce-CS-Mt in enhancing coating performance.

Nardeli et al. [88] focus on biobased organic polyurethane coatings for AA7475 aerospace alloy. Zinc micro-flakes were incorporated to enhance corrosion resistance, confirmed by FTIR-ATR and AFM analyses. EIS showed improved corrosion resistance with higher Zn content, and localized techniques revealed effective corrosion protection, especially with 7.5 wt% Zn flakes in the coating.

A novel eco-friendly corrosion protection coating was developed using waterborne polyurethane and Ce^{3+} modified with palygorskite nanocontainers. Ce^{3+} was successfully grafted into PAL nanofibers, and even a small addition (2 wt%) of Ce-PAL significantly improved corrosion resistance, as shown in salt immersion tests and electrochemical measurements. The study also proposed an active anti-corrosion mechanism for the Ce-PAL/WPU coating based on SEM with energy-dispersive X-ray spectroscopy results [93].

Li et al. [94] synthesize effective coatings to prevent corrosion by embedding inhibitors in nanocontainers that react to pH. Ce-MMT nanocomposites functionalized with tannic acid were created, in which Ce^{3+} serves as cathodic protection and MMT serves as a material barrier and container. In comparison to pure WPU, these coatings showed a markedly higher impedance (|Z|0.01Hz) and long-term anti-corrosion capabilities. Ce^{3+} and TA also functioned as self-healing agents, preventing corrosion at the interface between the coating and the metal and providing a viable method for high-efficiency anti-corrosion coatings.

Another work showcases the use of hybrid Polyurethane-modified ZrO_2 nanocomposites as carriers for corrosion protection coatings on steel. ZrO_2 and

modified ZrO_2 nanoparticles were synthesized and incorporated into the polyurethane matrix, enhancing thermal stability. These nanocomposites exhibit increased hydrophobicity, offering advantages for corrosion prevention. Electrochemical tests demonstrated that the polymer nanocomposite coatings, with 2 wt% Pd–ZrO_2, significantly improved corrosion protection efficiency, underscoring their enhanced anti-corrosion properties [95].

Diels-Alder bonds are formed when a PU prepolymer is bonded together with furan-modified CeO_2, resulting in a self-healing anti-corrosion coating that shields mild steel from corrosion damage. The coating exhibits impressive mechanical strength of around 39 MPa, strong adhesion (12 MPa), and an impedance modulus of around 1×10^9 Ω cm^2 at 0.01 Hz, remaining effective even after 100 days of immersion. Furthermore, the coating can rapidly self-heal within a few seconds under near-infrared light, with minimal impact on its mechanical and corrosion protection properties, offering a promising approach for excellent performance anti-corrosion polyurethane coatings [96].

Wang et al. [97] discuss the problem of getting the right balance between mechanical strength and self-healing efficiency in polymers. An outstanding mechanical property, around 132 MJ m^{-3} toughness and tensile strength of around 34 MPa are attained in a self-healing polyurethane nanocomposite, which is created by binding amidoxime-modified silica nanoparticles and isocyanate-terminated polyurethane with oxime-urethane linkages. The nanocomposite is useful for long-lasting, corrosion-resistant coatings in hostile settings since it also demonstrates a remarkable self-healing efficiency of 96% and corrosion protection for mild steel.

Lou et al. [98] explore waterborne polyurethane (WPU) composites with $Ti_3C_2T_x$ MXene and CNTs for the protection of corrosion. The nanocomposites show improved

thermal stability, surface properties, and mechanical strength. Electrochemical tests reveal that WPU with 0.95 wt% MXene and 0.05 wt% CNTs exhibits the lowest corrosion rate, highlighting its potential for effective corrosion protection on various surfaces.

One more study presents a composite waterborne polyurethane coating designed to offer sustained corrosion prevention for carbon steel, featuring a unique combination of self-healing and active corrosion inhibition. The coating incorporates both montmorillonite (MMT), acting as a corrosion inhibitor container with a labyrinth effect, and corrosion inhibitors Ce^{3+} and TA. After 50 days of immersion, the impedance modulus remained significantly higher (over 108 $\Omega \cdot cm^2$), demonstrating its superior corrosion resistance compared to pure PU coatings. Furthermore, the coating exhibited effective self-healing capabilities through disulfide bond exchange reactions, ensuring durable corrosion protection and making it a promising choice for long-term anti-corrosion applications [99].

Fabrication Techniques for the coatings

The fabrication process selection is influenced by several factors, including the geometry of the component that needs to be coated, aesthetics and appearance, production costs, coating thickness, and capital cost. Self-healing polymer coatings can be assembled using a variety of techniques, including the following: (1) dip coating, (2) Doctor blade coating, (3) spin coating, (4) spray coating, and (5) direct immersion approach. Numerous studies conducted in the last several years demonstrate that researchers are experimenting with these fabrication techniques and are attempting to increase their effectiveness by small-scale addition of additional elements. Every technique has limits that restrict its general application. For example, spin coating is a commonly used method for creating thin polymer coatings on flat surfaces, and the creation of nonplanar surfaces is accomplished through spray painting. The methods

for preparing polymeric coatings that are utilized to ensure that polymer material adheres to metal substrate surfaces are displayed in Figure 8.

Dip coating method

Among the most adaptable methods for coating deposition on metal substrates is dip coating, which offers great coating type versatility but limited coating thickness flexibility. The most basic coating methods create a connection between the form of the substrate material and the characteristics of the polymer solution [95]. There are three primary subprocesses in the dip coating process: (1) Immersion/dwell time: The polymer liquid solution is continually poured onto the surface that will get the coating. For a predetermined period of time, the substrate is allowed to be immersed in the solution to allow the coating solution to make contact with the surface and fully dry it. (2) The process of building up a thin polymeric film involves continuously removing the steel substrate from the coating solution, depositing a thin layer of solution on the metal substrate; (3) The thin film material is thermally treated to promote polymerization and strengthen the resulting polymer thin film following (4) dissolving the solution, which entails drying the solution that is available on the substrate to generate a fine film of polymer that is later prepared by heating and drying [95], [96]. Various manufacturing procedures enabling the use of protective coatings on metals have been the subject of numerous investigations.

Table 3 lists some of the methods that researchers have employed.

Table 3: Types of Coating Fabrication Techniques.

Matrix	Carrier/Inhibitor	Substrate	Coating technique	Ref.
PU	MAO/M16	Magnesium Alloy	Spray	[100]
PU	Maleic anhydride	Aluminum Alloy	Doctors blade	[101]
PU	Pda/CeO_2	Mild steel	Doctors blade	[102]
PU	Pd–ZrO_2	Mild steel	Spray	[103]
PU	Functionalized-GO	mild steel	Spray	[104]
PU	Zinc micro flakes	Aluminum Alloy	Doctors blade	[105]
PU	Tannin	Aluminum Alloy	Doctors blade	[106]
PU	ZnO	Mild steel	Spin coating	[107]
PU	MXene	Mg alloy	Spin coating	[108]
PU	Graphene Oxide	Steel	Doctors blade	[109]
PU	Silica (SiO_2)	steel	Spin coating	[110]
PU	Ceria (CeO_2)	Steel	Spray coating	[111]
PU	Silane grafted ZnO	Steel	Dip coating	[112]
PU	GO-CNTs	Steel	Spin coating	[113]
PU	Silica (SiO_2)	steel	Dip coating	[114]
PU	ZnO	Steel	Dip coating	[41]
PU	MXene/CeO_2	Steel	Doctors blade	[115]
PU	ZnO	steel	Spin coating	[116]

Doctor blade coating technique

Known alternatively as tape casting or doctor blade coating, this low-cost solution processing technique is the most often used for large-area thin film manufacturing. The name "doctor blade" coating was originally used in 1940 to refer especially to thin capacitor and piezoelectric material sheets. The fundamental principle of this procedure is the continuous movement between the substrate and the blade. This can be achieved by either sliding the substrate beneath the blade or passing the blade over it. Employing this method involves applying a well-mixed coating mixture to both sides of the blade-covered substrate. As the blade and surface move relative to each other, the resulting slurry effectively spreads across the metal, evaporating to form a film. The ultimate

consistency homogeneity and uniformity are highly dependent on the architecture of the doctor blade unit and the elastic property of the coating precursor, both of which need to be continuously monitored [117,118].

Spray method

An exciting method for atomizing and directing a small stream of compressed air into the surface coating stream while maintaining the size of nanostructured materials is compressed air spray. This process creates a fine surface coating by forcing the liquid stream into many tiny drops and violently framing it with bubbles. The difficulties in applying coatings with variable wettability. while maintaining control over both the surface's real and artificial characteristics. Using the compressed air spray technique described in this work, mild steel substrate was coated with anti-corrosion polyurethane coatings. ZrO_2 doped with polyurethane and Pd was utilised to deposit hydrophobic and anti-corrosion layers, providing a clear picture of possible coatings for maritime use [119].

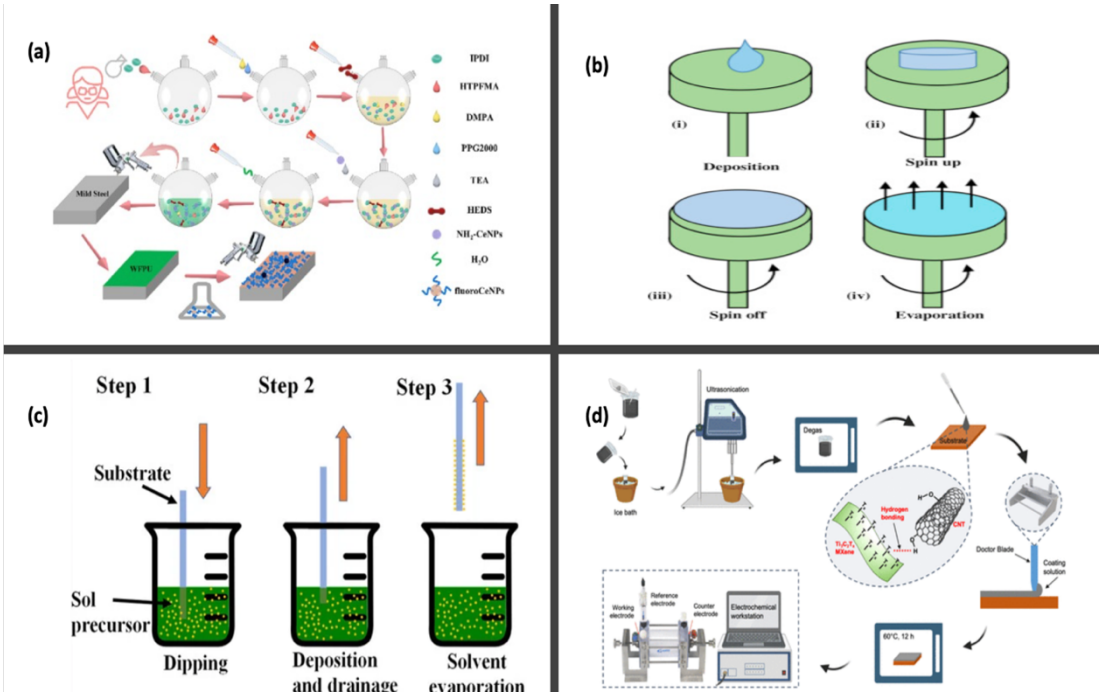

Figure 8: Representation of different fabrication techniques of polyurethane coating. (a) spray coating, (b) spin coating, (c) dip coating[120], and (d) doctor's blade. Reproduced with permission of Elsevier, [121][122].

Spin coating technique

Spin coating represents a technique utilized to generate uniform coatings of organic compounds on smooth surfaces [28]. Through spin coating, Fu et al. created a transparent superhydrophobic coating [29]. As illustrated in Figure 8 spin coating is carried out in four stages: deposition, spin up, spin-off, and evaporation. After the material is put on the spin in the first phase, the evaporation stage continues constantly while the material rotates up and down successively. The applied solution is distributed on the turntable via centrifugal force. The fast rotating speed causes the layer to thin. This is followed by allowing the applied layer to dry. It is feasible that the solvent that is used to evaporate evenly when there is rapid rotation. High volatile solution components evaporate or just dry off from the substrate, while low volatile solution components remain on the metal's surface. The thickness of the coated layer is determined by the spinning speed and the viscosity of the coating solution.

Table 4: Pros and Cons of Coating Techniques.

Techniques	Pros	Cons	Reference
Dip Coating	Easy to use, minimum paint loss	sagging	[123,124]
Spray coating	Smooth & even, time effective	Paint loss	[111,125]
Spin coating	Uniform thickness	Waste resources, depend on speed and size of substrate.	[116], [126]
Doctors blade	Less material waste, large scale application	Non uniform thickness	[115],[127]

Performance Evaluation

Methods for testing corrosion resistance and performance of polyurethane coatings:

Evaluation and testing are crucial steps to confirm corrosion protection coatings' efficacy and dependability in practical applications. A range of testing techniques, including accelerated corrosion testing methods and standard laboratory tests, have been produced to evaluate the efficiency of these coatings. Furthermore, assessing coatings' long-term dependability and durability is essential to comprehend how well they function over time. This section provides a summary of commonly used testing methods to assess coating performance, recent advancements in accelerated corrosion testing, and an evaluation of the long-term reliability and durability of corrosion protection coatings. The performance of corrosion protection coatings can be evaluated using a variety of methods. The salt spray test is a rapid corrosion assessment method that discloses a coating's ability to resist corrosive environments. The corrosion resistance and electrochemical behaviour of the coating can be better understood through the use of electrochemical techniques. Accelerated weathering tests evaluate coatings' resilience to deterioration and durability, offering a thorough assessment of their performance by simulating real-world environmental conditions.

Salt-spray test

One notable method of assessing accelerated corrosion is the salt spray test, which is also called the salt fog test. This test is especially useful for comparing the corresponding corrosion resistance of related coating materials rather than concentrating on quantitative performance metrics. Even with this focus on comparison, many test parameters still depend on meeting predetermined performance

thresholds during predetermined exposure times. During the test, an appropriate corrosive environment that mimics accelerated maritime conditions is generated. Checking coated metal surfaces for issues such as corrosion intensity and chipping, the saltwater spray test is often conducted in a self-contained setting. The substrates are left in a slightly heated fog that contains 3.5% salt water. As observed from Figure 9, the coated samples have a "X" marked on them to allow the coating to permeate the substrate. This evaluation aims to accelerate the spread of degradation or creep (beneath polymeric layer). Basically, salt spray tests work really well for quickly detecting coating deterioration, porosity, and cracks. As a result, when comparing coatings with comparable corrosion behavior, the salt spray test becomes the most appropriate test. Salt spray tests are particularly useful for evaluating the effectiveness of self-healing mechanisms in corrosion inhibitors incorporated into intact coatings. Experiments with salt spray applied to self-healing coatings have produced several interesting findings [128].

Jothi et al. studied this phenomenon in their paper. The mild metal surface is easily accessible to corrosion-causing agents (Na^+, Cl^-, and H_2O), which makes it vulnerable to high corrosion in the blank NaCl solution. Reactive ions can enter the coating interface due to the porosity caused by the uneven coating. As a result, the process of corrosion initiation is expedited. On the other hand, reactive ions are less likely to penetrate the coating/metal interface when Pd–ZrO_2 is present to fill the pores on the PU matrix. The corrosion process is significantly slowed down after adding Pd–ZrO_2 inhibitor to polyurethane, and the inhibitory effects are enhanced when Pd and ZrO_2 inhibitors are present together, per the results of EIS, potentiodynamic polarization, and weight loss. With the addition of primer and Pd–ZrO_2, it can preferentially adsorb on the mild steel surface due to its lower electronegativity, strong hydrophobicity, and

higher ionic radius than Cl− ions [129].

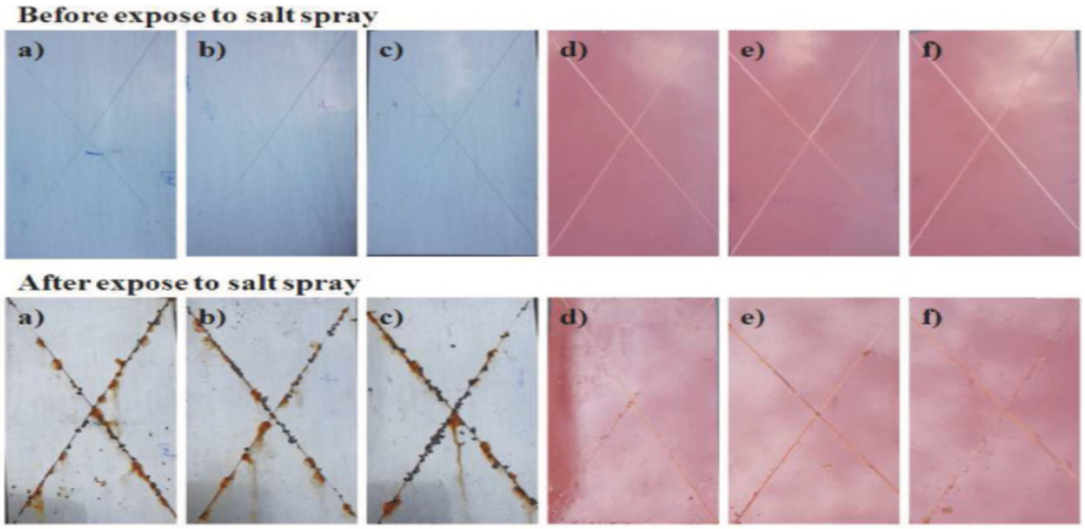

Figure 9: Coated Substrate before and after exposure to the salt spray chamber. (Copyright Elsevier 2022, [129]).

Open circuit potential (OCP)

The potential of a functional electrode when no current is supplied to the cell is known as the open-circuit potential. Through the use of electrochemistry, the free potential can be used to determine how a material will behave when submerged in a corrosive solution and how likely it is to interact with the surrounding environment. Since the OPC value decreases on the metal substrate as electrons pass through the coating, tracking the OCP is a helpful technique for keeping an eye on the deterioration of barrier coatings. It is widely recognized that an increase in positive potentials during time-potential measurements indicates the initiation of a protective film formation. Conversely, a decrease in potentials may signify the removal of oxide layers from the surface, marking the onset of corrosion measurements are usually used prior to EIS measurements to confirm the stability of the system. The technique's primary benefits stem from its straightforward setup, which offers the user an indirect assessment of

coatings that can be linked to electrochemical impedance spectroscopy findings. Benea et al. study the OCP measurements of different polyurethane films in seawater. For fourteen weeks, the open circuit potential was monitored. Measurements were taken every week at the same time on Monday in order to establish a stationary value. Figure 10 presents a summary figure that encompasses all of the OCP data obtained during the 14th week. The assessment of open circuit potential demonstrated that steel coated with polyurethane for corrosion protection exhibited a shift in free potential towards higher positive values compared to unprotected sandblasted steel. This shift suggests a more corrosion-resistant behaviour [122], while Rajitha et al. also studied the anti-corrosive efficiency of PU coatings decorated with reduced GO and ZnO [130]. Additionally, Nardeli et al. address the polyurethane-modified tannins' barrier qualities and capacity to prevent corrosion through open circuit potential [61] and Xue et al. [131].

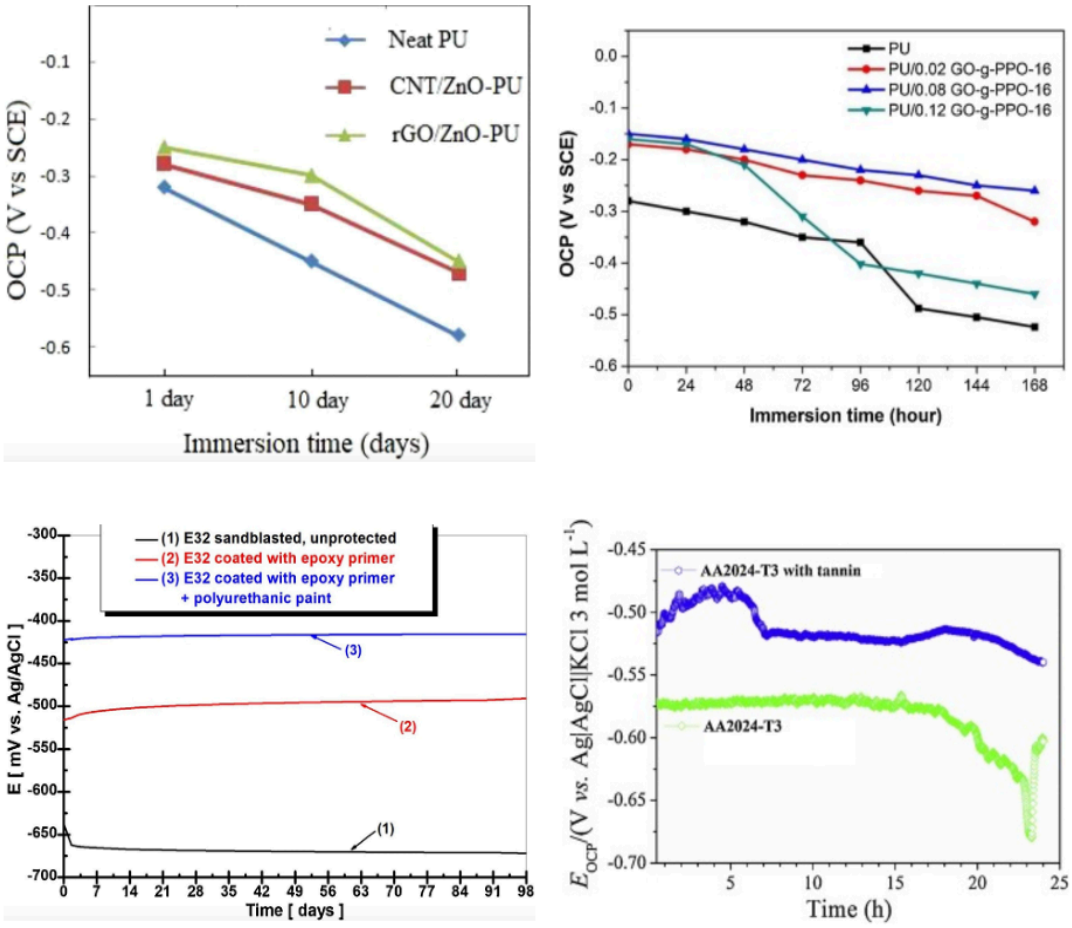

Figure 10: (a) represents the circuit potential for the following three types of E32 naval steel: (1) unprotected sandblasted steel; (2) naval steel protected with polymeric epoxy primer; and (3) naval steel coated with polyurethane acrylic paint as the final layer and epoxy primer as an intermediate layer. The steel was submerged in seawater for 98 days. (b) OCP values of samples coated with pure PU, CNT/ZnO, and rGO/ZnO after they were immersed in a 3.5 weight percent NaCl solution for one, ten, and twenty days. (c) EOCP vs. time for the AA2024-T3 alloy submerged in 0.6 mol L−1 NaCl for 24 hours, both with and without tannin addition. (d) OCP value variation for GO-PPO samples submerged in 3.5 weight per cent NaCl (aq.). Reproduced with permission Elsevier,2020 [130–132].

Electrochemical Impedance Spectroscopy (EIS)

Due to its ability to measure coating barrier properties, water absorption, defect presence, interface reactivity, and coating adherence, EIS is one of the most suitable tests for evaluating coating efficiency. In addition, it is capable of evaluating characteristics such as the high-frequency phase angle, breakpoint frequency, low-frequency impedance, coating damage index, and coating delamination index. All things considered, electrochemical sensing (EIS) is a highly useful technique for studying the electrochemical processes that occur during corrosion, as well as for monitoring and tracking the pace at which polyurethane coatings are exposed to electrolytes degrade or swell. Some of EIS's main advantages in the research of polymeric materials include its non-destructive nature, its power to assess film deterioration or regeneration, and, essentially, its ability to generate numerical values for the electrochemical reactions that are taking place inside the system. Nevertheless, the modelling and interpretation of diffusing or corrosion environments can be difficult because the results are averages over the surface [14,133][134].

Xavier studied the electrochemical impedance of polyurethane and fillers. In a 3.5% NaCl solution, the corrosion resistance of polyurethane (PU) and PU combined with SiO_2-Al_2O_3 nanoparticle coatings was evaluated using Electrochemical Impedance Spectroscopy (EIS) as shown by Figure 11. In contrast to pure PU coating, the PU/SiO_2-Al_2O_3 composite demonstrated better corrosion protection, a wider Nyquist loop, and a higher charge transfer resistance (Rct). This suggests that SiO_2-Al_2O_3 nanoparticles decreased porosity and prevented the onset of corrosion. PU/SiO_2-Al_2O_3's improved modulus resistance and wider phase angle provided additional evidence of its efficacy. According to the study's findings, PU/SiO_2-Al_2O_3 coating offers superior protection

against strong corrosive ions compared to PU alone [135].

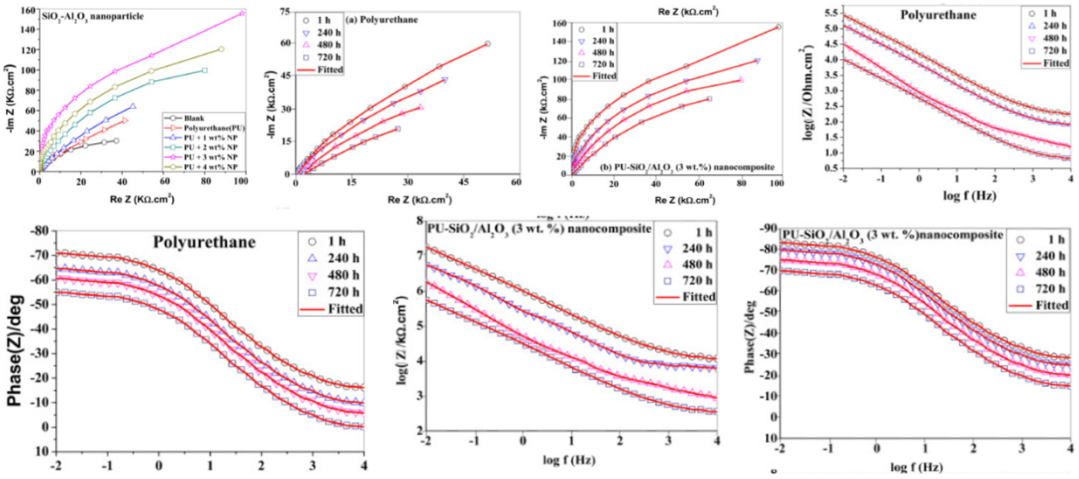

Figure 11: Nyquist plot and Bode plots obtained for polyurethane and PU-SiO_2/Al_2O_3 nanocomposite coated mild steel immersed in NaCl solution for 1, 10, 20, and 30 days. Reproduced with permission from Elsevier 2021 [135].

Localized electrochemical impedance spectroscopy (LEIS)

The EIS and LEIS techniques are both predicated on the same idea. Between a sample and a counter electrode, the ratio between the applied AC voltage and density is determined. LEIS calculates the local impedance by measuring the local resultant current. LEIS is a regionally determined technique that is primarily used for polymeric coatings to track corrosion inhibition and initiate and propagate delamination. Another effective method for examining substrate reactions beneath the coating is LEIS. Nonetheless, two vital factors that may impact the resolution of the data are the probe's size and the separation between it and the substrate. For example, it has been noted that smaller probes offer higher spatial resolutions.

Nardeli et al. conducted LEIS mapping on an aluminum alloy coated with oil-based polyurethane, examining both non-destructive and destructive areas in an aerated 0.005

mol L−1 NaCl solution over various immersion times. The admittance outside the scratched area remained low, indicating the coating's high impedance and effective protection. The maximum value was observed on the scratched area, decreasing over time, suggesting substrate protection, potentially attributed to coating recovery. This finding aligns with values of localized SVET, confirming the self-healing nature of the coating and highlighting its role in reducing substrate corrosion activity under the specified conditions [136].

By creating a fake flaw on the coated surface and exposing the alloy, Silva et al. studied the self-healing effect. During a 48-hour period in a NaCl solution, routine measurements of LEIS were conducted. The analysis was done on admittance maps in the defect region for the following coatings: 7.5 wt% Zn coating (Figure 12c), 2.0 wt% Zn coating (Figure 12b), and blank coating (Figure 12a). There was an increase in corrosion activity on the blank coating. Though not as much as the blank coating, the 2.0 weight per cent Zn coating did exhibit some corrosion activity over time. Weak early corrosion activity was shown by the 7.5 weight per cent Zn coating, but it gradually decreased, showing substantial corrosion inhibition. Lower Zn concentrations delayed corrosion but were unable to prevent it completely, according to LEIS data, whereas 7.5 weight per cent Zn demonstrated considerable inhibition.

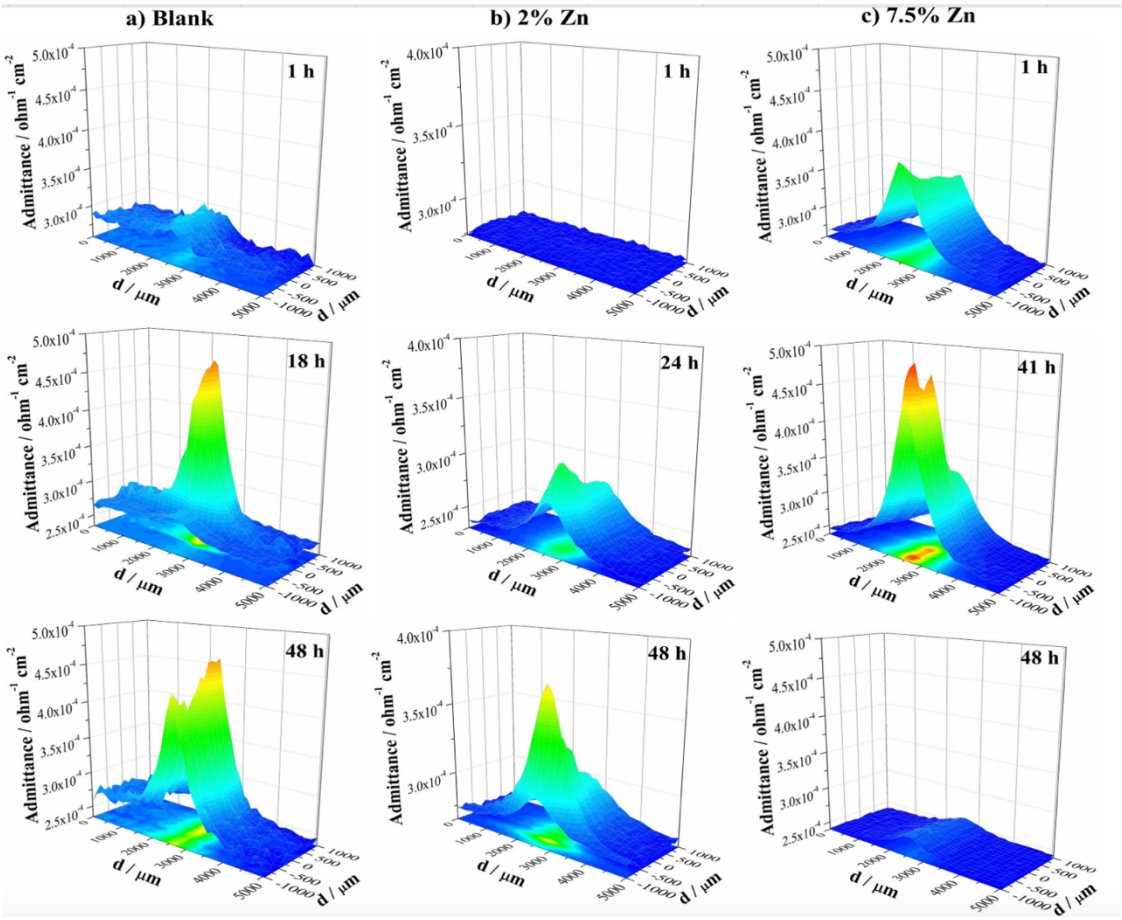

Figure 12: LEIS maps of the coated AA7475 alloy at different wt.% of Zn coating during immersion in NaCl solution at different immersion times. Reproduced with permission of Elsevier 2021 [137].

Scanning Vibrating Electrode Technique (SVET)

One of the most important methods for analyzing polyurethane coatings is the use of a micro-tip to investigate current distribution in solutions[138]. The main outcomes of the Scanning Vibrating Electrode Technique (SVET) are maps of the ionic current density that are measured in a corroding system's micrometer range, as exhibited in Figure 13. Reduction reactions at cathode sites and oxidation reactions at anode sites can be seen on these maps. The microelectrode is subjected to vibrations caused by a piezo-oscillator system, which bends the coating surface (usually with false defects)

during the measurements. After the solution is immersed in a conducting electrolyte, DC potential gradients cause the creation of current density distribution maps. While SVET has been commonly applied to the study of effective systems containing self-healing agents or corrosion inhibitors, its use is restricted to systems that are electrochemically active in which direct currents flow through the solution, making it impossible to evaluate corrosion reactions under intact coatings. In addition to its fragility and short lifespan, the probe may require labour-intensive platinization and calibration. However, the scanning ion-selective electrode technique (SIET) can be integrated with SVET mapping to acquire SVET maps and pH maps simultaneously, improving the method's ability to analyze local changes in both variables [14].

In recent years, there has been a notable increase in publications reporting the use of SVET due to the growing interest in active and smart anti-corrosion systems. For example, Nardeli et al. represented the SVET maps of unmodified and tannin-modified polyurethane coatings, explaining the healing process [61].

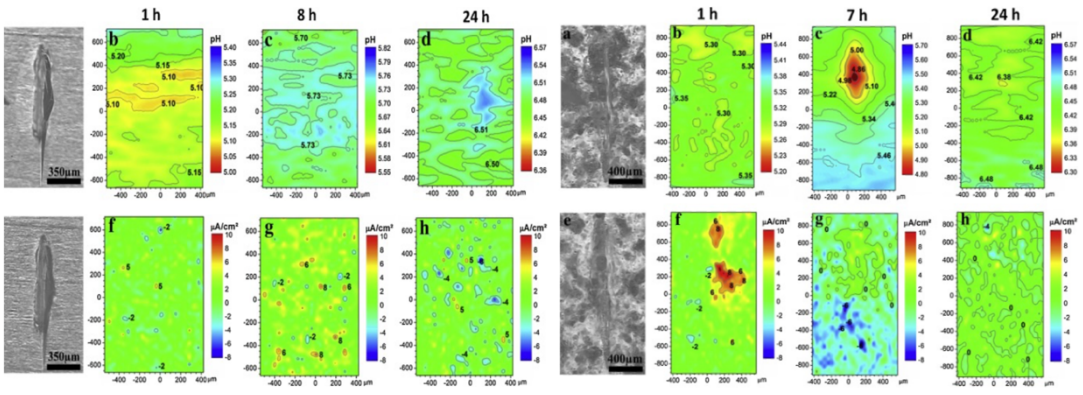

Figure 13: The optical micrographs (left a, e) show the specimen coated with the reference coating after 1 hour and 24 hours, respectively. The distributions of pH (b, c, d) and current density (f, g, h) were obtained after 1 hour, 8 hours, and 24 hours of immersion in NaCl, respectively. The modified coated sample with tannin was shown

in optical micrographs (a, e) corresponding to the scanned area after 1 and 24 hours, respectively. The pH (b, c, d) and current density (f, g, h) distributions were obtained after 1 hour, 7 hours, and 24 hours of immersion in NaCl, respectively. Reproduced with permission Elsevier 2022 [61].

Self-healing property of polyurethane coatings by SEM & Stress-Strain curves

Wand et al. in their study, using a maleimide end-capped polyurethane, the anti-corrosion coatings with multiple furan groups underwent a Diels-Alder (DA) reaction to form thermally reversible cross-linked materials. It was anticipated that these materials would exhibit heat-driven self-healing properties. Near-infrared (NIR) light was used to purposefully scratch the sample (PU-DA-d@CeNPs5) that exhibited the best anti-corrosion performance and healed it. Electrochemical impedance spectroscopy (EIS), stress-strain curves, polarized optical microscopy (POM), and scanning electron microscopy (SEM) were used to analyze the healing process. The formation and de-bonding of the DA bond were identified as the cause of the self-healing property. The DA reaction was aided by the PDA's exceptional photo-thermal conversion efficiency, which allowed for a quick temperature rise under NIR illumination. Within 20 seconds, crack healing was seen in POM and SEM images. The stress-strain curve showed that after two hours of heating or 30 seconds of NIR repair, the composite performance was restored to over 90%. The anti-corrosive performance was almost the same before and after healing, according to EIS tests. The outcomes demonstrated how well the coatings self-healed, retaining their initial anti-corrosion efficacy after healing. The accompanying Figure 14 provides an illustration of the procedure [53].

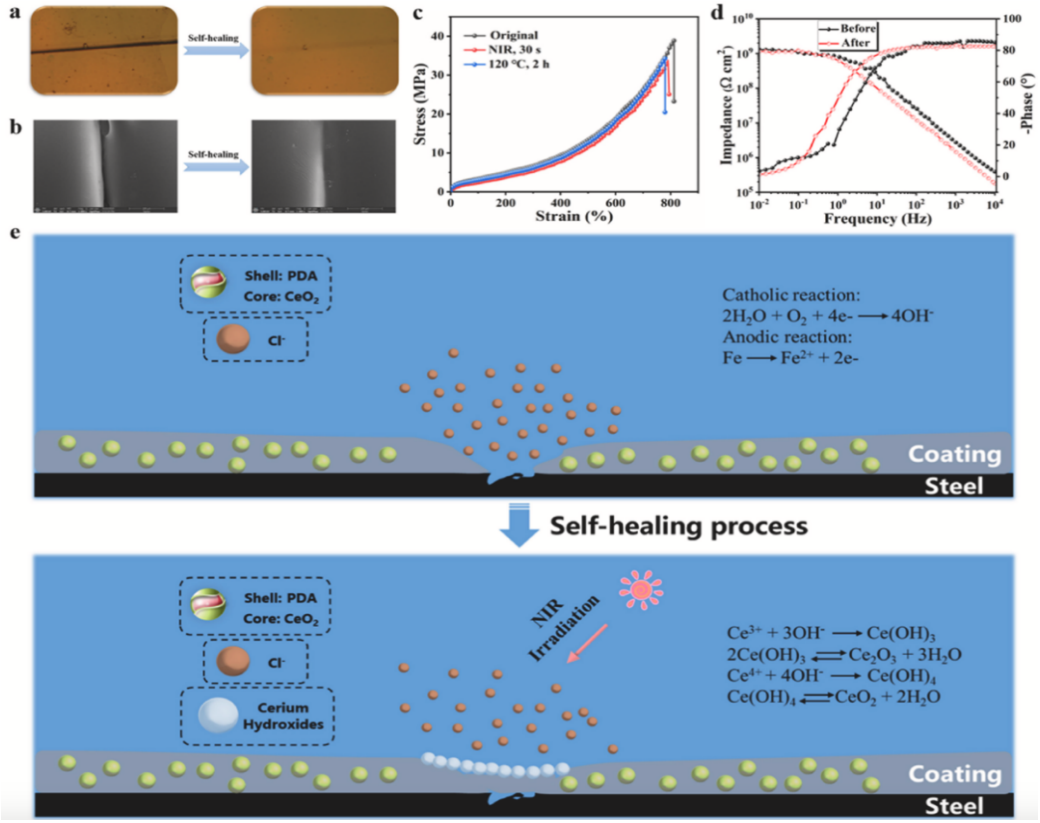

Figure 14: The coating's capacity for self-healing (a) pictures from optical microscope and (b) SEM pictures showing the crack both before and after NIR irradiation (0.5 W/cm2, 30 s irritation time). (c) The PU was modified with ceria hydroxide composite's strain-stress curves under various healing circumstances. (d) The PU-DA-d@CeNPs5 coatings bode plots before and after healing. (e) An example of the anti-corrosion and self-healing processes. Copy with consent 2021 Elsevier [44].

Self-healing and atomic force microscopy (AFM)

The excellent perseverance, capability to preserve the actual sample condition and low requirement for sample preparation of AFM have made it a popular tool in nanotechnology for coating substrate inspection [139]. To enable up-and-down oscillation of the cantilever probe, the apparatus modifies the specimen to keep a fixed-

point value. Through the use of light and dim areas to denote high and low regions, these oscillations yield useful height information. This makes the production of deflection-displacement loaded curves and surface topography possible as can be observed from Figure 15. Based on the material's inherent ability to heal itself, these curves act as markers of self-healing characteristics. The adaptability and power of AFM make it an invaluable instrument for examining and evaluating coatings' self-healing properties. Researchers like Nardeli [140], Liu [141] and Sheng [142] confirm the homogeneity and self-healing mechanism of polyurethane coatings by AFM analysis.

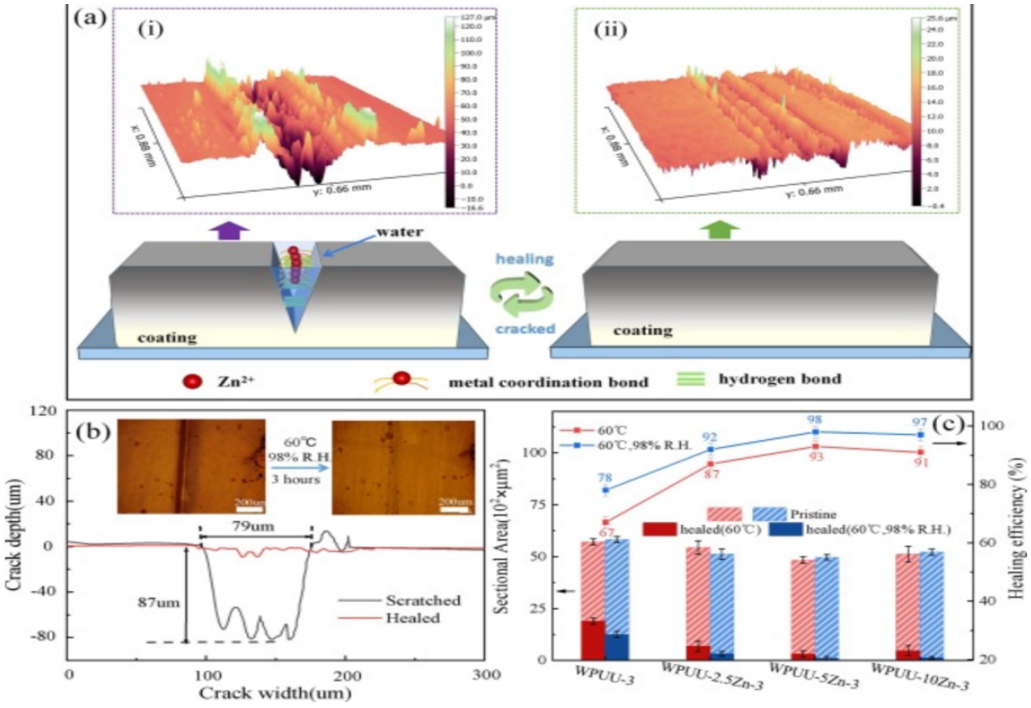

Figure 15: (a) Shows the evolution of the three-dimensional topography for WPU-Zn coatings before and after repair (i) and (ii), respectively; (b) Shows the equivalent depth profiles of the WPU-Zn coatings that have been scratched before and after healing in a hot, humid environment (60 °C, 98% relative humidity). The healing efficacy of various WPU-Zn coatings (c) Repair Condition: 98% RH for 12 hours at 60 °C or 60

°C. Reproduced with permission of Elsevier 2021 [142].

Physical and Mechanical Strength of PU coatings

The inclusion of nanoparticles may result in a sizable interfacial surface, which alters the modified PU coating's protective and mechanical qualities considerably. Nguyen et al. investigated tensile stress, adhesion, and impact resistance in PU films by evaluating their mechanical and physical strength as shown in Figure 16. Adhesive strength increased with increasing CNT content in TiO_2 but declined at 5%wt CNTs. For each individual piece of PU film, the tensile stress was around 28 MPa. At about 41MPa, Sample 4 displayed the maximum tensile stress, which was double that of the individual PU film. The overall improvement of the mechanical characteristics of the films was facilitated by the combination of PU paint and CNTs/TiO_2 composites [143].

Haghdadeh et al. performed mechanical analyses of graphene oxide and PU. Graphene Oxide has a Young's modulus of around 1.0 TPa and a fractural modulus of 130 GPa. However, because there is inadequate interfacial adhesion between the polymer chains and the nanoparticles, the stress-strain curves in the given figures show that adding GO to the PU matrix does not appreciably influence the strain at break. On the other hand, microscopic investigations show that the incorporation of functionalized graphene oxide into PU leads to a significant 31% increase in elongation at break, which improves the modulus. Higher stress at break and double increase in energy point of break for the PU-fGO sample, which shows the effective functionalization of the silane group and improvement of mechanical characteristics [144].

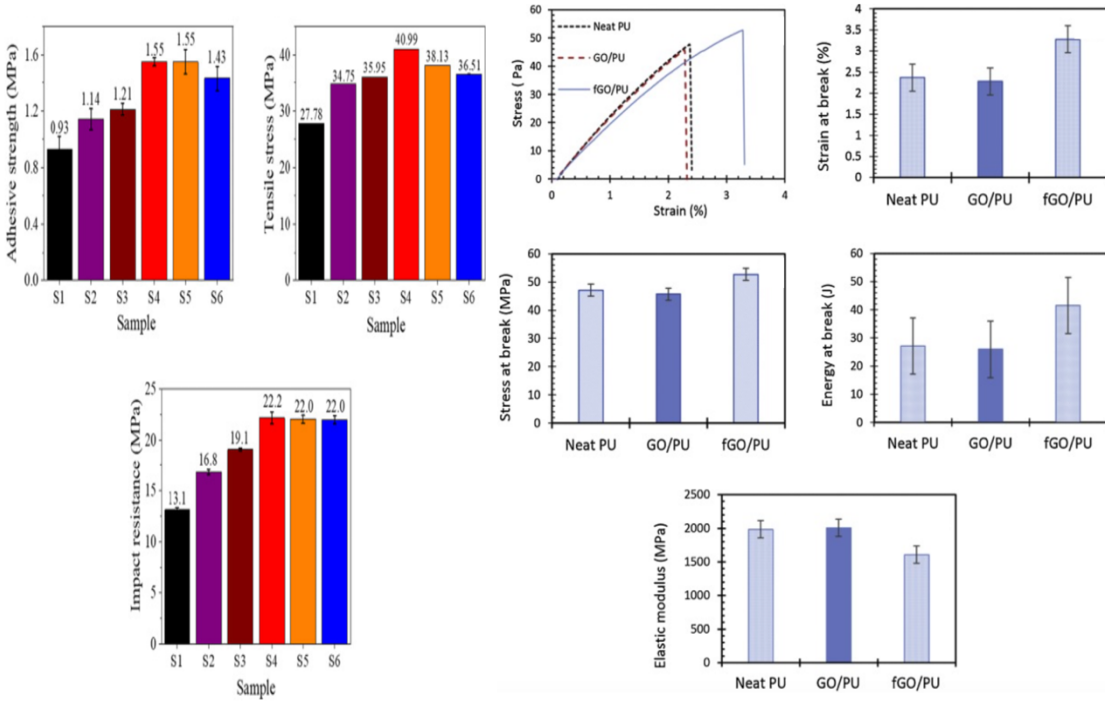

Figure 16: (Left) Mechanical properties of PU coatings modified with TiO_2 and CNTs. (Right) Stress-strain, tensile and elastic properties of PU and PU reinforced with Graphene Oxide. Reproduced with permission of Elsevier (2019 – 2022). [143,144].

Application of polyurethane coatings

Polyurethane coatings are extensively used in a variety of industries as a malleable and protective solution. Polyurethane coatings are widely used in the automotive industry to improve the exterior look and provide resistance to corrosion in vehicles. These coatings offer strong, weather-resistant finishes for surfaces like walls and floors in the construction sector. Furthermore, polyurethane coatings are essential in industrial environments because they provide defence against abrasion, chemical exposure, and adverse weather. They aid in the marine industry's anti-fouling qualities, which stop marine organisms from growing on surfaces. Furthermore, polyurethane coatings' adaptability and efficacy in preserving and enhancing a variety of materials are demonstrated by their applications in infrastructure, furniture, and aerospace.

Oil and Gas Industry

Smart nano-based materials are being used to develop superhydrophobic coatings, which will serve as protective layers for metallic parts against fouling agents, corrosion, and mechanical aggressors. Polyurethane coatings have been shown to be excellent choices for steel pipeline protection[145]. As illustrated in Figure 17 using a sol-gel technique, a strong superhydrophobic and extremely oleophobic PU–SiO_2 nanoparticle coating is created by Yousefi et al.[146]. With contact angles of 159° and 140°, the coating repels both oil and water. The PU-SiO_2 composite retains its amphiphobicity with contact angles of 150° and 130° for water and oil, respectively, even after a 7-day submersion in water. The exceptional characteristics of the coating are ascribed to its decreased surface energy, structured micro- and nanoscale roughness, stable adhesion of SiO_2 NP, and enhanced chemical interaction with the substrate. These attributes present an advanced approach for the development of high-performance superamphiphobic surfaces.

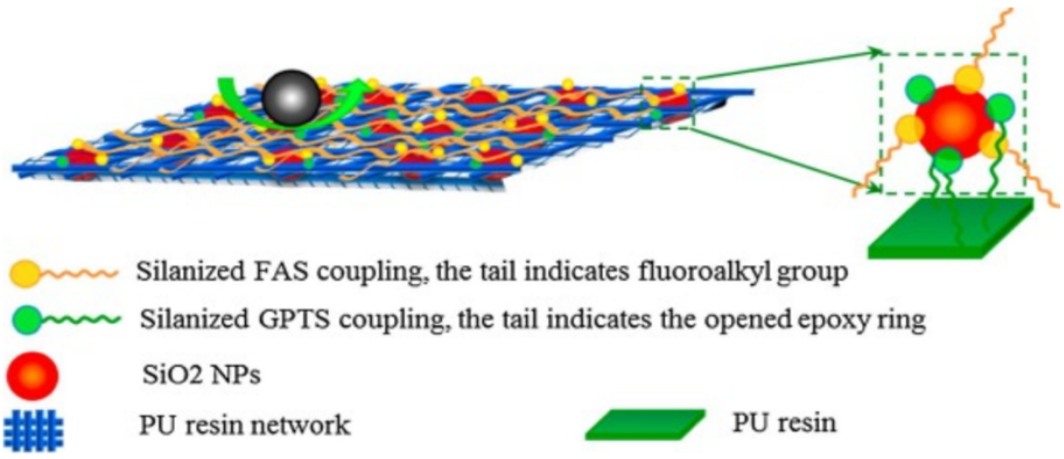

Figure 17: Fabrication of superhydrophobic PU-SiO_2 coating. Reproduced with permission Elsevier, 2018.

Automotive industry

As depicted in Figure 18 polyurethanes find application in automotive coatings, which play a crucial role in offering corrosion resistance to metal components used in vehicle body parts. Additionally, these coatings contribute to a glossy finish, enhancing the durability, weather resistance, and aesthetic appeal of automobiles. To bolster safety, flame retardants are incorporated into coatings by both the automobile and furniture industries. Bio-based polyurethanes are emerging as substitutes for conventional fossil fuel-derived foams, while bio-based polyamides exhibit promise in replacing petrochemical by-products. In the current automotive industry, structural components are predominantly crafted from steel, comprising 70–75% of a vehicle's total weight[147]. Rigid polyurethanes are used in heat and soundproofing in the automotive industry, while flexible polyurethanes are used in the production of car seats[148].

In response to the phase-out of certain flame retardants, there is a growing use of an alternative flame retardant referred to as V6. Researchers, including Fang et al., conducted a study to assess V6 levels in the environment, particularly in foam from baby products and dust samples from automobiles and houses in the Boston, MA, area. Concentrations of V6 in baby product foam ranged from 24,500,000 to 59,500,000 ng/g. V6 was also detected in car and house dust samples, with significantly higher concentrations in car dust, suggesting potentially greater usage of V6 in automobiles. Notably, an associated flame retardant, known for its carcinogenic properties, was found as an impurity in the V6 commercial mixture. This compound was constantly detected alongside V6 in samples of dust and foam, indicating that V6 usage might be a notable source of this carcinogenic substance in indoor environments [149].

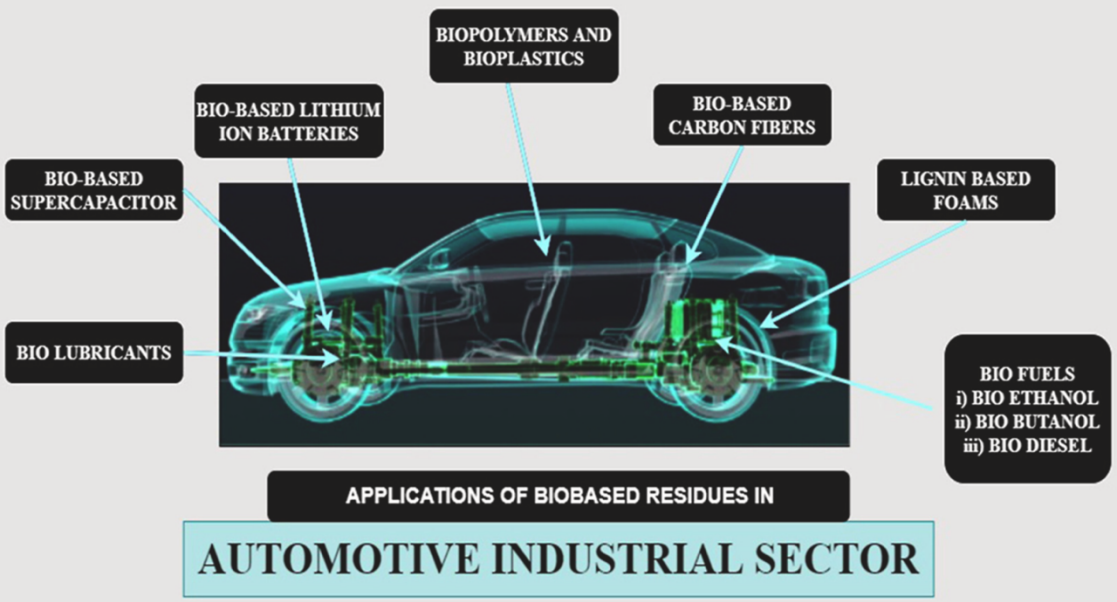

Figure 18: Application of polyurethane in the automotive industry. Reproduced with permission, Elsevier 2021 [147].

Medical, drugs and tissue engineering Applications

PU's have mechanical and physical characteristics similar to those of natural tissue, in contrast with various other artificial and natural biodegradable polymers. This makes numerous applications of PU in the biomedical sector possible, along with minimal adhesion to platelets and in vitro protein adsorption [150].

Regenerative medicine and tissue engineering depend on our ability to understand how cells respond to stem cell niches. Using organic-inorganic polyurethane (PU) nanocomposites, the investigation aimed to study cell signaling and the impact of magnetite nanoparticles on cell responses and proliferation. Many methods employed to characterize the PU-IONs showed that the inclusion of iron oxide nanoparticles altered their bulk shape as well as their mechanical, electrochemical, and natural characteristics. Cell survival, water absorption, and breakdown were all impacted by the increased hydrophilic nature and electrical conductivity of the

magnetite nanoparticles. Biocompatibility experiments such as cell adhesion, staining, and MTT assay demonstrated the promise of magnetite-PU nanotechnology for tissue engineering and cell treatment, particularly in nerve repair applications [151]. As illustrated in Figure 19, Chen and colleagues examined the layered framework of drug-loaded PLGA pellets in polyurethane coating as a potential coating for the stents for the airways that deliver anticancer medicines locally and continuously [152].

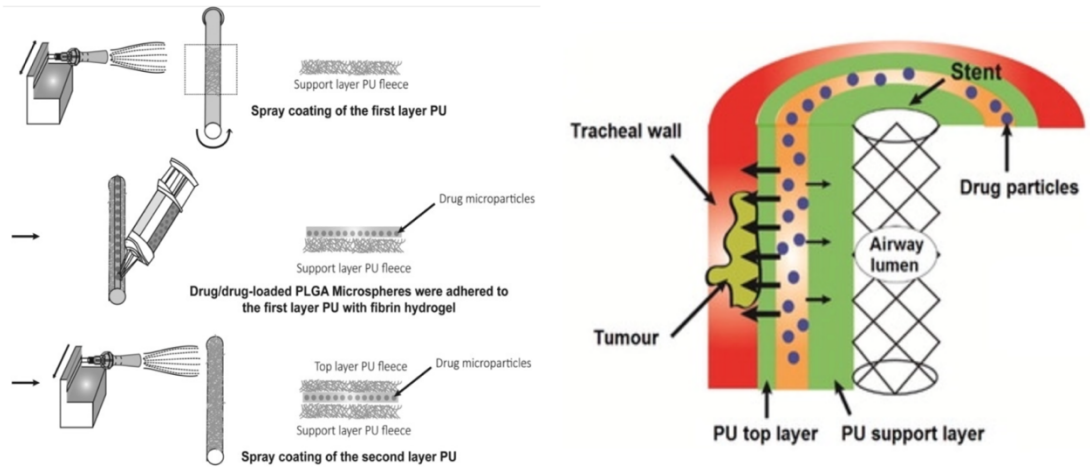

Figure 19: Schematic drawing of the three-step PU spray-coating procedure and broncho tracheal stent implanted in the upper airways after bronchoscope-assisted surgical resection [152].

Textile

Polyurethane stands out as a distinctive type of thermoset elastomer, combining the favorable characteristics of conventional polyurethane with unique features such as high impact strength, extended cycle life, and outstanding surface finish. Consequently, PU emerges as an excellent choice for surface coating applications, particularly as a coating for flame-resistant textiles. This is attributed to its ability to provide a combination of desirable properties, including effective flame retardancy, flexibility, and prolonged cycle life, even after repeated deformation[153][154].

ZnO-PU was used by Kumar et al. to create a nanocomposite through an in-situ polymerization technique. EDS and FTIR were used to confirm the structure of the nanocomposite. ZnO-PU and regular polyurethane were compared in terms of their physicochemical characteristics and structure. ZnO-PU outperformed conventional polyurethane in terms of heat and UV protection. According to rheological investigations, PU functions as a non-Newtonian fluid with exceptional viscoelastic qualities that make it appropriate for the preparation of composite films. ZnO-PU showed notable antibacterial activity in contrast to regular polyurethane, equivalent partition ratios and coloring intensity were revealed by the pigmentation characteristics of PU-PET/ZnO. The combined results point to the possibility of using PU-ZnO nanocomposites as functionally flexible substances in the textile sector [155].

Nguyen et al. conducted a study involving the preparation of a flexible polyurethane derived from renewable-sourced polyol. This PU was subsequently enhanced with halogen-free flame retardants, specifically ATH and TPP, to augment its flame-resistant characteristics. The best amount of additive loading was identified by evaluating the altered PU materials' thermal, mechanical, and fire-resistant characteristics. Next, a PU-coated textile was made, and its flammability and ability to produce smoke were evaluated against those of pure fabric, neat PU, and their corresponding modified PU. The findings demonstrated a positive synergistic effect between ATH and TPP, enhancing the fire-resistant properties of the advanced materials while maintaining reasonable flexibility for fabric-coating applications[154].

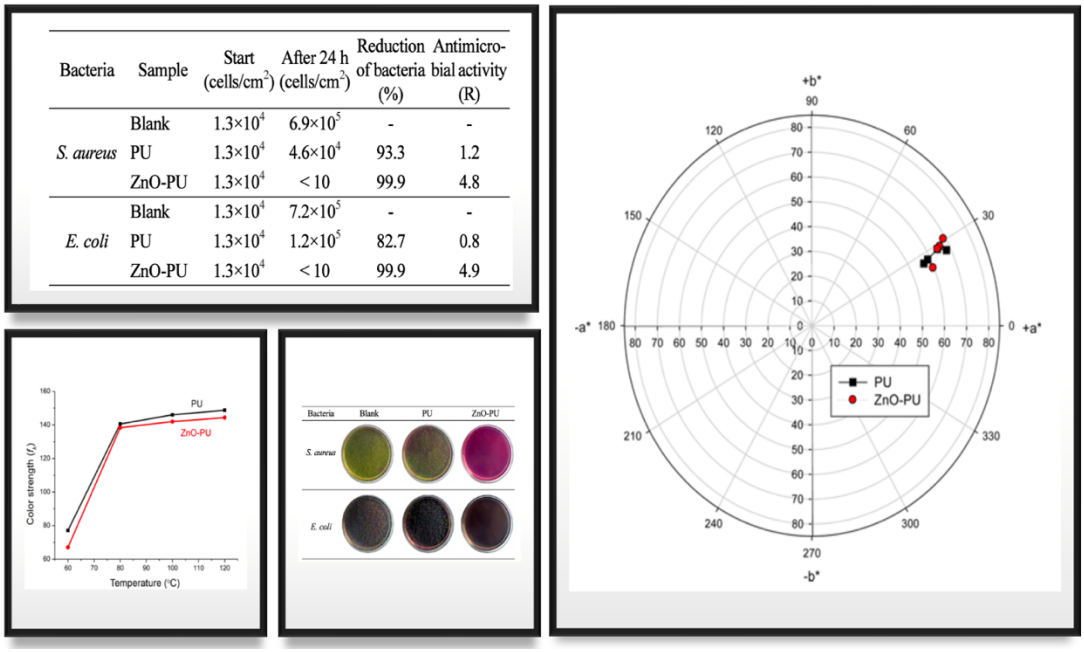

Figure 20: Polyurethane (PU) and (ZnO-PU) film samples were used to test for antibacterial activity, and the results were obtained after a 24-hour incubation period. Further pictures were taken of the microorganisms Escherichia coli and staphylococcus aureus after they had been cultured for 24 hours on the PU, ZnO-PU, and blank films. A 1.0% omf dyeing concentration was used to evaluate the color intensity (f) of dyed PU and ZnO-PU films at different dyeing rates (60, 80, 100, and 120 °C). We identified the dyed PU films' CIELAB color coordinates (a* and b*). Copyright permission Springer Nature, 2021 [155].

Marine

Surface chemistry is one of the most crucial design criteria for fouling release or antifouling coatings. Hydrophilic coatings eliminate any thermodynamic benefit from the adhesion of biomolecules because it is more actively beneficial for the surface to stay in contact with water than with an amphiphilic organism like a protein. Hydrophilic coatings have high surface energies similar to water and an intense attraction for polar molecules of water. Conversely, materials with low surface energies and hydrophobic

surfaces are made to reduce contact with biomolecules by removing the possibility of strong polar interactions. Because biomolecules and bio-organisms can only cling to these surfaces very weakly, a fouling discharge mechanism can facilitate their removal [156].

Chungprempree et al. devised an effective method to prevent fouling on marine structures using a hydrophobic polymer film. In field testing conducted in the Gulf of Thailand, the film—which was created by blending polydimethylsiloxane elastomer and polyurethane—displayed better antifouling qualities. With soft lithography micro-patterning, the PDMS: PU blend demonstrated a water contact point of 128.8° ± 1.6° and a lower barnacle bonding strength (0.07 MPa) than carbon steel (1.16 MPa). The findings imply that this mix is a viable option for real-world anti-fouling applications in the maritime sector, especially when combined with micro-patterning [157].

Waterborne polyurethane dispersions improved with polydimethylsiloxane and were studied by Kim et al. This change entailed adding PDMS to the polyurethane chains' pliable sections. Overall, the results indicate that the PS-WPU samples from this investigation have a lot of potential for use as coatings in maritime environments [158].

Xu et al. developed polyurethane using poly(ε-caprolactone)PCL as the main chain and poly(triisopropylsilyl acrylate) (PTIPSA) as side chains via radical polymerization and condensation. Their studies showed that polyurethane degrades in enzyme presence, with degradation slowing as PTIPSA content increases. A hydrophilic surface that lowers frictional drag is produced when the substance hydrolyzes in simulated saltwater, and the rate of hydrolysis increases with increasing PTIPSA concentration. Marine tests demonstrated effective antifouling due to the self-renewing surface from the biodegradable PCL main chain and hydrolysable PTIPSA side chains. Polyurethane, carrying an environmentally friendly antifoulant, exhibited significantly

improved antifouling performance even in stagnant marine atmospheres [159].

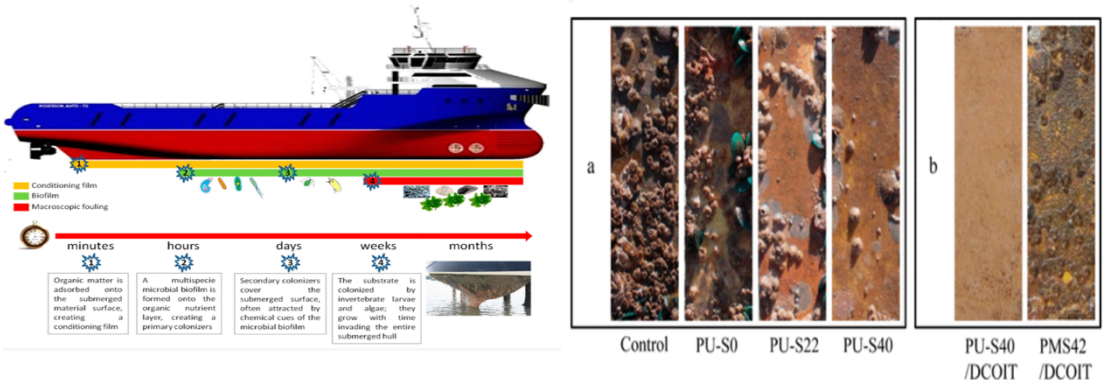

Figure 21: The process through which fouling forms on the surface of submerged structures. Sample photos of the panels that were put through testing are as follows: (a) Sample coated with PU; (b) Samples coated with PU-S40 and PMS-42 along with 10% DCOIT after three months of soaking in seawater. Reproduced with permission ACS, 2014.

Real-world case studies demonstrating the effectiveness of polyurethane coatings

Research has focused on the use of superhydrophobic coatings as an anti-icing solution. A lot of coatings with superhydrophobic properties have been produced for anti-icing because of the pioneering work, which is inspiring. Li et al. presents a significant advancement in bioinspired superhydrophobic coatings, tackling important issues like poor mechanical stability and environmentally hazardous preparation techniques. The new coatings are entirely waterborne, nonfluorinated, mechanically strong, and self-healing as illustrated in Figure 22. They are produced by spray-coating a waterborne polyurethane (PU) solution and a SiO_2 suspension modified with hexadecyl polysiloxane. The distinct hierarchical nanostructure and solid lubrication of the coatings are attributed to the PU-SiO_2 suspension, which is produced via HCl-catalyzed

reactions. Superior mechanical stability is exhibited against sandpaper abrasion and tape-peeling, and the migration of the healing agent (HD-POS) facilitates rapid and stable self-healing. The coatings' potential for a variety of applications is demonstrated by their effective static and dynamic anti-icing performance in outdoor environments. Superhydrophobic coatings have never been this promising for real-world applications, but this work has overcome some of their prior drawbacks [160].

A scalable and economical atmospheric methodology is used to synthesize superhydrophobic surfaces without the need for a substrate. Highly hydrophobic F-SiO_2 nanoparticles are anchored by a sprayable IPN colloidal solution that offers a hierarchical structure that is impervious to both mechanical and chemical forces. After 120 typical abrasion cycles, the resultant IPN-F-SiO2 coatings still show remarkable erosion resistance, retaining considerable water contact angles. The yielding elastic deformities of the IPN texture provide the coatings with exceptional mechanical characteristics. Tests of real-world damage can readily be withstood with negligible effects on transparency and super hydrophobicity. With potential uses in protective coatings and self-cleaning, this sprayable polyurethane–acrylic IPN colloid provides an affordable, scalable foundation for creating transparent, ultradurable superhydrophobic surfaces [161].

Holder et al. [162] developed a method to protect polyurethane foam, commonly used in furniture, from fire using eco-friendly materials. They coated the foam with nanocomposite films made from multi-walled carbon nanotubes (MWCNTs) using water-based solutions. The coating, applied in layers, significantly reduced the foam's flammability and smoke release. Even a small number of layers showed substantial improvement, and thicker coatings made the foam self-extinguish after a vertical burn test. This protection is attributed to a carbon-based layer formed by the coating, acting

as a fire barrier.

Figure 22: Anti-icing behavior of Polyurethane coating. Reproduced with permission ASC, 2018.

Challenges and Future Directions

The issues and prospects for polyurethane coatings include resolving health and safety and environmental concerns, optimizing performance attributes, integrating intelligent features, and adhering to changing legal requirements [163]. The goal of ongoing research and development in these fields is to increase the sustainability, functionality, and overall performance of polyurethane coatings to unprecedented levels. The utilization of polyurethane coatings for safeguarding diverse surfaces such as metals, glass, wood, plastics, and related materials has been increasing [164]. Consequently, steel is coated with polyurethane-based coatings to provide enhanced wear resistance, effective corrosion protection, and superior barrier properties. The nanocomposite coatings exhibit better protection for steel with prolonged immersion times, although there is a lack of comprehensive exploration into their microhardness. Evaluating the microhardness properties of coated systems is crucial to determine their suitability for

specific substrates, as variations in these parameters may reveal a significant correlation with corrosion protection features. Moreover, while polyurethane coatings are commonly used in various technical applications as topcoats, there is a notable absence of polyurethane nanocomposite coatings in these applications. The substitution of polyurethane with polyurethane nanocomposite coatings in automotive and aerospace industries could extend the lifespan of these coatings. Different micron-sized particles or additives can be incorporated into the base matrix to impart hydrophobic nature and corrosion protection, which might be used to build multi-functional coating systems; however, the practical applicability of these materials is limited due to their high cost. Furthermore, because they are so delicate, it seems difficult to synthesize very hydrophobic coatings with outstanding abrasion resistance because they are readily harmed by mechanical abrasion after a hydrophobic loss [165]. The primary challenge in this context is the degradation of polyurethane coating systems caused by weathering during natural outdoor exposure. Exposure to environmental factors like temperature, Ultraviolet rays, water content, and chemicals can lead to the deterioration of polyurethane, generating free radicals that affect polymeric chains. As a result, the outdoor service life of polymers is constrained by weathering. Various physical methods are utilized to evaluate the weathering properties of polyurethane and nanocomposite coatings. Progress in this area can be made by improving and designing polyurethane nanocomposite coatings with increased resistance to weathering. Opting for different coating techniques such as the solution method, solvent-free method, spraying, and advanced methods like spin coating and inkjet printing can greatly improve the overall coating features. Conventional polyurethane (PU) coatings often lack sufficient heat resistance and experience significant pyrolysis at temperatures exceeding 200°C. These drawbacks restrict the use of traditional UV-cured

polyurethane coatings. Consequently, attempts should be undertaken to address the standard UV-cured PUs' low hardness and inadequate heat resistance. Emphasis should be placed on developing polyurethane nanocomposite coatings with UV radiation resistance and high-temperature stability [166]. The integration of nanoparticles in polyurethane strengthens the nanocomposite structure against weathering. Technologies like polyurethane-carbon nanotubes and polyurethane-graphene coatings show promise in the industrial coating market due to their high performance in challenging conditions. WPU coatings' non-toxicity, environmental friendliness, adaptability, UV and chemical resistance, and superior mechanical qualities have all contributed to their increased popularity. Yet, diverse types of nanoparticles must be employed to enhance the resistance to solvents, tensile strength and thermal stability of polyurethane coatings. Areas of research yet to be explored in polyurethane nanocomposite coatings encompass potential applications in the sports sectors, aerospace, energy devices, automotive and electronics.

Chapter 3: Methodology

Silane Functionalization of Titania-Graphene Oxide Nanocomposite for Superior Anticorrosion Polyurethane Coatings on Steel

Materials

Graphene oxide (GO) (quality level 100) and Titanium (IV) Dioxide nanopowder, <25 nm particle size (TiO_2) (Purity ≥ 99%), also known as Titania, were purchased from Sigma Aldrich, Darmstadt, Germany, absolute ethanol C2H5OH) ≥99.8 %, Sodium Chloride (NaCl) ≥99.0 %, N-(2-Aminoethyl)-3-aminopropyltrimethoxysilane (DAMO)(Purity ≥ 97.0%) and Dimethylformamide (DMF)(Purity 99.8%) were acquired from Sigma Aldrich and used as received. Hemple company provided Polyurethane (HS 55610) and a curing agent (hemple curing agent 95,370). Steel substrates were purchased from a local company in Qatar. The size of the samples was 3x3cm^2. Silicon carbide abrasive papers of 80 and 120 were purchased from Hebei Yineng Pipeline Group Co., Ltd., China, and used to polish the steel samples. Distilled water used for the experimental procedures was obtained from the department laboratory.

Synthesis of GO-TiO_2 modified with DAMO.

Figure 23 illustrates the synthesis procedure for fGO hybrids. For this synthesis, 0.4 grams of TiO_2 and 8 grams of DAMO were first added to 200 g of anhydrous ethanol. After this, the mixture was heated and stirred using a magnetic stirrer for 4 to 5 hours at 78 ◦C. Then, 16 g of Deionized Water was added slowly to the solution, followed by centrifugation. The solution was washed with anhydrous ethanol and DI water and dried in an oven at 60 ◦C for one day to obtain modified TiO_2. After this, 100 mg of modified TiO_2 and 400 mg of GO were dispersed in 250 ml DMF to form a homogeneous suspension, which was added to the suspension via ultrasonication for 60 sec. The

mixture was again stirred for more than 5 hours at a temperature of 105 ◦C, and the product obtained was centrifuged, washed, and dried for 24 h at 60 ◦C in an oven.

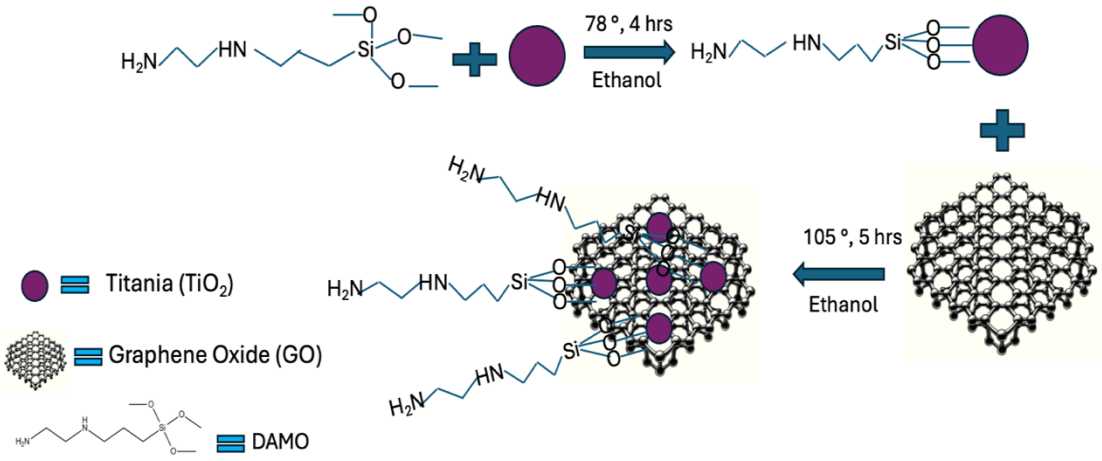

Figure 23: Synthesis procedure of GO-TiO_2.

Preparation of steel substrate and coating application

Proper surface preparation of steel substrates is critical to ensure optimal adhesion and performance of the applied coatings. The steel substrates were systematically cleaned and polished to remove surface contaminants such as dust, oxides, and other impurities. Initially, the substrates were polished and ground using Silicon Carbide (SiC) abrasive papers with grit sizes of 80 and 120. This process was performed on a precision polishing and grinding machine (Metkon ForcoPol IV), ensuring uniform surface treatment and removing any visible imperfections or surface irregularities. The coarse grit (80) was employed to eliminate the oxide layer and rough imperfections.In contrast, the finer grit (120) further smoothed the surface to achieve a more refined finish suitable for coating application. To ensure the removal of residual dust, debris, and any remaining oxide layer after mechanical polishing, the substrates were thoroughly rinsed with deionized water. Following this step, the substrates were cleaned using ethanol to

eliminate any organic contaminants or grease hindering the coating's adhesion. Ethanol was chosen due to its quick-drying properties and effectiveness in dissolving oils and fine particulates. Once the cleaning and polishing steps were completed, the steel substrates were allowed to dry thoroughly under ambient conditions. This ensures a clean, contaminant-free surface, essential for successfully applying the coating in the subsequent steps. The final step before further characterization involves applying a coating to the polished steel substrate. The composite coatings were prepared by adding 1 wt.% of fGO synthesized particles into 9 g of PU formulation. The ratio of PU and the curing agent was (8:1). The formulated PU coatings were deposited on polished steel substrates by doctor's blade technique. After deposition on steel substrates, the coatings were left to cure at room temperature for one week. The resultant coating thickness was 100 μm. For reference and comparison purposes, we needed Blank PU coatings, whose data is available in previous work of our research group [167,168].

Characterization

The morphological analysis of Pristine GO, TiO_2, and fGO involved the use of a Transmission Electron Microscope (TALOS F200X, USA) and a Field Emission Scanning Electron Microscope (Nano-450, FEI, NY, USA) equipped with an EDS system. Chemical interaction between GO and TiO_2 was examined using an FTIR spectrometer (PerkinElmer, Waltham, USA) in the 4000–500 cm^{-1} range. Thermal stability and mass loss of pristine GO and fGO were evaluated through Thermogravimetric Analysis (TGA) and Differential Thermal Analysis (DTA) (Pyris 4000 PerkinElmer-USA) performed in the temperature range of 30–700 °C and at a heating rate of 10 °C/min under a N_2 environment. The specific surface area and pore volume of pristine GO and fGO were determined using Brunauer–Emmett–Teller (BET) analysis (Micromeritics ASAP 2420, USA). Structural and phase purity of

pristine GO and fGO were examined through X-ray Diffraction (PANalytical, Empyrean, United Kingdom) with a scanning rate of 2°/min and scanning angle ranging between $10° \leq 20° \leq 90°$.

The anti-corrosion performance of the coatings was assessed via electrochemical impedance spectroscopic measurements (EIS) conducted on samples immersed in a 3.5 wt.% NaCl solution for four weeks at room temperature. EIS measurements were performed using a Gamry 3000 potentiate/galvanostatic/ZRA (USA) with a scan frequency rate of 10 points per decade. In Gamry, each EIS test utilized three types of electrodes: a coated steel substrate as the working electrode, a Carbon counter electrode, and an Ag/AgCl reference electrode. Additionally, a Salt Spray test was conducted at room temperature to evaluate the coatings' corrosion inhibition and barrier activity.

Enhanced Steel Surface Protection Using TiO_2/MS30 Modified Polyurethane Coatings: Synthesis and Performance Evaluation

Chemicals used

Titania nano powder (TiO_2) with 99.7% trace metal basis used as carrier, piperazine Bis-Urea (MS30-synthesized in-house) used as corrosion inhibitor, Isopropanol ≥99.5% , Sodium Chloride (NaCl) ≥99.0%, Absolute Ethanol (C_2H_5OH) ≥99.0%, was acquired from Sigma Aldrich. Distilled water was attained from the center laboratory. Steel substrate (3.5 cm x 3.5 cm x 0.1 cm) was purchased from a local seller. The steel substrate exhibits the following chemical composition: 0.21% carbon, 0.30% phosphorus, 0.04% silicon, 0.20% copper, and 99.18% iron. The silicon abrasive paper (120-2c) used for polishing steel substrates is obtained from Able Group W.L.L. Doha, Qatar. Polyurethane (Hempathane HS 55610) and its curing agent (Hemple's curing agent 95,370) were acquired from Hemple company.

Loading of MS30 into TiO_2

The compound 1,1'-(1,4-phenylene)bis(3-(pyridin-2-ylmethyl)urea) named MS30, which is used as an inhibitor, was synthesized in-house using proprietary methods. Detailed information on the synthesis process, including reaction conditions, reagents, and characterization data, will be provided in a forthcoming publication following the acceptance of the corresponding patent application (US Provisional Patent Application No. 63/462,316). The structure of synthesized MS30 is given in Figure 24.

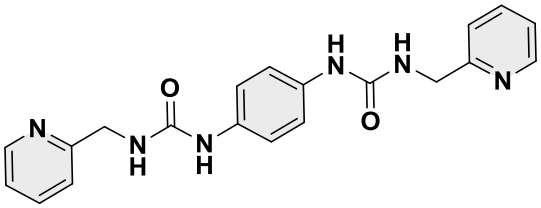

Figure 24: Structure of synthesized MS30 inhibitor.

The M30 was loaded into pristine TiO_2 using the method already reported in our previous work [169,170].The schematic of loading is represented in Figure 25. For this purpose, 2 g MS30 was dissolved into 25 mL of isopropanol (solvent) to make a saturated solution. After this, 1 g of pristine TiO_2 was added into the MS30 solution and kept overnight, stirring on a magnetic stirrer at room temperature (25 °C). After being stirred for 24 h, the solution was placed in a vacuum chamber for 3 h with vacuum cycling after each hour. This treatment in a vacuum chamber guarantees the loading of MS30 into TiO_2. The solution was centrifuged for 10 mins at 5000 rpm after vacuum cycling. The particles were washed with ethanol and distilled water 2-3 times to ensure the resultant product is free of any impurity. The resultant product was then collected and dried in an oven at 80 °C for 8 hours. The product TiO_2/MS30 was then pulverized

in mortar and pastel to make small particles and will be utilized for further characterization.

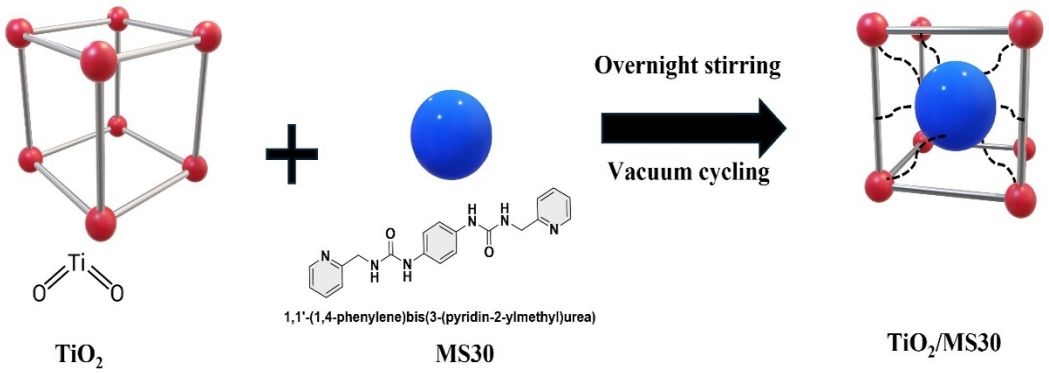

Figure 25: Schematics of loading of MS30 into TiO_2.

Preparation of steel substrate and development of PU based coatings

The steel substrate utilized for coating was grinded and polished prior to the coating application to make the surface rough and free from any residues. For this purpose, the steel substrate was polished by utilizing a silicon carbide abrasive appearance (120-2c). Following this, the surface was cleaned with ethanol to prevent formation of any oxide layer. PU based coatings were synthesized by adding 1 wt. % (0.09 g) of loaded TiO_2 into PU (8 g) and curing agent (1 g). First, 0.9 g of product was added into 8 g of PU and kept on ultrasonication to remove any air bubbles. Then 1 g of curing agent was added and gently mixed with glass rod to avoid any air entrapment. The synthesized PU-based coating mixture was then deposited on a polished steel substrate via a doctor blade and left for curing at room temperature (25°C) for 5 days until fully cured. The final thickness of developed coatings was 100 µm. These coatings were labeled as PU/TiO_2/MS30. For reference purposes, blank PU-based coatings were also needed, but the data of blank PU coatings for the EIS study is available in our previous work

[171]. However, for salt spray analysis blank PU coatings were synthesized by mixing 8 g of PU with 1 g of curing agent and left for curing at room temperature (25°C) for 5 days. The blank PU coatings were labeled as blank PU coatings with a final thickness of 90 µm. The coatings were also scratched by using a hand scalpel with a scratch length of 1cm.

Characterization of synthesized particles and developed PU-based coatings

The synthesized TiO_2/MS particles were characterized by employing various characterization techniques. Transmission electron microscopy (TEM, FEI, TALOS F200X, USA) was utilized to analyze the morphology of pristine TiO_2 and TiO_2/MS particles. Brunauer–Emmett–Teller (BET Micromertitcs ASAP 2420, USA) was employed to study the surface area and pore volume of pristine TiO_2 and TiO_2/MS particles. To study the composition and chemical composition of pristine TiO_2 and TiO_2/MS particles, Fourier transform infrared (FTIR PerkinElmer, Waltham, MA, USA) was employed in the range of 500-4000 cm^{-1}. Thermogravimetric analysis (TGA analyzer pyris 4000 (PerkinElmer-USA) with a temperature range of 50-700 ° (10°/min) was utilized to study the thermal stability and weight loss of the pristine TiO_2 and TiO_2/MS particles. Differential scanning calorimetry (DSC 8500 PerkinElmer-USA) was used to study the transition temperatures and cross linking of the developed PU coatings. The electrochemical measurements were done employing Gamry 3000 (30 K BOOSTER Potentiostat/Galvanstate/ZRA, USA), which utilized three-electrode system, the coated steel sample as the working electrode, whereas the carbon plate and silver/silver chloride as the counter and reference electrodes. The frequency range was 0.01 Hz-100 kHz, and the RMS signal was 10.0 mV. Gamry E-Chem 3000 software was employed to analyze the measured EIS data. All EIS measurements were accomplished at 25°C. The coatings also experienced 5 h of exposure to 3.5 wt. % NaCl

solution in potentiodynamic polarization (PP) analysis. After PP analysis, the steel surface was studied via Raman (Raman Thermo Scientific DXR3) analysis. The scratched coatings were also subjected to the salt spray analysis for 4 weeks in 3.5 wt. % NaCl solution.

Chapter 4: Results & Discussion

Silane Functionalization of Titania-Graphene Oxide Nanocomposite for Superior Anticorrosion Polyurethane Coatings on Steel

SEM, TEM and EDX

The SEM images in Figure 26, provide detailed insights into the morphology and structure of the materials involved in our study. For Titania (TiO_2), the SEM Figure 26(a) reveals that it consists of small, spherical particles [172]. This morphology indicates well-defined and uniform titania nanoparticles, which is a desirable feature for enhancing the dispersion and interaction within composite materials [173]. In contrast, the SEM Figure 26(d) of graphene oxide (GO) displays a characteristic flake-like and layered structure [174,175]. This morphology is typical of graphene oxide, confirming its sheet-like nature and extensive surface area, which are crucial for its role as a support matrix in nanocomposites [176]. Upon modification with titania, the SEM Figure 26(g) shows that titania nanoparticles are effectively integrated into the graphene oxide layers. The titania appears to be intercalated within the GO sheets, suggesting a successful composite formation. This intimate interaction between titania and graphene oxide layers is essential for the synergistic properties anticipated in the nanocomposite, particularly for enhancing anticorrosion performance [177].

The EDS analysis complements the SEM observations by providing elemental composition data for the materials. For pristine Titania Figure 26(b), the EDS spectrum shows prominent peaks corresponding to titanium (Ti) and oxygen (O) [178]. The absence of other significant peaks confirms the purity of the Titania used. Similarly, the EDS spectrum of pristine Graphene Oxide Figure 26(e) displays distinct peaks for carbon (C) and oxygen (O). These peaks are characteristic of GO, indicating that the material primarily comprises these elements and is free from significant contamination.

For the TiO_2-GO nanocomposite, the EDS spectrum, Figure 26(h) reveals the presence of carbon (C), oxygen (O), and Titanium (Ti). The simultaneous detection of these elements confirms the successful functionalization of Graphene Oxide with Titania. The integration of TiO_2 within the GO layers, as evidenced by the SEM images, is further corroborated by Titanium peaks alongside carbon and oxygen in the EDS spectrum. EDX mapping of the TiO_2 and $fTiO_2$ before and after modification and functionalized Graphene Oxide (fGO) clearly confirms the composition distribution. The images show a uniform distribution of oxygen (O), carbon (C), silicon (Si), nitrogen (N), and titanium (Ti) across the sample, which confirms the successful functionalization and incorporation of these elements into the fGO structure Figure 41, Figure 42, and Figure 43.

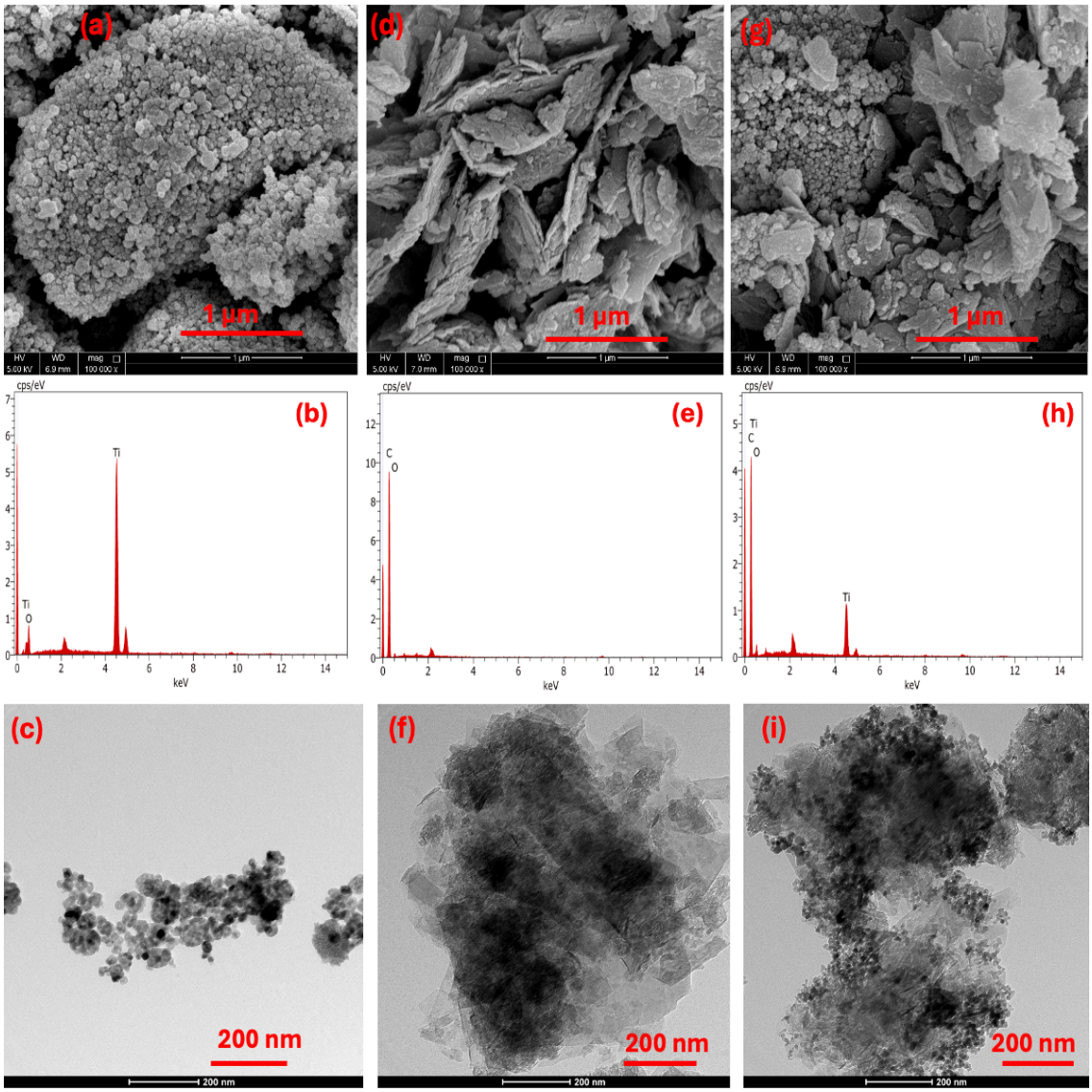

Figure 26: SEM, EDS, and TEM analysis of TiO_2 (a,b,c), GO (d,e,f), and fGO (g,h,i).

The TEM images provided further insights into the structural characteristics of TiO_2, GO, and the fGO nanocomposite. The TEM image of Titania, Figure 26(c) shows small spherical structures, confirming the nanoparticulate nature of TiO_2 [179]. On the other hand, the TEM image of GO, Figure 26(f) reveals a flaky structure. This morphology is typically disadvantageous for dispersing GO into polymers as a nanofiller due to its tendency to agglomerate [180]. Upon functionalization, the TEM image, Figure 26(i)

clearly shows that TiO_2 nanoparticles are effectively intercalated with the GO sheets. The characteristic flaky structure of GO is still visible in the TEM micrographs of the fGO nanocomposite, indicating that the fundamental structure of GO is retained even after decoration with TiO_2. This decoration is done with the help of a silane group that acts as a source of bridging between TiO_2 and GO and is advantageous as it can inhibit the agglomeration of TiO_2 nanoparticles, enhancing their dispersion within the GO matrix [181]. This improved dispersion is crucial for the effectiveness of the nanocomposite as a nanofiller in polymer coatings.

The TEM results corroborate the findings from SEM and EDS analysis. The intimate interaction between TiO_2 nanoparticles and GO layers observed in TEM images aligns with the SEM observations of titania intercalated between the layers of graphene oxide. Additionally, the existence of oxygen, carbon, and titanium peaks in the EDS spectra of the functionalized nanocomposite supports the successful loading of TiO_2 onto GO. This comprehensive analysis confirms that the structural and compositional characteristics of the fGO nanocomposite are as expected, making it a potential material for improving the anticorrosion performance of polyurethane coatings on steel.

FTIR and XRD analysis

In Figure 27(a), The FTIR spectrum of GO revealed the existence of various oxygen-containing functional groups indicative of its highly oxidized nature. Notable peaks were observed at 2961 cm^{-1} (C–H stretching), 2355 and 2318 cm^{-1} (CO_2 absorption), and 1564 cm^{-1} (C=C stretching in aromatic rings). Peaks at 1259 cm^{-1} and 1090, 1022 cm^{-1} corresponded to C–O stretching vibrations, highlighting the presence of epoxide and alkoxy groups. Additionally, peaks at 796 cm^{-1} and 742 cm^{-1} were associated with bending vibrations of C–H bonds in aromatic rings [182,183]. The FTIR spectrum of TiO_2 in Figure 27(a) displayed distinct peaks associated with the titanium-oxygen

structure. Ti–O–Ti and Ti–O stretching vibrations were confirmed by peaks at 904, 834, and 798 cm^{-1}, which are characteristic of the titania structure [184,185]. The FTIR spectrum of fGO from Figure 27(a), a composite of GO and TiO_2, exhibited features from both parent materials, confirming successful functionalization. The peak at 2965 cm^{-1} (C–H stretching) was present in all spectra, indicating residual organic compounds. An upward hump at 2322 cm^{-1}, similar to GO, suggested retained CO_2 characteristics. Peaks at 2150 and 1981 cm^{-1} indicated the presence of C≡C stretches akin to both GO and TiO_2 [186]. A significant peak at 1267 cm^{-1}, close to the C–O stretching peaks in GO and TiO_2, pointed to the integration of C–O groups. Peaks at 1087 and 1026 cm^{-1} confirmed the presence of C–O stretching vibrations, retained from GO and influenced by TiO_2. The critical evidence of successful functionalization was seen in the Si-O-Si stretching at 1094 cm^{-1} and Ti–O–Ti stretching vibrations at 850 and 796 cm^{-1}, characteristic of TiO_2, indicating the incorporation of TiO_2 into the GO structure [183,187]. The FTIR spectra of TiO_2 and $fTiO_2$ has been added into the supplement file as Figure 44.

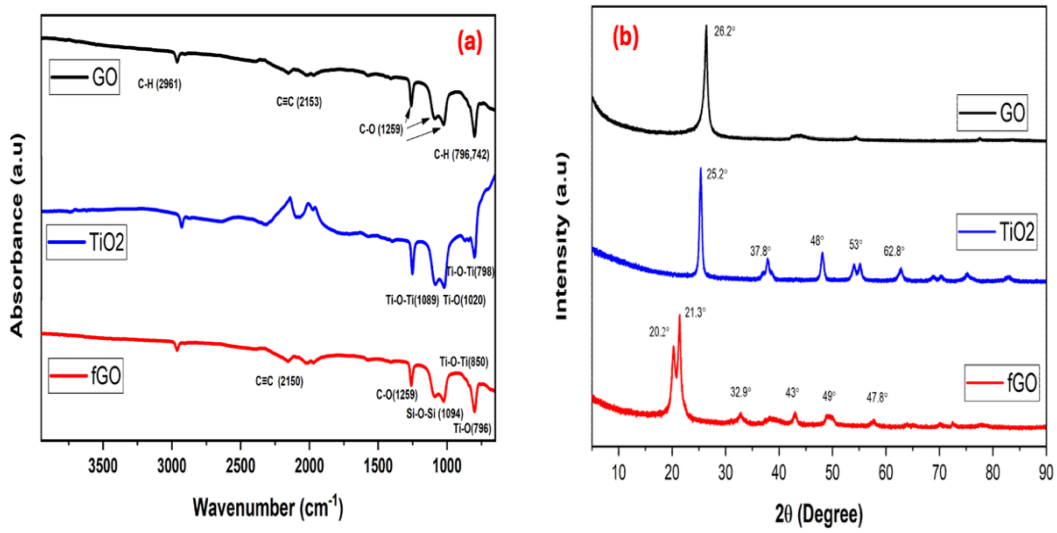

Figure 27: (a) FTIR analysis and (b) XRD analysis of GO, TiO_2, and fGO particles.

In Figure 27(b), the XRD patterns for graphene oxide (GO), titanium dioxide (TiO_2), and functionalized graphene oxide (fGO) reveal distinct features corresponding to their respective crystalline structures and demonstrate the successful integration of TiO_2 into the GO matrix. The GO XRD pattern shows a prominent peak at 26.2°. This peak relates to the (002) reflection of Graphene Oxide, indicating the GO's layered structure with an interlayer spacing consistent with oxygen-containing functional groups [188]. The XRD pattern of TiO_2 displays several characteristic peaks. The peak at 25.2° is associated with the (101) plane of anatase TiO_2, indicating its crystalline nature. The peaks at 37.8°, 48°, 53°, and 62.8° correspond to the (004), (200), (105), and (204) planes of anatase TiO_2, respectively [189]. The occurrence of these peaks affirms the anatase phase of TiO_2 in the sample. The XRD pattern of fGO shows peaks at multiple angles, demonstrating the incorporation of TiO_2 into the GO matrix. These peaks at 20.2° and 21.3°suggest modifications to the GO structure, possibly due to interactions with TiO_2 nanoparticles. These peaks at 32.9°, 43°, 49°, and 47.8° correspond to the reflections of TiO_2, indicating the presence of TiO_2 nanoparticles within the fGO. The peaks align with the anatase TiO_2 phase, confirming that TiO_2 retains its crystalline structure upon functionalization [190].

BET analysis

A BET analysis of graphene oxide (GO) and functionalized GO-TiO_2 was performed, and the findings are demonstrated in Table 5. The Nitrogen Adsorption and Desorption isotherms are represented to show BET analysis results in Figure 28. The specific surface area (SSA) and pore volume (P_V) showed a considerable decrease after the synthesis of fGO. The SSA of the GO emerged to be 505.540 m^2/g and pore volume as 0.867 cc/g, which is decreased to 211.622 m^2/g and 0.708 cc/g in the case of fGO after modification due to the incorporation of TiO_2 into GO[191]. These outcomes aligned

with previous studies [192] that the modification of nanoparticles decreases specific surface area and pore volume [193].

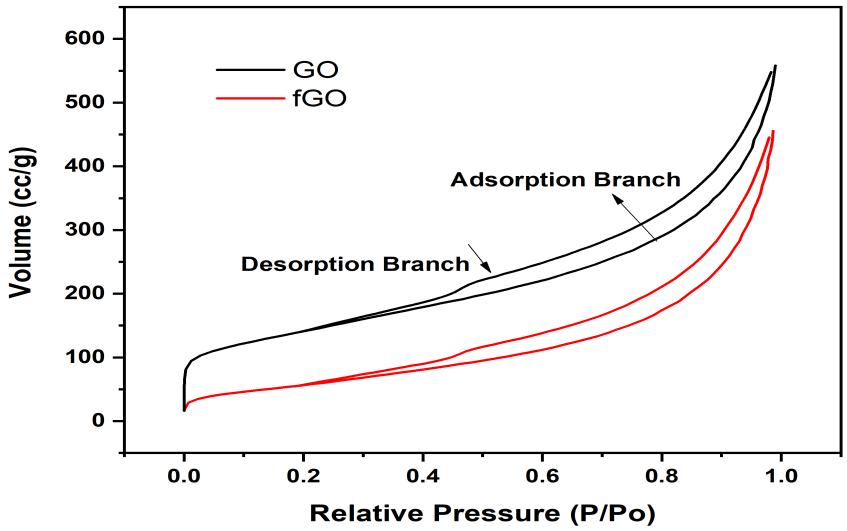

Figure 28: BET analysis of GO and fGO.

Table 5: BET Analysis of GO and GO-TiO_2.

Particles	**Specific surface area (m^2/g)**	**Pore volume (cc/g)**
Graphene Oxide (GO)	505.540	0.867790
fGO	211.622	0.708235

Thermal gravimetric analysis (TGA and DTA)

Figure 29(a) shows the TGA analysis of Pristine GO and fGO, conducted to evaluate their thermal stability. The TGA curves for both particles show weight loss occurring in three distinct stages, each corresponding to different thermal events. In the first stage, observed between 0°C and 55°C, both GO and fGO exhibit a minor weight loss of about

1-2%. This initial weight loss is ascribed to removing absorbed water molecules from the samples' surfaces. Water is common in GO due to its hydrophilic nature and its surface's various oxygen-containing functional groups.

$$GO{\cdot}H_2O\ (adsorbed) \rightarrow GO + H_2O(g) \text{ --------}\quad \text{Equation 1}$$

$$fGO{\cdot}H_2O\ (adsorbed) \rightarrow fGO + H_2O(g) \text{ --------}\quad \text{Equation 2}$$

This represents the evaporation of physically adsorbed water molecules from the surface of the graphene oxide (GO) or functionalized graphene oxide (fGO). The second stage of weight loss occurs between 55°C and 500°C, where both GO and fGO experience a weight loss of approximately 10%. This stage corresponds to the decomposition of oxygen-containing functional groups and other volatile substances present in the samples. The similar weight loss in this stage for both GO and fGO indicates that the initial functional groups are largely retained even after the modification with titania. The third stage, between 500°C and 700°C, shows a significant difference between GO and fGO. Pristine GO undergoes a substantial weight loss of about 45%, which can be attributed to the decomposition of the more stable oxygen-containing functional groups and the carbon framework [194]. In contrast, fGO exhibits a much lower weight loss of about 15% in the same temperature range. This marked difference in thermal stability is due to the incorporation of titania nanoparticles into the graphene oxide matrix. The presence of TiO_2 enhances the thermal stability of GO by reducing the rate of decomposition and providing a more thermally stable composite structure [195]. These TGA results are further supported by the Differential Thermal Analysis (DTA). In Figure 29(b), The DTA analysis reveals distinct thermal events for GO, with four peaks observed at approximately 50°C, 200°C, 350°C, and 450°C. These peaks correspond to the endothermic decomposition of different functional groups in GO. In contrast, the DTA curve for fGO shows no

sharp peaks, indicating more stable thermal behavior due to the presence of titania, which inhibits the thermal degradation of the graphene oxide.

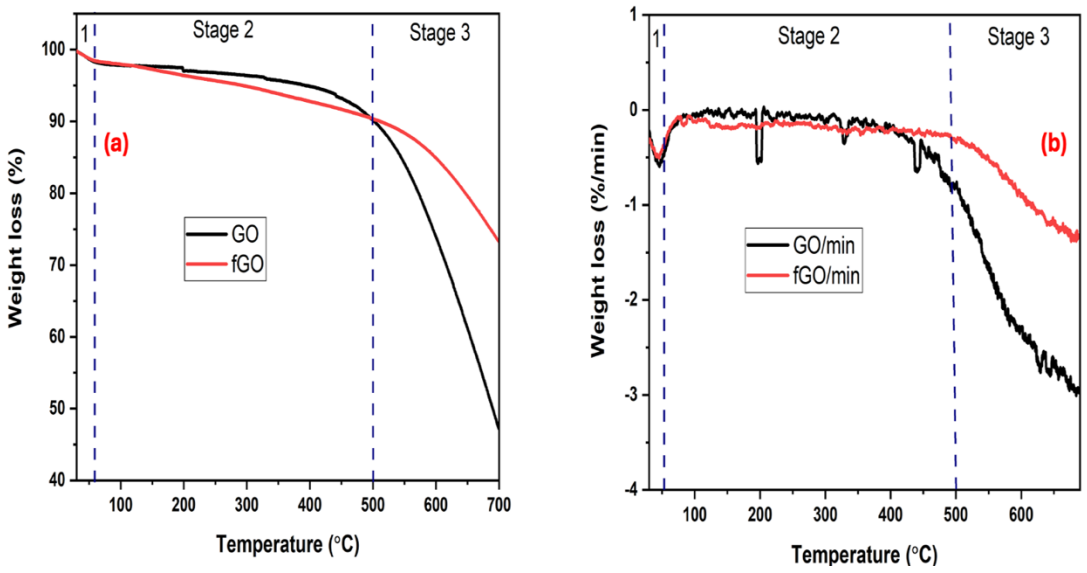

Figure 29: TGA analysis (a) and DTA analysis (b) of GO & fGO particles.

Electrochemical analysis of the coatings

To compare the effectiveness of corrosion inhibition, the blank PU and fGO coatings were examined for four weeks at room temperature in a 3.5 wt% NaCl solution. The coatings were subjected to open circuit potential (OCP) (Figure 30b) measurements over a period of 1800 seconds to evaluate system stability before the EIS analysis. Phase angle and bode graphs of coating are displayed in the Figure 30(c and d). The characteristics of blank PU coatings were thoroughly examined in an earlier study by our research group [167,168]. The data from that study will be used here for comparison and reference purposes. We used an analogous circuit model with two-time constants to analyze the data Figure 30(a). Several variables, including R_s (solution resistance), R_{ct} (charge transfer resistance), R_{po} (pore resistance), and capacitance relevant to these resistances as CPE2 and CPE1 (constant phase elements), were obtained through the

fitting data. The values of these variables are summarized in Table 6. The initial impedance for blank PU coatings was 6.81 GΩ.cm² on the first day, and after 4 weeks, it dropped to 0.37 GΩ.cm². The slow decrease in impedance over time suggests that the blank PU coatings have inadequate barrier qualities. Occurrences of intrinsic pores in the matrix are responsible for the decline in corrosion inhibition performance [196]. These pores let the electrolyte pass through the coatings and cause surface rust to occur. Rust first creates a barrier, but as time passes, it starts to lose its ability to protect. The phase angle plot demonstrated resistive behavior at low frequencies but capacitive behavior at the start of immersion, suggesting coating degradation [167,168].

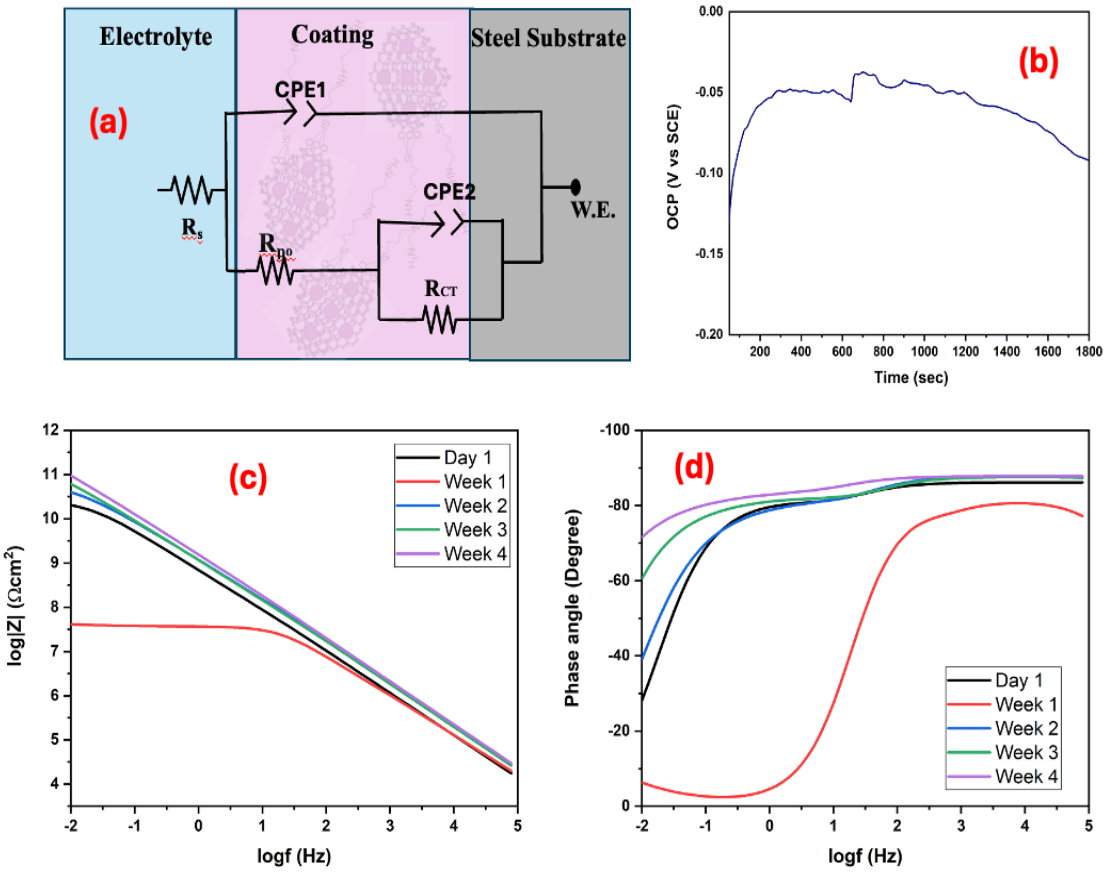

Figure 30 : Equivalent circuit (a) OCP plot (b) Bode plot (c) and phase angle plot analysis (d) of fGO-modified PU coatings.

The fGO-modified PU coating has outstanding initial barrier qualities, as seen by the impedance value of 25.5 GΩ.cm^2 on the first day. This high value is because the TiO_2 nanoparticles are uniformly dispersed throughout the GO matrix, forming a dense, compact covering that initially inhibits electrolyte penetration. fGO silane functionalization improves the coating's adherence to the steel substrate by reducing flaws and micropores that could allow ions to enter [174,193,196]. The electrolyte may start to seep through any inherent micro-pores or faults in the coating, which would account for the notable decline in impedance to 0.019 GΩ.cm^2 at the end of the first week. The abrupt drop indicates that the resistance is significantly reduced as ionic routes are formed and the electrolyte fills the open pores. The impedance value increases significantly to 67.7 GΩ.cm^2 by the second week, which could be caused by the formation of the passivation layer. A passivation layer may form as a result of the electrolyte and TiO_2 nanoparticles interacting [197]. By acting as an extra barrier, this layer prevents further ion transit. When the coating's constituents react with the electrolyte to seal micropores and flaws, the functionalized graphene oxide (GO) and titanium dioxide (TiO_2) may promote self-healing characteristics [198]. In the third week, the impedance measurement rises to 211 GΩ.cm^2, suggesting improved barrier qualities. The earlier-formed passivation layer keeps developing and is stronger at keeping ions out. Reorganization of the TiO_2 and GO within the coating matrix, due to the cross linking of functional groups on fGO, could result in decreased permeability and enhanced structural integrity. The impedance value reaches an incredible 821 GΩ.cm^2 by the fourth week. Extended contact with the saline medium creates an extremely robust and efficient barrier that greatly suppresses electrochemical processes. A similar growth trend was also seen in the Rpore values, which increased from an impedance value of 0.4 GΩ.cm^2 on the first day of immersion to 1.59 GΩ.cm^2 on the

fourth week of immersion. The good protective and barrier capabilities of the modified coatings are indicated by the trend of lowering CPE1 and CPE2 values. The presence of GO and TiO_2 together in the coating matrix leads to a compact and tightly packed structure. TiO_2 nanoparticles intercalated the spaces between GO sheets, reducing the porosity of the coating and, because of minimizing pathways for ion diffusion. The synergistic effects of modified GO-TiO_2 enhance the coating's overall performance [198–200], making it highly effective in protecting the steel substrate from corrosion with an exceptional efficiency of 99.9%. The following formula [168,201] can be used to determine the inhibition efficiency of the modified PU coatings; the results are given in Table 6.

The inhibition efficiency (η) % = $1 - (R_{ct\ blank} / R_{ct\ modified}) \times 100$ ----- Equation 3

Where:

$R_{ct\ blank}$ = Charge transfer resistance of blank PU coating

$R_{ct\ modified}$ = Charge transfer resistance of fGO-modified PU coating

Table 6: The Electrochemical Impedance Data Values of Modified PU Coatings.

Week	**R_{pore} xE1**	**CPE_1 xE-10**	**n**	**R_{ct}**	**CPE_2 xE-12**	**m**	**R_s**	**R^2 xE-3**	**η**
	$G\Omega.cm^2$	$s^n.\Omega^{-1}.cm^{-2}$		$G\Omega.cm^2$	$s^n.\Omega^{-1}.cm^{-2}$		Ω		%
1	0.1	3.42	1	0.02	36.7	0.91	1548	11.6	-
2	3.45	1.02	0.7	67.7	71.5	0.97	239	0.4	98.5
3	3.12	1.08	0.7	211	59.7	0.97	91	0.4	99.7
4	15.9	0.93	0.7	821	30	0.97	1.7	0.2	99.9

Salt Spray test

The salt spray analysis test was carried out to evaluate the corrosion protection ability

of scratched blank polyurethane (PU) coatings and PU coatings modified with fGO on steel substrates [202]. These substrates were immersed in a 3.5wt % NaCl solution at room temperature for four weeks. The observations were made at regular intervals to assess the extent of corrosion. Figure 31 shows the photographs of scratched blank PU and PU-fGO coated samples. For the blank PU coatings, noticeable deterioration began after just one week of immersion in the saline solution. Early signs of corrosion were evident, characterized by the rust formation on the surface of the coatings. By the second week, the scratched areas exhibited significant corrosion, which continued to propagate into the coatings in the third and fourth weeks. The deterioration can be attributed to the development of conductive paths for electrolyte uptake. Due to the inherent micro-pores in the blank PU coatings, the electrolyte penetrated these paths, leading to accelerated corrosion. The PU coatings modified with fGO showed remarkable resistance to corrosion in the initial stages. During the first week, there was no visible change in the coating's appearance, indicating the effectiveness of the fGO in providing a protective barrier. This can be related to the formation of a protective barrier within the coatings, which inhibits the penetration of electrolytes into the steel substrate. also, TiO_2 nanoparticles were intercalated within the graphene oxide layers, as confirmed by SEM and TEM images, creating a more impermeable and cohesive barrier. In the second week, slight signs of corrosion started to appear. However, the extent of corrosion was minimal compared to the blank PU coatings. From the second week onward, a low corrosion rate observed and it gradually increased up to the fourth week. The slight increase in corrosion might be due to the gradual breakdown of some weak spots in the coating, but overall, the protective layer remained highly effective. These results highlight the increased durability and corrosion resistance of the PU-fGO coatings, demonstrating their superior performance and protective capabilities against

corrosion in harsh environments as compared to blank PU coatings.

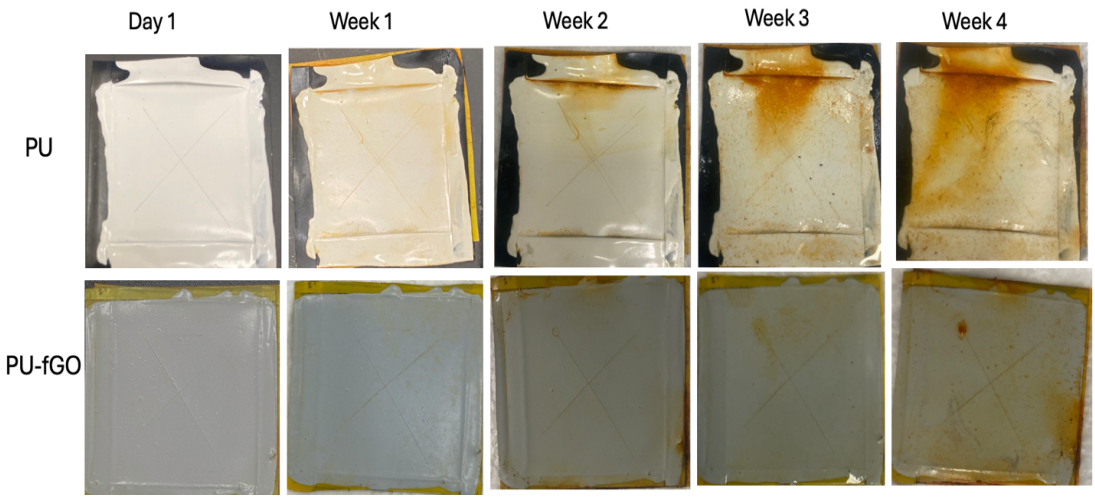

Figure 31: Images of salt spray analysis of blank PU coatings and fGO-modified PU coatings in 3.5wt % NaCl solution at room temperature.

Proposed Mechanism for Inhibiting Corrosion

The remarkable protective characteristics of polyurethane (PU) coatings modified by fGO can be ascribed to various cooperative mechanisms, one of which is the passivation of the steel surface. Let's examine the interaction between the Fe of the steel substrate and the fGO to give improved corrosion protection. When the fGO-modified PU coating is applied to the steel surface, it forms a dense, uniform barrier. Graphene oxide (GO) and titania (TiO_2) nanoparticles enhance the physical barrier properties, preventing the initial connection between the steel surface and the corrosive conditions. Electrolyte penetration may be possible due to micro-pores or imperfections in the coating, even after the initial barrier is present. This is particularly clear from our statistics, which show a significant drop in impedance over the first week. When a steel substrate is immersed in a NaCl solution, several initial electrochemical reactions occur, leading to corrosion. The first electrochemical reaction can happen when the electrolyte

reaches the steel substrate. Iron hydroxides and oxides are formed when the iron (Fe) in the steel combines with the oxygen and water in the electrolyte [203,204] :

$$Fe \rightarrow Fe^{+2} + 2e^{-} \text{ (reaction occur at anode) -------- Equation 4}$$

$$O_2 + 2H_2O + 4e^{-} \rightarrow 4OH^{-} \text{ (reaction occur at cathode) -------- Equation 5}$$

$$4Fe + 3O_2 + 6H_2O \rightarrow 4Fe(OH)_3. \text{ -------- Equation 6}$$

$$Fe(OH)_3 \rightarrow Fe_2O_3.H_2O \text{ (rust) -------- Equation 7}$$

To elucidate the corrosion inhibition performance of the fGO-modified coatings within a polyurethane matrix, we propose three distinct mechanisms, as shown in Figure 32. These mechanisms are based on the composite coating's unique structural and chemical properties and its interaction with the corrosive environment. Each route contributes to the overall corrosion resistance through different pathways, enhancing the protective capabilities of the coating. The detailed mechanisms are as follows:

Route 1: Impediment of Electrolyte Diffusion by Graphene Oxide Layers

Figure 32(a) shows the first proposed route for corrosion inhibition. In the first proposed mechanism, the GO within the polyurethane matrix acts as a formidable barrier against the diffusion of corrosive species. The GO sheets are arranged in a layered structure, creating a tortuous path for the electrolyte movement. This alignment restricts the perpendicular diffusion of electrolytes, thereby significantly impeding the transport of corrosive agents such as chloride ions towards the steel substrate [174,205]. The physical obstruction provided by the GO layers effectively enhances the barrier properties of the coating, reducing the rate of corrosion initiation and propagation

Route 2: Formation of Passive Iron Titanate Layer

Figure 32(b) shows the second route suggests that Titania (TiO_2) in the coating reacts with iron (Fe) present on the steel substrate to form Iron Titanate ($FeTiO_3$). This chemical reaction leads to the development of a passive layer on the steel surface. The $FeTiO_3$ layer acts as a protective barrier, preventing further interaction between the steel

and the corrosive environment. This passive layer is crucial in enhancing the corrosion resistance of the coated steel substrate. The second proposed mechanism involves the chemical interaction between titania (TiO_2) nanoparticles and the iron (Fe) from the steel substrate. Upon exposure to the corrosive environment, TiO_2 reacts with Fe to form iron titanate ($FeTiO_3$) [206]. The formation of $FeTiO_3$ occurs through the following reaction [207]:

$$TiO_2 + Fe \rightarrow FeTiO_3 \text{ --------} \quad \text{Equation 8}$$

The resultant $FeTiO_3$ forms a stable, adhesive passive layer on the steel surface, which acts as a protective barrier. This passive layer inhibits further electrochemical reactions by blocking the access of corrosive agents to the underlying metal, thereby enhancing the overall corrosion resistance of the coated substrate [208,209].

Route 3: Enhanced Adhesion Through Silane Functionalization and Epoxy Group Reactions

Figure 32(c) shows the third proposed mechanism based on the chemical modification of the epoxy groups present on the surface of GO through a ring-opening reaction facilitated by silane molecules. The alkoxy groups in silane molecules undergo hydrolysis to form unstable silyl alcohols (Si-OH) [174] :

$$R{-}Si(OR')_3 + H_2O \rightarrow R{-}Si(OH)_3 + 3R'OH \text{ --------} \quad \text{Equation 9}$$

These silyl alcohols can then react with hydroxyl groups present on the metal surface, leading to the formation of strong covalent bonds such as -Si-O-Fe and -Si-O-Si- [210]:

$$Si(OH)_3 + Fe(OH)_2 \rightarrow Fe{-}O{-}Si + H_2O \text{ --------} \quad \text{Equation 10}$$

$$Si(OH)_3 + Si(OH)_3 \rightarrow Si{-}O{-}Si + H_2O \text{ --------} \quad \text{Equation 11}$$

These reactions result in a robust chemical bonding network between the coating and the metal substrate, significantly improving the coating's adhesion and mechanical stability. This enhanced adhesion prevents delamination and ensures long-term protection of the steel surface against corrosion. These proposed mechanisms

collectively contribute to the superior corrosion inhibition performance of the silane-functionalized graphene oxide-titania coatings in a polyurethane matrix, offering a multi-faceted defense against corrosive environments.

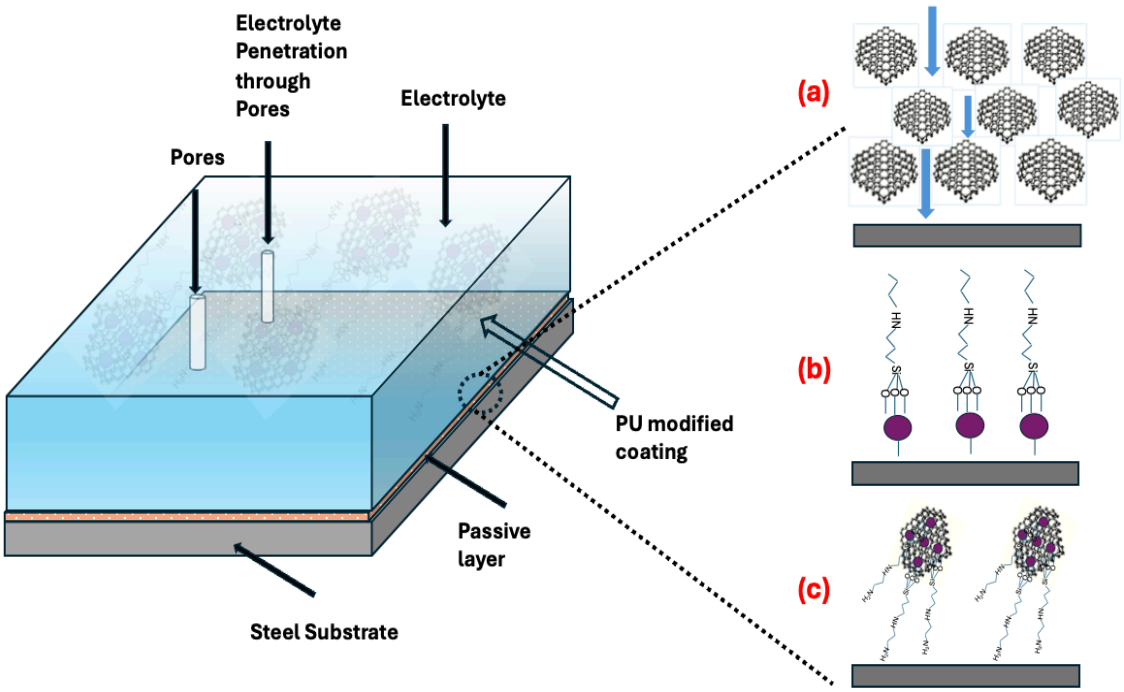

Figure 32 : Proposed schematic of corrosion inhibition mechanism.

Enhanced Steel Surface Protection Using TiO_2/MS30 Modified Polyurethane Coatings: Synthesis and Performance Evaluation

Structural and Morphological analysis of synthesized particles

Figure 33 represents the TEM images of the pristine TiO_2 and TiO_2/MS30 particles. The TEM images of pristine TiO_2 particles (Figure 33a) demonstrated that particles are uniformly distributed with more of spherical morphology. As most of the particles are in spherical shape, it seems that TiO_2 appeared to be in the anatase phase. It can also be seen that the boundaries among particles are clearly visible, which is also one of the unique characteristics of anatase phase TiO_2 [211,212]. Figure 33 (b1 and b2) corresponds to the TEM images of the TiO_2/MS particles, suggesting that after the

loading of MS30 particles into TiO_2, the agglomeration of particles can be seen. The shape of the particles appeared to be pseudo-spherical with different size distributions [213]. This is due to the chemical interaction of M30 with TiO_2 particles. The size of the particles also appeared to be smaller due to the addition of MS30 [214].

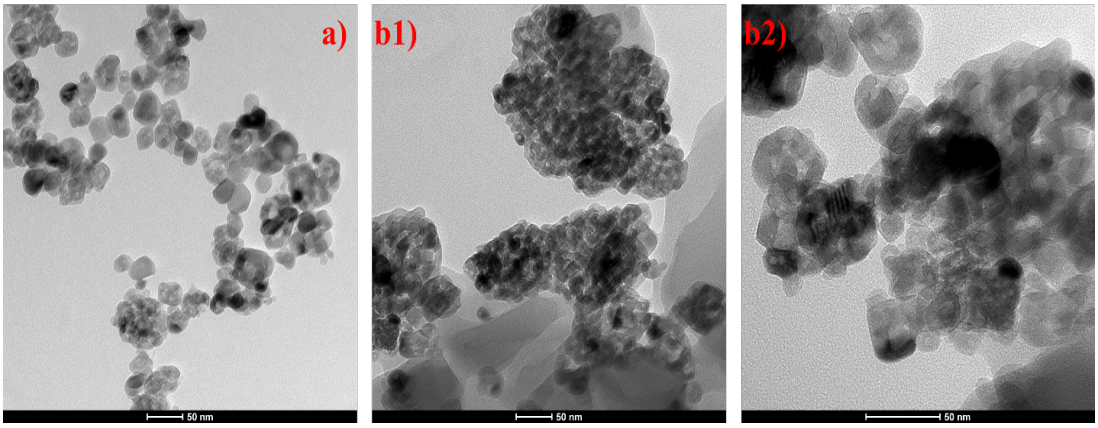

Figure 33: TEM images of the (a) Pristine TiO_2 (b1 and b2) TiO_2/MS30 particles.

Figure 34 represents the N_2 adsorption-desorption isotherm of pristine TiO_2, MS30 and TiO_2/MS30. The isotherm attained from BET analysis suggests that these particles exhibited typical type IV isotherm with H1 hysteresis loop, which is indicative of the mesoporous form of particles and anatase TiO_2 [215–217]. The specific surface area and pore volume results obtained from BET analysis are tabulated in Table 7. The specific surface area (SSA) and pore volume (PV) of pristine TiO_2 and MS30 appeared to be 135.01 m^2/g / 0.64 cc/g and 72.63 m^2/g / 0.41 cc/g, respectively. After being loaded with MS30, the SSA and PV of TiO_2/MS30 is observed to be decreased to 72.74 m^2/g and 0.33 cc/g. This decrease in SSA and PV of loaded TiO_2 particles is related to successfully incorporating MS30 into TiO_2. Moreover, there is also a decrease in the pore radius of TiO2 from 94.4 A to 90.5 A after being loaded with MS30, which is also suggesting that most of the volume of TiO2 particles is occupied by MS30 inhibitor

particles [171,218].

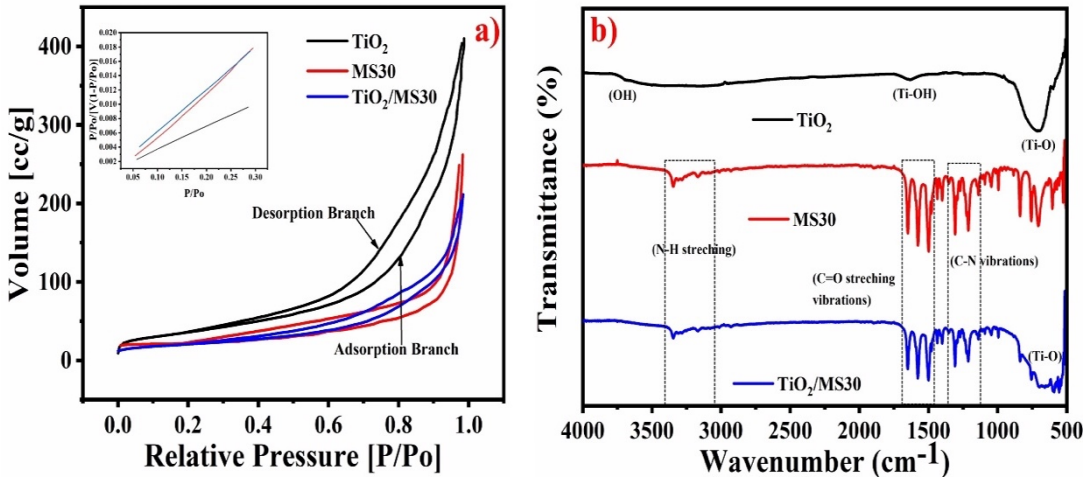

Figure 34: BET analysis (a) and FTIR analysis (b) Pristine TiO_2, MS30 and TiO_2/MS30 particles.

Table 7: BET Analysis of Pristine TiO_2, MS30 and TiO_2/MS30.

Sample	**Specific Surface area**	**Pore volume**	**Average Pore radius**
	(m^2/g)	**(cc/g)**	**(A)**
Pristine TiO_2	135.01	0.64	94.40
MS30	72.63	0.41	112.20
TiO_2/MS30	72.74	0.33	90.50

FTIR analysis (Figure 34b) was done to study and confirm the composition and chemical bonding in the pristine TiO_2, MS30, and TiO_2/MS30. In FTIR analysis results of pristine TiO_2, three peaks are observed at wavenumber 701, 1642, and 3696 cm^{-1}. The broad, sharp peak at 701 cm-1 is attributed to the Ti-OH stretching deformative vibrations, which confirms the presence of anatase TiO_2 [219]. The peak at 1642 cm^{-1}

is attributed to the Ti-O bending mode [220], and in some literature, it is said to be attributed to the hydroxyl group from the adsorbed water content [219]. The small peak at 3696 cm^{-1} is also linked to the symmetric stretching vibrations of OH group from adsorbed water molecules. The results are in agreement with previous literature [220]. In the case of the MS30, since the synthesized inhibitor possesses a piperazine bis-urea structure. The main absorbance peak is observed at 1307, 1652, and 3350 cm^{-1}. These peaks are related to the C-N, C=O and N-H stretching vibrations. The observance of these peaks demonstrates the confirmation of the piperazine bis-urea structure [221]. Further detailed results and comprehensive data analysis will be published in a subsequent manuscript, which will be made available following the acceptance of the corresponding patent application (US Provisional Patent Application No. 63/462,316). The FTIR analysis of TiO_2/MS30 displayed the peaks, which are a combination of peaks of both MS30 and TiO_2. However, some displacement and shift in the peaks have been observed, which demonstrated that MS30 has interacted with TiO_2. The peak for C-N has been shifted to 1305, C=O to 1643, and N-H to 3354 cm^{-1}. This indicates that the functional group in MS30 has coordinated with TiO_2, resulting in the successful loading of the MS30.

Thermal analysis of synthesized particles

TGA and DTA analysis was done to study the thermal stability of particles at high temperatures in the range of 50-700°C. Figure 35 represents the TGA and DTA analysis of Pristine TiO_2, MS30, and TiO_2/MS30 particles which shows that the thermal degradation of these particles is divided into four distinct stages. The TGA analysis of pristine TiO_2 suggests that the particles possess high thermal stability as no degradation or decomposition is seen in the TGA and DTA analysis of pristine TiO_2 up to 700°C. Similarly, no sharp or apparent peak can be seen in the DTA analysis of pristine

samples. The TGA analysis of MS30 suggests that the sample was quite stable in the first stage, and no degradation is seen in the first stage which is also evident from DTA analysis. These results suggest that MS30 sample was properly dried and there was no water content in it. The main degradation of MS30 can be seen in the second stage in the temperature range of 232-287 °C. Almost 26.7 % of the product has been degraded in this range. This is due to the decomposition of the MS30 urea group into -NH_3 and CO_2. The second phase of decomposition is seen in the third stage of TGA, in the temperature range of 288.35-376.81°C. In this stage, almost 44% of weight loss can be seen. The rest of the weight loss can be observed in the fourth stage, when almost all of the product has been degraded. Similar results can be observed in the DTA analysis of MS30. The two endothermic peaks can be seen at 276.57 °C and 328.77°C which is by the TGA analysis of the sample. In the case of TiO_2/MS30, the main degradation can be seen in the second and third stages. About 2% of weight loss is seen in the first stage which is due to the evaporation of adsorbed water content in the sample [222]. The degradation in the second stage follows the same path as that of MS30 with a temperature of little less than 276.57°. This may be due to degradation of the MS30 particles loosely attached to the TiO_2 particles. The total weight loss observed in this stage is about 35%. In the third stage, almost 5% weight loss is seen, and after that,the particles seem to become more stable at high temperatures. This suggests that the MS30 has been successfully loaded into TiO_2 particles. So, 46% weight loss can be seen in the TiO_2/MS30 particles. This is also by DTA analysis where the main endothermic degradation peak is seen at 257.05°C.

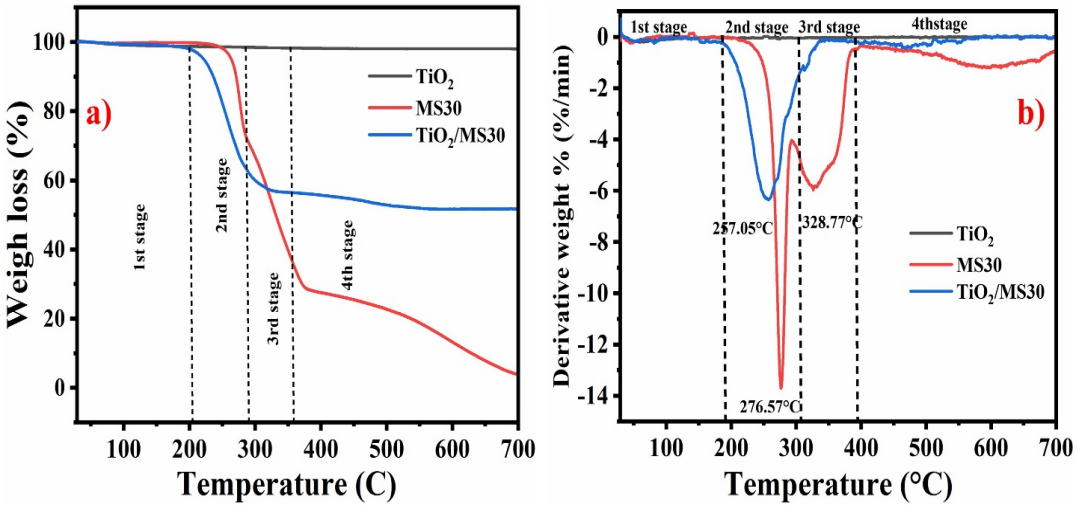

Figure 35: TGA (a) and DTA (b) analysis of Pristine TiO_2, MS30 and TiO_2/MS30 particles.

TGA analysis results can also be utilized to calculate the loading amount of inhibitor into TiO_2. For this purpose, the following equation [223,224] is used:

$$\text{Ratio mass loss} = \frac{\Delta W}{W1} \text{ x } 100 \qquad \text{Equation 1}$$

Where ΔW is $W_2 - W_1$. W_2 is the weight loss % at higher temperatures (final temperature) and W_1 is the weight loss at lower temperatures (initial temperature). The initial weight loss as W_1 for TiO_2/MS30 is observed at 202.16 °C, and the final weight loss as W_2 it 473.88°C. So, ΔW will be 46%. Hence, the ratio of mass loss for TiO_2/MS30 will be 46% w/w.

DSC analysis of developed coatings

Figure 36 illustrates the DSC analysis for blank and modified PU composite coatings. The DSC curves provide critical insights into the thermal transitions of these materials, highlighting four distinct points corresponding to the glass transition temperature (Tg) and melting point (Tm) of both the soft and hard segments of the polymer chains. The DSC analysis for the blank PU coatings identifies two primary thermal transitions for

the soft segments of the polymer chains. The first transition, the glass transition temperature (Tg), occurs at -56 °C, followed by the melting point (Tm) at 27 °C. These transitions indicate the thermal behavior of the soft segments within the PU matrix. The Tg represents the temperature at which the polymer transitions from a brittle, glassy state to a more pliable, rubbery state. The Tm indicates the temperature at which the crystalline regions of the soft segments melt, signifying a breakdown of the crystalline structure. The sharp endothermic peak at the soft segments' Tg indicates imperfections and voids, leading to a pronounced thermal response [225]. This is followed by the melting of these segments at 27 °C, further confirming the presence of crystalline structures within the soft segments. For the hard segments of the blank PU coatings, the DSC curve reveals an endothermic peak at 106 °C, corresponding to the glass transition temperature, and another peak at 148 °C indicating the melting point. These transitions are crucial as they reflect the thermal stability and structural integrity of the hard segments within the polymer matrix.

The modified PU coatings, incorporating TiO_2 and MS30, exhibit slight variations in the thermal transitions compared to the blank PU coatings. The Tg and Tm of the soft segments for the modified PU coatings are observed at -55 °C and 29 °C, respectively. These slight shifts in temperature indicate a minor interaction between the PU matrix and the modified particles. The presence of these particles appears to restrict the mobility of the polymer chains, leading to a slight increase in the thermal transition temperatures [226]. For the hard segments, the modified PU coatings show Tg and Tm at 107 °C and 148 °C, respectively. This slight elevation in the thermal transition temperatures compared to the blank PU coatings suggests a more robust interaction between the hard segments and the modified particles. Introducing TiO_2 and MS30 likely enhances the crosslinking within the PU matrix, resulting in improved thermal

stability and mechanical properties [227].

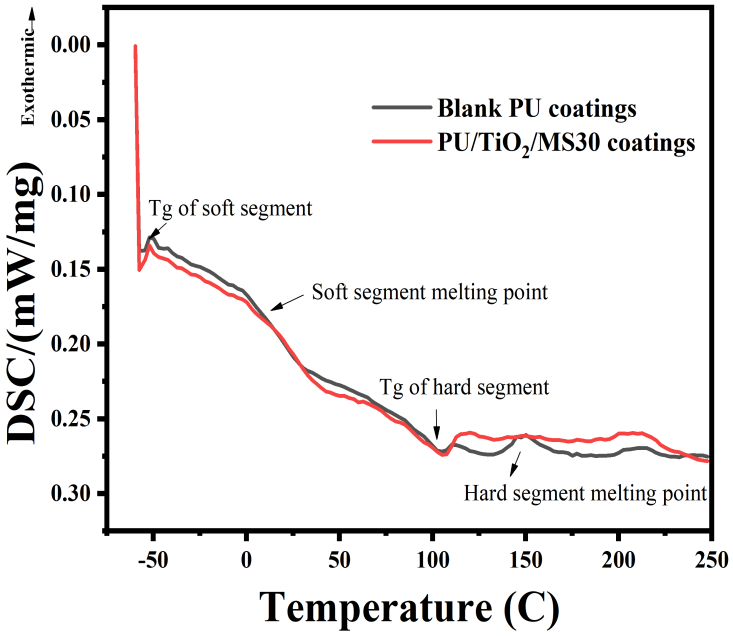

Figure 36: DSC analysis of blank PU coatings and PU/TiO_2/MS30.

Corrosion Inhibition Analysis

Potentiodynamic polarization analysis

Potentiodynamic polarization (PDP) scans were conducted to investigate the corrosion inhibition performance and the corrosion rate of steel specimen after 5 hours of immersion in a 3.5 wt.% NaCl solution, both in the absence and presence of TiO_2/M30 particles (Figure 37a). The Tafel parameters, derived from fitting the PDP data (Table 8) were evaluated to assess the corrosion resistance of the steel specimen. Key parameters include the corrosion potential (Ecorr), corrosion current density (Icorr), and the anodic (βa) and cathodic (βc) slopes. The results indicate a significant improvement in corrosion resistance when the steel substrate was immersed in the saline solution containing TiO_2/M30 particles. Specifically, the corrosion current

density (Icorr) decreased markedly from 82.1 μA/cm² in the absence of particles to 39.1 μA/cm² in their presence. This reduction in Icorr is accompanied by a positive shift in the corrosion potential (Ecorr) from -875 V to -767 V, suggesting a more thermodynamically stable surface and less corrosion susceptibility. Furthermore, the corrosion rate decreased from 13.2 mpy to 6.3 mpy, indicating the efficacy of the TiO_2/M30 particles in enhancing the protective barrier on the steel surface. The observed changes in the PDP parameters can be attributed to the formation of a film on both the cathodic and anodic regions of the steel substrate due to the adsorption of TiO_2 and M30 particles. This film acts as a barrier, mitigating the electrochemical reactions responsible for corrosion. Moreover, the inhibitor has a larger cathodic Tafel slope indicating it is more towards a cathodic inhibitor type. The inhibition efficiency, a critical parameter for evaluating the performance of corrosion inhibitors, was calculated using the following equation [171] .

$$\text{Inhibition Efficiency} = 1-\frac{Icorr2}{Icorr1} \times 100 \qquad \text{Equation 2}$$

where Icorr2 is the corrosion current density in the presence of TiO_2/M30 particles, and Icorr1 is the corrosion current density in their absence. The inhibition efficiency for the steel substrate in the presence of TiO_2/M30 particles was determined to be 53%. This significant value underscores the considerable adsorption of these particles onto the steel surface, providing an effective barrier against the corrosive NaCl medium. These findings support the suggestion that TiO_2/M30 particles enhance the corrosion resistance of steel in saline environments by forming a protective film. The subsequent section will delve into a detailed surface analysis post-PP testing to further elucidate the nature and effectiveness of this film.

Table 8: Tafel Parameters Calculated from Polarization Test of Steel substrate After 5 Hours of Immersion in 3.5 wt. % NaCl Solution with and without TiO_2/MS30.

Sample in 3.5 wt.% NaCl Solution	**E_{corr}**	**I_{corr}**	**β_a**	**β_c**	**Corrosion rate**	**Inhibition efficiency**
	V	**µA.cm²**	V/dec	V/dec	mpy	%
Blank	-875.0	82.10	0.33	0.38	13.21	-
TiO_2/MS30	-767.0	39.10	0.32	0.21	6.29	53

Raman analysis

Raman analysis was conducted on a steel substrate after 5 hours of immersion in a 3.5 wt.% NaCl solution containing TiO_2/MS30 particles, following PP analysis. This study aimed to examine the surface chemistry of the steel substrate and identify the chemical composition of the adsorbed particles. The Raman spectra, presented in Figure 37 (b), provide critical insights into the corrosion products and adsorbed species on the steel surface. The Raman spectra exhibited bands at 134, 306, 382, and 525 cm^{-1}, corresponding to the lepidocrocite (γ-FeOOH) phase [228]. This indicates the formation of corrosion products on the steel surface, as lepidocrocite is a common iron oxyhydroxide formed during the corrosion process. Additionally, bands were observed at 602, 711, 1014, 1139, 1346, and 1424 cm^{-1}. These bands are associated with amine ring bending, benzene ring bending, in-plane trigonal breathing, NH in-plane bending, amine ring stretching, and benzene ring stretching, respectively [229]. The band at 602 cm^{-1} may also indicate the anatase phase of TiO_2 [230]. The presence of these Raman bands suggests that MS30 has been successfully absorbed onto the steel substrate. The appearance of peaks corresponding to both MS30 and TiO_2 implies that titania also

contributes to protection at the cathodic region. The adsorption of MS30 onto the steel surface is likely facilitated by forming Fe(II)-MS30 complexes. This complexation occurs due to the interaction of π-electrons from the aromatic ring and lone pairs of electrons from nitrogen atoms with iron [229]. Such interactions enhance the adherence of MS30 to the steel surface, forming a protective layer that mitigates further corrosion. The Raman analysis thus confirms the successful adsorption of MS30 onto the steel surface, which is crucial for its corrosion protection properties. The complexation and electrostatic interactions between MS30 and the steel surface not only improve the adhesion of the inhibitor but also contribute to forming a stable protective film. This film acts as a barrier, reducing the diffusion of corrosive species to the steel surface and inhibiting further corrosion. Furthermore, the presence of TiO_2 in the Raman spectra suggests that titania particles also contribute to the corrosion protection mechanism. The TiO_2 particles, upon dissociation, release Ti^{4+} ions, which interact with hydroxide ions to form a passive $Ti(OH)_4$ layer on the cathodic sites. This passive layer further enhances the corrosion resistance by blocking the cathodic reactions and reducing the overall corrosion rate.

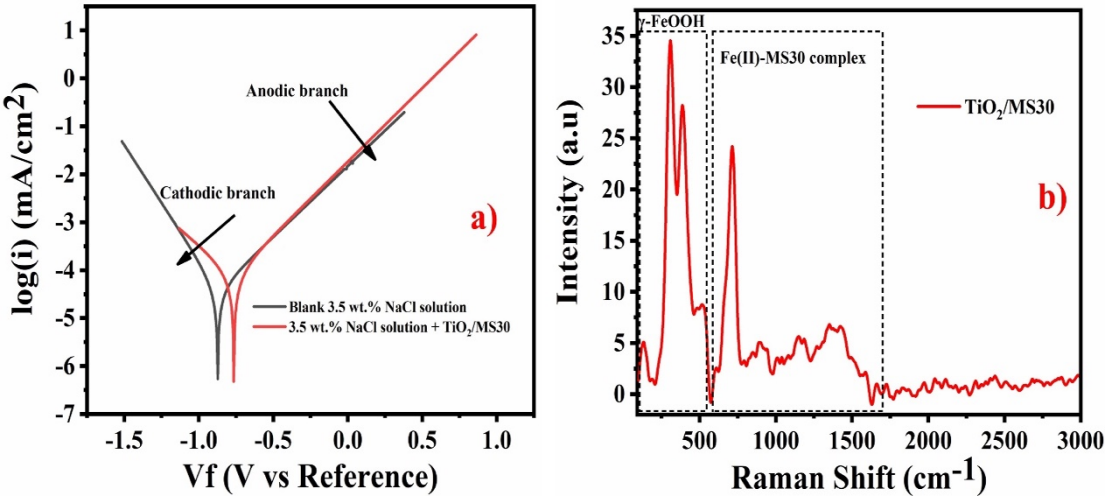

Figure 37: Potentiodynamic polarization (a) of steel substrate after 5 h of immersion in

3.5 wt. % NaCl solution containing TiO_2/MS30 particles and raman analysis (b) of steel substrate after 5 h of immersion in 3.5 wt. % NaCl solution containing TiO_2/MS30 particles post PP.

EIS analysis

The EIS analysis was done to study the coating's protection and corrosion inhibition capability. For this purpose, the scratched PU-based modified coatings were immersed in 3.5 wt. % NaCl solution for 7 weeks. Open circuit potential (OCP) measurements (Figure 45) were done to record the variations in system and system stability over the period of 1500 seconds. Figure 38 (a) represents the two-times constant equivalent circuit utilized to fit the data obtained from the Gamry 3000 during EIS analysis. Figure 38 (b, c) displays the bode and phase angle plots of the modified PU coatings immersed in 3.5 wt. % NaCl solution for the period of 7 weeks. For reference purposes, the blank PU coatings were analyzed to compare the corrosion inhibition efficiency of the blank PU coatings and modified PU coatings. The impedance results of the blank PU coatings have already been published in our previous work [171].

The impedance measurements of the blank PU coatings indicated that they initially provided effective corrosion inhibition, with an impedance value of 0.63 $G\Omega.cm^2$ at the start of immersion. However, this impedance value significantly decreased, reaching 0.002 $G\Omega.cm^2$ by the final week of immersion in a 3.5 wt.% NaCl solution. This notable decline in impedance suggests that the electrolyte infiltrated the coatings, forming conductive paths and progressively degrading the coating material. The penetration of the electrolyte not only compromised the integrity of the coatings but also likely led to delamination, as the adhesion of the coatings diminished with the passage of the electrolyte. This process is corroborated by the observed increase in capacitance values,

which will be discussed later.

The phase angle plot [171] results further elucidate the degradation process. Initially, the coatings exhibited capacitive behavior at high frequencies and resistive behavior at low frequencies. This capacitive behavior is indicative of the coating's ability to act as a barrier to charge transfer. However, over time, the capacitive behavior of the blank PU coatings decreased, suggesting that the coatings began to fail and deteriorate. The progressive loss of capacitive properties indicates that the electrolyte could penetrate the coating more easily, leading to an increase in conductive pathways and a subsequent decrease in impedance. Moreover, the increase in capacitance values over time supports the conclusion that the coatings were deteriorating. As the electrolyte infiltrated the coatings, it likely caused microstructural changes that increased the dielectric constant of the material, resulting in higher capacitance readings. These changes further suggest a breakdown in the coating’s ability to act as an effective barrier against corrosion.

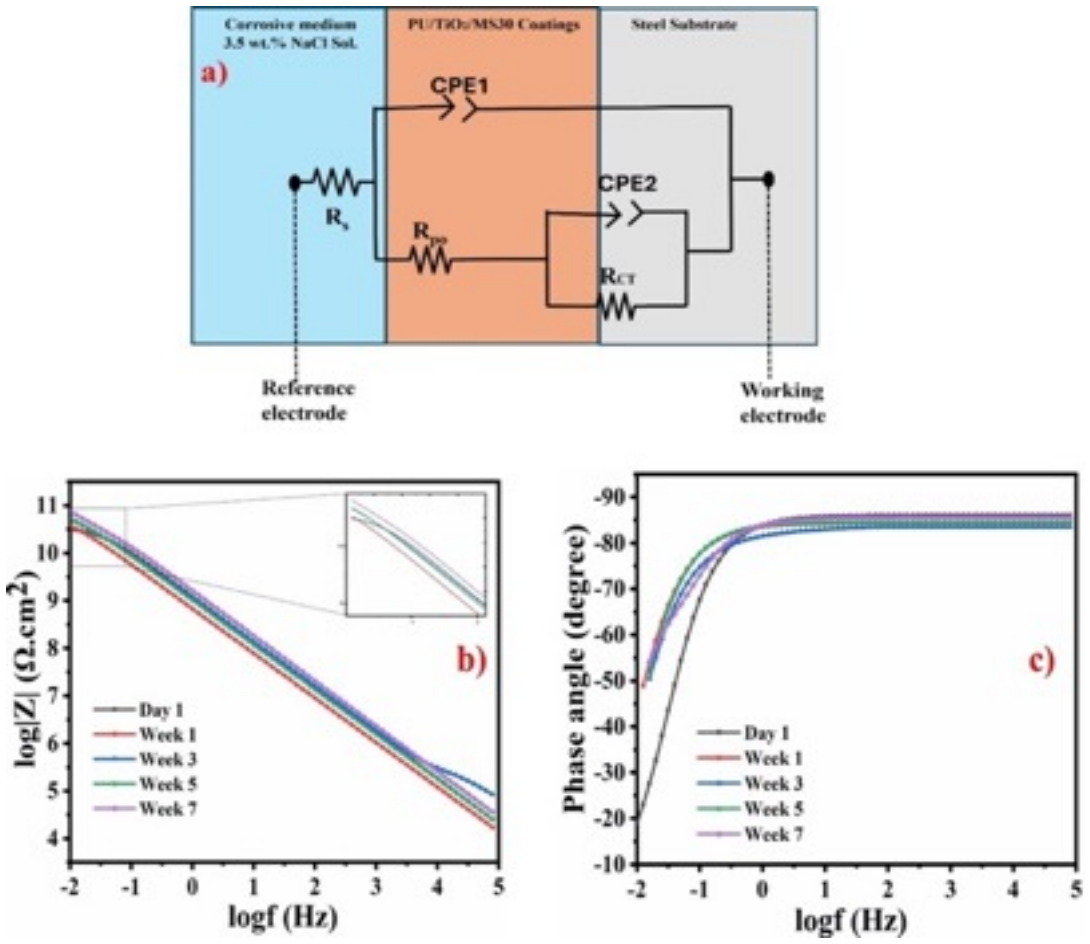

Figure 38: (a) Equivalent circuit utilized to fit the data, (b) Bode and (c) Phase angle plot of the scratched PU/TiO_2/MS30 coatings immersed in 3.5 wt. % NaCl solution for the period of 7 weeks.

The PU/TiO_2/MS coatings demonstrated exceptional barrier properties. As illustrated in Figure 38 (b), these modified coatings exhibited an initial impedance value of 39.2 GΩ.cm² on the first immersion day in a 3.5 wt.% NaCl solution. The high impedance values observed at low frequencies indicate robust corrosion resistance. Specifically, after 7 weeks of immersion, the high impedance values suggest that the coatings remained intact and effectively inhibited corrosion at the metal-coating interface. This conclusion is further supported by the low capacitance values of the modified coatings, indicating that they remained undamaged and provided superior protection compared

to the blank PU coatings due to better adhesion. The immersion period for the modified coatings (7 weeks) exceeded that of the blank PU coatings (4 weeks), yet they continued to provide excellent corrosion protection, with an impedance of 83.3 GΩ.cm² after 7 weeks. This significant disparity in impedance between the modified and blank coatings can be attributed to the corrosion inhibition effect of MS30. At defect sites (e.g., scratches), the local pH decrease triggers the release of MS30 from its TiO_2 carrier. This release process also leads to the dissociation of TiO_2, forming $Ti(OH)_4$, which subsequently creates a protective layer at the cathodic region of the steel substrate. This synergistic corrosion inhibition mechanism protects both the cathodic and anodic regions, resulting in increased impedance values and decreased capacitance values. The detailed corrosion inhibition mechanism will be explained in a later section. The phase angle plot in Figure 38 (c) of the modified coatings indicated that the coatings exhibited capacitance behavior over a wider frequency range. The phase angle above -80° is an indication of capacitance behavior. Even at low frequency, the more than -50° phase angle after 7 weeks of immersion suggests that coatings are still unscathed.

Table 9: The Electrochemical Impedance Data Values Attained for the Scratched Polyurethane Coatings Reinforced with Modified TiO_2/MS30 Particles Immersed in 3.5 wt. % NaCl for Different Immersion Times at Room Temperature.

Week	R_{pore}	**CPE$_1$ x10^{-10}**	n_1	R_{ct}	**CPE$_2$ x10^{-9}**	n_2	R_s	η
	GΩ.cm^2	s^n Ω^{-1}cm^{-2}		GΩ.cm^2	s^n Ω^{-1}cm^{-2}		Ω	%
1	47.0	2.65	0.93	46.2	2.90	0.99	406	99.9
2	61.4	1.76	0.87	57.3	2.27	0.99	477	99.9
3	73.1	1.65	0.93	74.6	2.13	0.87	480	99.9
4	75.8	1.40	0.95	83.3	1.71	0.93	468	99.9

The values of the impedance parameters attained from the equivalent circuit (Figure 38 (a)) after fitting data from EIS analysis are tabulated in

Table 9. The parameters to quantify the impedance are pore resistance as Rpo, the capacitance associated with Rpo as CPE1 (Constant phase element), charge transfer resistance as Rct, the capacitance associated with Rct as CPE2, also called double layer

capacitance (constant phase elements), and solution resistance as Rs. The double layer capacitance is usually expressed by equation [231].

$$C_{dl} = Y_o * \omega^{n-1} \qquad \textit{Equation 3}$$

Where Y_o is the CPE2 (Constant phase element), ω is the angular frequency, and n is the factor that decides the capacitor and resistive behavior of the coatings. When n=0, the CPE suggests the resistive behavior, when n=1 the CPE represents the ideal capacitance behavior. Since in our coatings, n is nearly equal to the ideal capacitor behavior, that's why CPE is also represented as C_{dl}. The values attained after fitting data suggested that the modified coatings exhibited excellent corrosion resistance. The investigation of the electrochemical properties of both blank and modified PU coatings reveals distinct trends indicative of their corrosion protection efficacy over time. Initially, the blank PU coatings demonstrate a diminishing resistance against corrosion, as evidenced by a decline in both the R_{po} and R_{ct} values after 4 week of immersion it decreased to 0.001 GΩ.cm² and 0.002 GΩ.cm² respectively. This decay is primarily attributed to the inherent porosity within the PU matrix, facilitating the ingress of electrolyte and subsequent chloride ion penetration, thus compromising the coatings' barrier properties. The consequential increase in capacitance suggests heightened electrolyte uptake, exacerbating coating delamination. Conversely, the modified PU coatings exhibit a progressive enhancement in corrosion resistance parameters over the immersion period. Notably, both R_{po} and R_{ct} values exhibit an upward trajectory from 32.29 GΩ.cm^2 to 75.83 GΩ.cm^2 (R_{po}) and 39.19 GΩ.cm^2 to 83.31 GΩ.cm^2 (R_{ct}) after 7 weeks of immersion, indicative of superior corrosion inhibition. This improvement is attributed to the synergistic effect of the corrosion inhibitor MS30 and the carrier TiO_2, which collectively impede the ingress of electrolytes and mitigate chloride ion penetration. Consequently, the reduced electrolyte uptake is reflected in decreased

capacitance values (CPE), underscoring the sustained integrity of the modified coatings.

Salt spray analysis

The scratched blank PU and modified PU based coated steel substrates were subjected to continuous immersion in saline solution (3.5 wt. % NaCl solution) for 7 weeks. The salt spray analysis was performed to study the corrosion inhibition performance of steel substrate without applying external voltage and under salt environmental conditions. Figure 39 presents photographic images of coated steel substrates immersed in NaCl solution over various time intervals, illustrating the degradation process of blank polyurethane (PU) coatings. On the first immersion day, the PU coatings appeared neat and intact, showing no visible signs of damage or corrosion. After one week of immersion, the coatings remained undamaged, with no apparent signs of corrosion. However, deposition of salt particles was observed on the scratched area. By the third week of immersion, noticeable deterioration and discoloration of the coatings had commenced. Corrosion was evident on the left scratch, and substantial rust formed on the coating's surface. This degradation is attributed to the penetration of the electrolyte through the scratch, which likely created conductive paths within the coating, leading to further damage. After five weeks of immersion, delamination of the coatings was observed, particularly from the corners and edges of the substrates. The corrosion propagated from the initial scratch towards the top of the coating. By the seventh week, the extent of rust and corroded areas had significantly increased, with more pronounced delamination from the edges. These observations indicate that the blank PU coatings exhibited limited durability during prolonged immersion in NaCl solution. Although the coatings maintained their integrity during the first week, significant deterioration occurred subsequently, resulting in poor corrosion resistance. The findings from the

electrochemical impedance spectroscopy (EIS) analysis corroborate these visual assessments, further demonstrating the insufficient long-term protective performance of the blank PU coatings.

For the modified polyurethane (PU) coatings incorporating PU/TiO_2/MS30, Figure 39 depicts their performance during immersion in NaCl solution, revealing a notable enhancement compared to blank PU coatings. On the first day, the PU/TiO_2/MS30 coatings appeared intact and pristine, like the blank PU coatings. SEM images showed an average scratch width of 29.15 μm. After one week of immersion, the coatings remained unchanged, performing well. Notably, the scratch width reduced to an average of 19.05 μm. This trend persisted through the third week, with the coatings still providing a robust barrier against the corrosive medium, as evidenced by a further reduction in scratch width to an average of 11.35 μm. By the fifth week, slight corrosion discoloration was observed on the right side of the scratch, indicating the initiation but limited propagation of corrosion. SEM images confirmed that the scratch width remained relatively stable on average. After seven weeks of immersion, the corrosion spot on the right side of the coating had not propagated further. The average scratch width decreased to 10.33 μm, demonstrating the coating's continued protective efficacy. The sustained protection is attributed to the synergistic corrosion inhibition performance of the TiO_2 and MS30. The effective release of the inhibitor and carrier from the coating matrix likely contributed to maintaining the integrity of the coating and preventing significant corrosion propagation. These findings underscore the enhanced durability and corrosion resistance of the PU/TiO_2/MS30 coatings, highlighting their superior performance in aggressive environments compared to blank PU coatings. The results suggest that incorporating TiO_2/MS30 into PU coatings significantly improves their long-term protective capabilities, providing a green and

effective barrier against corrosive elements.

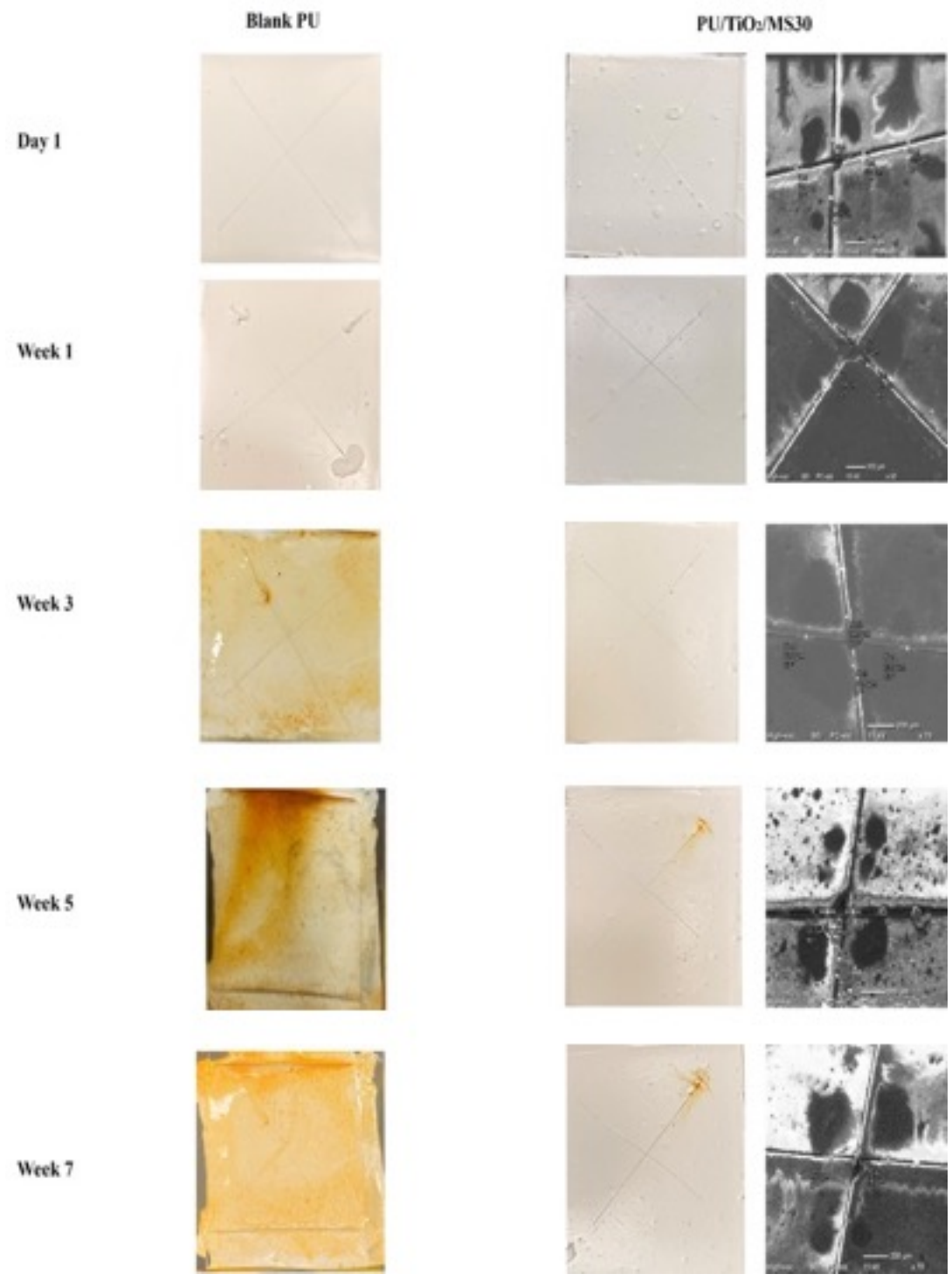

Figure 39: Photographs of scratched PU-based coated steel substrates subjected to 3.5

wt. % NaCl solution in the chamber for the period of 7 weeks at room temperature (25 °C).

Proposed corrosion inhibition mechanism

The PU/TiO_2/MS30-based coatings function as advanced corrosion-resistant layers, integrating TiO_2/MS30 particles into the PU matrix to provide active and passive protection for steel substrates. Figure 40 illustrates the schematic representation of the proposed corrosion inhibition mechanism utilized by the PU/TiO_2/MS30 coatings. These coatings enhance the PU matrix's barrier properties by obstructing the corrosive electrolytes' diffusion pathways, thereby hindering their access to the steel/coating interface. This effective barrier formation underscores the excellent compatibility of TiO_2/MS30 particles within the PU matrix.

Upon scratching the blank PU coatings, the coatings exhibited a limited ability to resist prolonged immersion in corrosive environments, leading to the rapid progression of corrosion on the steel substrate. This analysis emphasizes the need for improved protective measures or alternative modified coatings to enhance the corrosion resistance of steel substrates in harsh environments.

When corrosion initiates on steel in an electrolyte such as NaCl solution, a series of electrochemical reactions typically occur. The primary anodic reaction involves the dissolution of iron:

$$Fe \rightarrow Fe^{2+} + 2e^{-} \text{ (Anodic reaction)} \qquad \text{Equation 4}$$

Simultaneously, the cathodic reaction involves the reduction of oxygen in the presence of water:

$$O_2 + 2H_2O + 4e^{-} \rightarrow 4OH^{-} \text{ (Cathodic reaction)} \qquad \text{Equation 5}$$

These reactions collectively lead to a localized decrease in pH at the defect site,

fostering the creation of micro-anodic and cathodic regions. This environment stimulates the dissociation of TiO_2 [232] following the reaction:

$$TiO_2 + 4H^+ \rightarrow Ti^{4+} + 2H_2O \qquad \textit{Equation 6}$$

The dissociated titanium ions (Ti^{4+}) subsequently interact with hydroxide ions (OH^-) produced during the cathodic reaction, resulting in the formation of titanium hydroxide:

$$Ti^{4+} + 4OH \rightarrow Ti(OH)_4 \qquad \textit{Equation 7}$$

$Ti(OH)_4$ formation establishes a protective passive layer on the cathodic regions, mitigating further corrosion. Concurrently, the dissociation of TiO_2 triggers the release of MS30 particles. These MS30 particles interact with Fe^{2+} ions generated at the anodic sites, forming an inhibitive film on the steel surface. This film is formed due to the adsorption of MS30, facilitated by the interaction between nitrogen atoms in MS30 and Fe^{2+} ions. The Fe^{2+} ions possess vacant d-orbitals, which become occupied by nitrogen atoms, rendering the Fe^{2+} ions unavailable for further reaction with hydroxide or oxygen to form corrosive products. at both cathodic and anodic regions leads to synergistic corrosion inhibition protection, thus enhancing the barrier properties of PU coatings.

This dual protective mechanism, involving both cathodic and anodic inhibition, results in synergistic corrosion inhibition, thereby significantly enhancing the barrier properties of the PU coatings. The presence of TiO_2/MS30 particles effectively blocks the diffusion pathways for corrosive species, while the active release and interaction of MS30 with corrosion products ensure continued protection even when the coating is damaged. Consequently, the PU/TiO_2/MS30 coatings exhibit superior corrosion resistance, maintaining the integrity of the steel substrate over extended periods of immersion in aggressive environments.

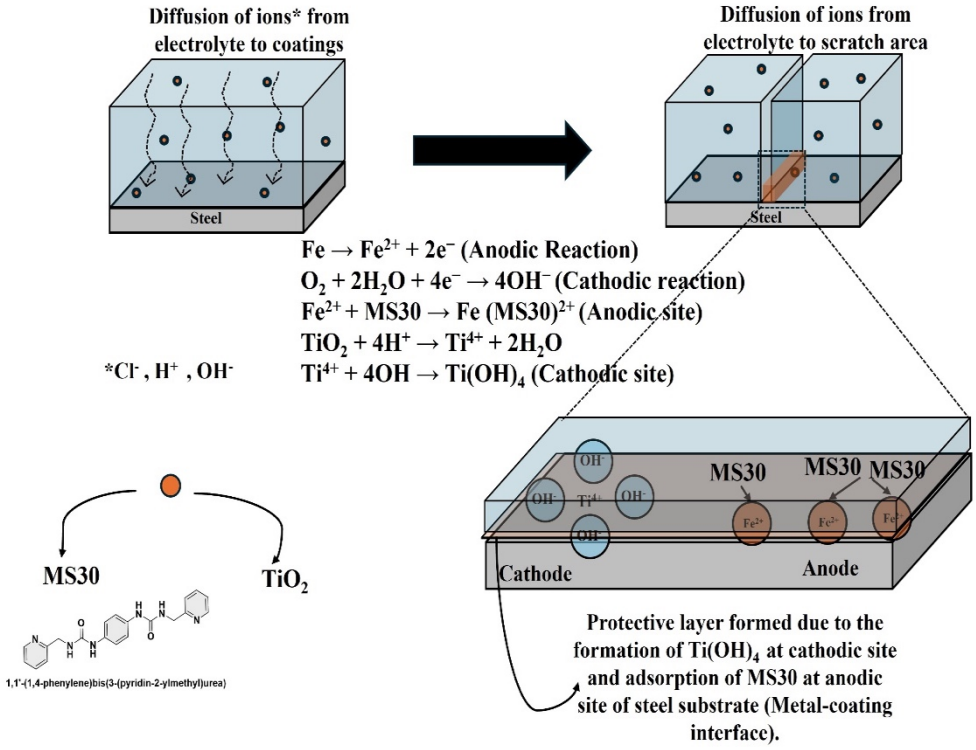

Figure 40: Schematics of the proposed self-healing mechanism of modified PU based coatings (PU/TiO_2/MS30).

Chapter 5: Conclusion

The field of polyurethane coatings is emphasized as a crucial component in corrosion prevention, regardless of its diversity. Thanks to their constantly growing number of formulations, application methods, and performance improvements, polyurethane coatings serve as adaptable guardians in a variety of industries. Investigating aquatic and biobased varieties demonstrates a dedication to sustainability, in line with the changing needs of a responsible global environment.

Upon navigating the complex chemistry, application techniques, and performance assessment standards, the resilience of polyurethane coatings is apparent. The ability of these coatings to heal itself further emphasises their versatility and toughness, indicating long-term durability in a variety of shifting environmental conditions.

Applications from the real world clearly show how polyurethane coatings can be used to protect important assets in the energy, automobiles, textile, and marine industries. On the other hand, progress necessitates acknowledging the challenges and obstacles that have been identified to facilitate potential development and research initiatives.

This thesis acts as a resource collection and a spur for ongoing innovation in the quest for superior corrosion protection. We map out a path towards more efficient, resilient, and sustainable polyurethane coatings with an eye towards challenges and future directions, guaranteeing a strengthened defence against the ubiquitous threat of corrosion.

The field of polyurethane coatings continues to be dynamic, offering continued advancements to explore long-lasting, eco-friendly, and highly effective corrosion even as industries and challenges change.

In this work, we have successfully synthesized fGO with the help of the Silane group.

Then, we made coatings by adding 1 wt% of fGO into the PU matrix. Incorporating fGO into PU coatings was systematically analyzed using various characterization techniques, including SEM, TEM, BET, TGA, FTIR, XRD, and electrochemical tests, along with performance tests like salt spray analysis.The SEM and TEM analyses confirmed the successful intercalation of TiO_2 nanoparticles within the GO layers, resulting in a well-dispersed and uniformly distributed composite material. This structural integration was further supported by EDS analysis, which consistently showed the presence of Ti, C, and O, N, and Si elements, confirming the effective production of fGO.TGA analysis showed that fGO had significantly improved thermal stability compared to pristine GO, due to the incorporation of TiO_2 nanoparticles. fGO exhibited a total weight loss of 25%, while pristine GO showed 53%. FTIR spectroscopy provided insights into the chemical bonding and functional groups present in the materials, demonstrating the formation of strong bonds between GO and TiO_2, which contribute to the structural integrity and stability of the composite.XRD analysis confirmed the crystalline nature of the TiO_2 nanoparticles and their successful incorporation into the GO matrix, further validating the effectiveness of the functionalization process. The electrochemical analysis indicated that the fGO modified PU coatings exhibited superior corrosion resistance with a maximum value of 0.821 T□-cm^2. Salt spray tests evaluated the coatings' practical performance. These findings show that fGO-modified PU coatings offer enhanced thermal stability, structural integrity, and corrosion resistance, making them a promising solution for extending the lifespan of steel structures in corrosive environments. This approach presents significant potential for applications in advanced protective coatings.

The PU/TiO_2/MS30-based coatings were successfully synthesized and deposited on steel substrate. Morphological and structural results obtained through TEM, FTIR and

BET confirmed the successful loading and interaction of inhibitor in TiO_2. TGA analysis results confirmed the excellent thermal stability of the synthesized particles upto 800°C. TGA results also demonstrated that almost 46% w/w of MS30 has been loaded into TiO_2. DSC results suggested that the introduction of TiO_2 and MS30 enhances the crosslinking within the PU matrix, resulting in improved thermal stability and mechanical properties. Tafel analysis results demonstrated that the inhibition efficiency of steel substrate has been enhanced to 53% in presence of TiO_2/MS30 particles. The Tafel results were also endorsed by Raman analysis which confirmed the interaction of inhibitor with steel substrate. EIS analysis results suggested that coatings modified with TiO2/MS30 resulted in superior corrosion inhibition with 99.9% of inhibition efficiency as compared to blank PU coatings after 4 weeks of immersion in 3.5 wt.% NaCl solution. Salt spray analysis results demonstrated the enhanced durability and corrosion resistance of the PU/TiO_2/MS30 coatings, highlighting their superior performance in aggressive environments compared to blank PU coatings.The PU/TiO2/MS30-based coatings provide a robust, green and multi-faceted approach to corrosion protection, combining the physical barrier properties of the PU matrix with the active and passive inhibition mechanisms offered by TiO_2 and MS30 particles. This advanced protective system highlights the potential of modified PU coatings to significantly enhance the durability and corrosion resistance of steel substrates in challenging environments.

Challenges and future directions

The issues and prospects for polyurethane coatings include resolving health and safety and environmental concerns, optimizing performance attributes, integrating intelligent features, and adhering to changing legal requirements. The goal of ongoing research and development in these fields is to increase the sustainability, functionality, and overall performance of polyurethane coatings to unprecedented levels. The utilization

of polyurethane coatings for safeguarding diverse surfaces such as metals, glass, wood, plastics, and related materials has been increasing. Consequently, steel is coated with polyurethane-based coatings to provide enhanced wear resistance, effective corrosion protection, and superior barrier properties. The nanocomposite coatings exhibit better protection for steel with prolonged immersion times, although there is a lack of comprehensive exploration into their microhardness. Evaluating the microhardness properties of coated systems is crucial to determine their suitability for specific substrates, as variations in these parameters may reveal a significant correlation with corrosion protection features. Moreover, while polyurethane coatings are commonly used in various technical applications as topcoats, there is a notable absence of polyurethane nanocomposite coatings in these applications. The substitution of polyurethane with polyurethane nanocomposite coatings in automotive and aerospace industries could extend the lifespan of these coatings. Different micron-sized particles or additives can be incorporated into the base matrix to impart hydrophobic nature and corrosion protection, which might be used to build multi-functional coating systems; however, the practical applicability of these materials is limited due to their high cost. Furthermore, because they are so delicate, it seems difficult to synthesize very hydrophobic coatings with outstanding abrasion resistance because they are readily harmed by mechanical abrasion after a hydrophobic loss. The primary challenge in this context is the degradation of polyurethane coating systems caused by weathering during natural outdoor exposure. Exposure to environmental factors like temperature, Ultraviolet rays, water content, and chemicals can lead to the deterioration of polyurethane, generating free radicals that affect polymeric chains. As a result, the outdoor service life of polymers is constrained by weathering. Various physical methods are utilized to evaluate the weathering properties of polyurethane and

nanocomposite coatings. Progress in this area can be made by improving and designing polyurethane nanocomposite coatings with increased resistance to weathering. Opting for different coating techniques such as the solution method, solvent-free method, spraying, and advanced methods like spin coating and inkjet printing can greatly improve the overall coating features. Conventional polyurethane (PU) coatings often lack sufficient heat resistance and experience significant pyrolysis at temperatures exceeding 200°C. These drawbacks restrict the use of traditional UV-cured polyurethane coatings. Consequently, attempts should be undertaken to address the standard UV-cured PUs' low hardness and inadequate heat resistance. Emphasis should be placed on developing polyurethane nanocomposite coatings with UV radiation resistance and high-temperature stability. The integration of nanoparticles in polyurethane strengthens the nanocomposite structure against weathering. Technologies like polyurethane-carbon nanotubes and polyurethane-graphene coatings show promise in the industrial coating market due to their high performance in challenging conditions. WPU coatings' non-toxicity, environmental friendliness, adaptability, UV and chemical resistance, and superior mechanical qualities have all contributed to their increased popularity. Yet, diverse types of nanoparticles must be employed to enhance the resistance to solvents, tensile strength and thermal stability of polyurethane coatings. In order to further advance the performance of polyurethane based coatings, it is essential to explore and develop a deeper understanding of self-healing mechanisms within these systems. Self-healing coatings have emerged as a promising solution for enhancing the long-term durability and corrosion resistance of steel substrates, particularly in harsh industrial environments like the oil and gas industry. For PU-based coatings, incorporating self-healing properties can be achieved through the integration of microcapsules, nanocarriers, or intrinsic polymeric networks

that enable autonomous recovery of mechanical and functional damage. Future work should focus on investigating the synergy between polyurethane matrices and smart additives such as encapsulated healing agents, nanocontainers with corrosion inhibitors, or supramolecular structures that allow reversible crosslinking. A detailed analysis of the healing kinetics, efficiency, and repeatability under real-world conditions (e.g., salt spray exposure, cyclic corrosion tests) will be essential to assess the practicality and durability of these systems. Understanding the relationship between polymer matrix design, filler distribution, and the triggering mechanisms (e.g., mechanical stress, pH, or environmental stimuli) can pave the way for designing PU coatings with self-healing capabilities that significantly prolong the service life of coated steel structures. Areas of research yet to be explored in polyurethane nanocomposite coatings encompass potential applications in the sports sectors, aerospace, energy devices, automotive, and electronics.

References

[1] M. Honarvar Nazari, Y. Zhang, A. Mahmoodi, G. Xu, J. Yu, J. Wu, X. Shi, Nanocomposite organic coatings for corrosion protection of metals: A review of recent advances, Prog Org Coat 162 (2022) 106573. https://doi.org/10.1016/J.PORGCOAT.2021.106573.

[2] H. Xu, Y. Zhang, A Review on Conducting Polymers and Nanopolymer Composite Coatings for Steel Corrosion Protection, Coatings 2019, Vol. 9, Page 807 9 (2019) 807. https://doi.org/10.3390/COATINGS9120807.

[3] M. Cui, B. Wang, Z. Wang, Nature-Inspired Strategy for Anticorrosion, Adv Eng Mater 21 (2019). https://doi.org/10.1002/ADEM.201801379.

[4] M. Salzano de Luna, Recent Trends in Waterborne and Bio-Based Polyurethane Coatings for Corrosion Protection, Adv Mater Interfaces 9 (2022) 2101775. https://doi.org/10.1002/ADMI.202101775.

[5] P. Vijayan, M. Al-Maadeed, materials Self-Repairing Composites for Corrosion Protection: A Review on Recent Strategies and Evaluation Methods, (2016). https://doi.org/10.3390/ma12172754.

[6] E. Bowman, N. Thompson, D. Gl, O. Moghissi, M. Gould, J. Payer, Project Manager, (2016).

[7] F.N. Jones, M.E. Nichols, S.P. Pappas, Corrosion Protection by Coatings, Organic Coatings (2017) 99–114. https://doi.org/10.1002/9781119337201.CH7.

[8] M.F. Montemor, Functional and smart coatings for corrosion protection: A review of recent advances, Surf Coat Technol 258 (2014) 17–37. https://doi.org/10.1016/J.SURFCOAT.2014.06.031.

[9] M. Salzano de Luna, Recent Trends in Waterborne and Bio-Based Polyurethane

Coatings for Corrosion Protection, Adv Mater Interfaces 9 (2022) 2101775. https://doi.org/10.1002/ADMI.202101775.

[10] A. Das, P. Mahanwar, A brief discussion on advances in polyurethane applications, Advanced Industrial and Engineering Polymer Research 3 (2020) 93–101. https://doi.org/10.1016/J.AIEPR.2020.07.002.

[11] S. Rabbani, E. Bakhshandeh, R. Jafari, G. Momen, Superhydrophobic and icephobic polyurethane coatings: Fundamentals, progress, challenges and opportunities, Prog Org Coat 165 (2022) 106715. https://doi.org/10.1016/J.PORGCOAT.2022.106715.

[12] G. Yeligbayeva, M. Khaldun, A.A. Alfergani, Zh. Tleugaliyeva, A. Karabayeva, L. Bekbayeva, D. Zhetpisbay, N. Shadin, Z. Atabekova, Polyurethane as a versatile polymer for coating and anti-corrosion applications: A review, Kompleksnoe Ispolzovanie Mineralnogo Syra = Complex Use of Mineral Resources 331 (2024) 21–41. https://doi.org/10.31643/2024/6445.36.

[13] What is Polyurethane? Composition, Preparation, Properties, Uses, and FAQs, (n.d.). https://byjus.com/chemistry/polyurethane/ (accessed August 19, 2024).

[14] A. Trentin, A. Pakseresht, A. Duran, Y. Castro, D. Galusek, Electrochemical Characterization of Polymeric Coatings for Corrosion Protection: A Review of Advances and Perspectives, Polymers (Basel) 14 (2022). https://doi.org/10.3390/POLYM14122306.

[15] Stages and Types of Steel Corrosion, (n.d.). https://www.huyett.com/blog/steel-corrosion (accessed October 18, 2023).

[16] (10) (PDF) The Principle Mechanisms of Corrosion, (n.d.). https://www.researchgate.net/publication/340948691_The_Principle_Mechanisms_of_Corrosion (accessed October 18, 2023).

[17] G. Lazorenko, A. Kasprzhitskii, T. Nazdracheva, Anti-corrosion coatings for protection of steel railway structures exposed to atmospheric environments: A review, Constr Build Mater 288 (2021) 123115. https://doi.org/10.1016/J.CONBUILDMAT.2021.123115.

[18] S.R. Taylor, Coatings for Corrosion Protection: Organic, Encyclopedia of Materials: Science and Technology (2001) 1274–1279. https://doi.org/10.1016/B0-08-043152-6/00240-0.

[19] G.E.C. Bell, S. Vp, BASIC MECHANISMS OF CORROSION AND CORROSION CONTROL FOR WATER AND WASTEWATER SYSTEMS, (n.d.).

[20] A. Das, P. Mahanwar, A brief discussion on advances in polyurethane applications, Advanced Industrial and Engineering Polymer Research 3 (2020) 93–101. https://doi.org/10.1016/J.AIEPR.2020.07.002.

[21] X. Jing, X. Li, Y. Di, Y. Zhao, J. Wang, M. Kang, Q. Li, Effect of the amide units in soft segment and urea units in hard segment on microstructures and physical properties of polyurethane elastomer, Polymer (Guildf) 233 (2021) 124205. https://doi.org/10.1016/J.POLYMER.2021.124205.

[22] C. Alkan, E. Günther, S. Hiebler, Ö.F. Ensari, D. Kahraman, Polyurethanes as solid-solid phase change materials for thermal energy storage, Solar Energy 86 (2012) 1761–1769. https://doi.org/10.1016/J.SOLENER.2012.03.012.

[23] X. Jin, N. Guo, Z. You, Y. Tan, Design and Performance of Polyurethane Elastomers Composed with Different Soft Segments, Materials 2020, Vol. 13, Page 4991 13 (2020) 4991. https://doi.org/10.3390/MA13214991.

[24] F.M. De Souza, P.K. Kahol, R.K. Gupta, Introduction to Polyurethane Chemistry, ACS Symposium Series 1380 (2021) 1–24.

https://doi.org/10.1021/BK-2021-1380.CH001/ASSET/IMAGES/LARGE/BK-2020-00517M_G020.JPEG.

[25] F.M. De Souza, P.K. Kahol, R.K. Gupta, Introduction to Polyurethane Chemistry, ACS Symposium Series 1380 (2021) 1–24. https://doi.org/10.1021/BK-2021-1380.CH001/ASSET/IMAGES/LARGE/BK-2020-00517M_G020.JPEG.

[26] S. Ahmad, S. Habib, M. Nawaz, R.A. Shakoor, R. Kahraman, T. Mohammed, A. Tahtamouni, The role of polymeric matrices on the performance of smart self-healing coatings: A review, (n.d.). https://doi.org/10.1016/j.jiec.2023.04.024.

[27] G. Avar, U. Meier-Westhues, H. Casselmann, D. Achten, Polyurethanes, Polymer Science: A Comprehensive Reference: Volume 1-10 1–10 (2012) 411–441. https://doi.org/10.1016/B978-0-444-53349-4.00275-2.

[28] O. Bayer, Das Di-Isocyanat-Polyadditionsverfahren (Polyurethane), Angewandte Chemie 59 (1947) 257–272. https://doi.org/10.1002/ANGE.19470590901.

[29] J. Li, J. Cui, J. Yang, Y. Li, H. Qiu, J. Yang, Reinforcement of graphene and its derivatives on the anticorrosive properties of waterborne polyurethane coatings, Compos Sci Technol 129 (2016) 30–37. https://doi.org/10.1016/J.COMPSCITECH.2016.04.017.

[30] F.E. Golling, R. Pires, A. Hecking, J. Weikard, F. Richter, K. Danielmeier, D. Dijkstra, Polyurethanes for coatings and adhesives – chemistry and applications, Polym Int 68 (2019) 848–855. https://doi.org/10.1002/PI.5665.

[31] F. Zafar, A. Ghosal, E. Sharmin, R. Chaturvedi, N. Nishat, A review on cleaner production of polymeric and nanocomposite coatings based on waterborne polyurethane dispersions from seed oils, Prog Org Coat 131 (2019) 259–275.

https://doi.org/10.1016/J.PORGCOAT.2019.02.014.

[32] M. Dai, J. Wang, Y. Zhang, Improving water resistance of waterborne polyurethane coating with high transparency and good mechanical properties, Colloids Surf A Physicochem Eng Asp 601 (2020) 124994. https://doi.org/10.1016/J.COLSURFA.2020.124994.

[33] B. Zhao, R. Jia, Preparation of super-hydrophobic films based on waterborne polyurethane and their hydrophobicity characteristics, Prog Org Coat 135 (2019) 440–448. https://doi.org/10.1016/J.PORGCOAT.2019.06.025.

[34] Y. Ahmadi, S. Ahmad, Recent Progress in the Synthesis and Property Enhancement of Waterborne Polyurethane Nanocomposites: Promising and Versatile Macromolecules for Advanced Applications, Polymer Reviews 60 (2020) 226–266. https://doi.org/10.1080/15583724.2019.1673403.

[35] M. Joshi, B. Adak, B.S. Butola, Polyurethane nanocomposite based gas barrier films, membranes and coatings: A review on synthesis, characterization and potential applications, Prog Mater Sci 97 (2018) 230–282. https://doi.org/10.1016/J.PMATSCI.2018.05.001.

[36] X. Sheng, S. Li, H. Huang, Y. Zhao, Y. Chen, L. Zhang, D. Xie, Anticorrosive and UV-blocking waterborne polyurethane composite coating containing novel two-dimensional Ti3C2 MXene nanosheets, J Mater Sci 56 (2021) 4212–4224. https://doi.org/10.1007/S10853-020-05525-2/FIGURES/11.

[37] J. Li, L. Gan, Y. Liu, S. Mateti, W. Lei, Y. Chen, J. Yang, Boron nitride nanosheets reinforced waterborne polyurethane coatings for improving corrosion resistance and antifriction properties, Eur Polym J 104 (2018) 57–63. https://doi.org/10.1016/J.EURPOLYMJ.2018.04.042.

[38] P.; Yi, J.; Mo, R.; Liu, B.; Fan, K.; Xiao, J.; Gao, H. Zhou, P. Yi, J. Mo, R. Liu,

B. Fan, K. Xiao, J. Gao, H. Zhou, Study on Corrosion Behavior of Waterborne Polyurethane Coating with High Thermal Conductivity, Applied Sciences 2022, Vol. 12, Page 2021 12 (2022) 2021. https://doi.org/10.3390/APP12042021.

[39] X. Wang, L. Hou, L.L. Xu, X. Li, H. Jiang, W.J. Zhou, Preparation and Corrosion Resistance of AKT-Waterborne Polyurethane Coating, Int J Electrochem Sci 15 (2020) 1450–1464. https://doi.org/10.20964/2020.02.28.

[40] J. Xu, F. Gao, H. Wang, R. Dai, S. Dong, H. Wang, Organic/inorganic hybrid waterborne polyurethane coatings with self-healing properties for anticorrosion application, Prog Org Coat 174 (2023) 107244. https://doi.org/10.1016/J.PORGCOAT.2022.107244.

[41] G. Christopher, M.A. Kulandainathan, G. Harichandran, Biopolymers nanocomposite for material protection: Enhancement of corrosion protection using waterborne polyurethane nanocomposite coatings, Prog Org Coat 99 (2016) 91–102. https://doi.org/10.1016/J.PORGCOAT.2016.05.012.

[42] M. Akbarian, M.E. Olya, M. Mahdavian, M. Ataeefard, Effects of nanoparticulate silver on the corrosion protection performance of polyurethane coatings on mild steel in sodium chloride solution, Prog Org Coat 77 (2014) 1233–1240. https://doi.org/10.1016/J.PORGCOAT.2014.03.023.

[43] M. Dai, J. Wang, Y. Zhang, Improving water resistance of waterborne polyurethane coating with high transparency and good mechanical properties, Colloids Surf A Physicochem Eng Asp 601 (2020) 124994. https://doi.org/10.1016/J.COLSURFA.2020.124994.

[44] B. Zhao, R. Jia, Preparation of super-hydrophobic films based on waterborne polyurethane and their hydrophobicity characteristics, Prog Org Coat 135 (2019) 440–448. https://doi.org/10.1016/J.PORGCOAT.2019.06.025.

[45] X. Sheng, S. Li, H. Huang, Y. Zhao, Y. Chen, L. Zhang, D. Xie, Anticorrosive and UV-blocking waterborne polyurethane composite coating containing novel two-dimensional Ti3C2 MXene nanosheets, J Mater Sci 56 (2021) 4212–4224. https://doi.org/10.1007/S10853-020-05525-2/FIGURES/11.

[46] J. Li, L. Gan, Y. Liu, S. Mateti, W. Lei, Y. Chen, J. Yang, Boron nitride nanosheets reinforced waterborne polyurethane coatings for improving corrosion resistance and antifriction properties, Eur Polym J 104 (2018) 57–63. https://doi.org/10.1016/J.EURPOLYMJ.2018.04.042.

[47] P.; Yi, J.; Mo, R.; Liu, B.; Fan, K.; Xiao, J.; Gao, H. Zhou, P. Yi, J. Mo, R. Liu, B. Fan, K. Xiao, J. Gao, H. Zhou, Study on Corrosion Behavior of Waterborne Polyurethane Coating with High Thermal Conductivity, Applied Sciences 2022, Vol. 12, Page 2021 12 (2022) 2021. https://doi.org/10.3390/APP12042021.

[48] X. Wang, L. Hou, L.-L. Xu, X. Li, H. Jiang, W.-J. Zhou, Preparation and Corrosion Resistance of AKT-Waterborne Polyurethane Coating, Int. J. Electrochem. Sci 15 (2020) 1450–1464. https://doi.org/10.20964/2020.02.28.

[49] E. Yousefi, A. Dolati, H. Najafkhani, Preparation of robust antistatic waterborne polyurethane coating, Prog Org Coat 139 (2020) 105450. https://doi.org/10.1016/J.PORGCOAT.2019.105450.

[50] H. Khatoon, S. Iqbal, S. Ahmad, Covalently functionalized ethylene diamine modified graphene oxide poly-paraphenylene diamine dispersed polyurethane anticorrosive nanocomposite coatings, Prog Org Coat 150 (2021) 105966. https://doi.org/10.1016/J.PORGCOAT.2020.105966.

[51] J. Cui, J. Xu, J. Li, H. Qiu, S. Zheng, J. Yang, A crosslinkable graphene oxide in waterborne polyurethane anticorrosive coatings: Experiments and simulation, Compos B Eng 188 (2020) 107889.

https://doi.org/10.1016/J.COMPOSITESB.2020.107889.

[52] H.J. Song, Z.Z. Zhang, X.H. Men, Tribological behavior of polyurethane-based composite coating reinforced with TiO2 nanotubes, Eur Polym J 44 (2008) 1012–1022. https://doi.org/10.1016/J.EURPOLYMJ.2008.02.004.

[53] H. Wang, J. Xu, X. Du, Z. Du, X. Cheng, H. Wang, A self-healing polyurethane-based composite coating with high strength and anti-corrosion properties for metal protection, Compos B Eng 225 (2021) 109273. https://doi.org/10.1016/J.COMPOSITESB.2021.109273.

[54] M.J. Palimi, M. Rostami, M. Mahdavian, B. Ramezanzadeh, The Corrosion Protection Performance of the Polyurethane Coatings Containing Surface Modified Fe2O3 Nanoparticles, Corrosion 71 (2015) 1012–1026. https://doi.org/10.5006/1365.

[55] H.S. Karmakar, R. Arukula, A. Thota, R. Narayan, C.R.K. Rao, Polyaniline-grafted polyurethane coatings for corrosion protection of mild steel surfaces, J Appl Polym Sci 135 (2018) 45806. https://doi.org/10.1002/APP.45806.

[56] H. Wang, J. Xu, X. Du, H. Wang, X. Cheng, Z. Du, Stretchable and self-healing polyurethane coating with synergistic anticorrosion effect for the corrosion protection of stainless steels, Prog Org Coat 164 (2022) 106672. https://doi.org/10.1016/J.PORGCOAT.2021.106672.

[57] M.M. Ariffin, M.M. Aung, L.C. Abdullah, M.Z. Salleh, Assessment of corrosion protection and performance of bio-based polyurethane acrylate incorporated with nano zinc oxide coating, Polym Test 87 (2020) 106526. https://doi.org/10.1016/J.POLYMERTESTING.2020.106526.

[58] M.S. Pawar, A.S. Kadam, O.S. Yemul, Development of polyetheramide based corrosion protective polyurethane coating from mahua oil, Prog Org Coat 89

(2015) 143–149. https://doi.org/10.1016/J.PORGCOAT.2015.08.017.

[59] G. Christopher, M. Anbu Kulandainathan, G. Harichandran, Highly dispersive waterborne polyurethane/ZnO nanocomposites for corrosion protection, J Coat Technol Res 12 (2015) 657–667. https://doi.org/10.1007/S11998-015-9674-3/SCHEMES/1.

[60] Q. Mo, W. Li, H. Yang, F. Gu, Q. Chen, R. Yang, Water resistance and corrosion protection properties of waterborne polyurethane coating enhanced by montmorillonite modified with Ce3+, Prog Org Coat 136 (2019) 105213. https://doi.org/10.1016/J.PORGCOAT.2019.105213.

[61] J. V. Nardeli, C.S. Fugivara, M. Taryba, M.F. Montemor, S.J.L. Ribeiro, A. V. Benedetti, Novel healing coatings based on natural-derived polyurethane modified with tannins for corrosion protection of AA2024-T3, Corros Sci 162 (2020) 108213. https://doi.org/10.1016/J.CORSCI.2019.108213.

[62] J. Li, L. Gan, Y. Liu, S. Mateti, W. Lei, Y. Chen, J. Yang, Boron nitride nanosheets reinforced waterborne polyurethane coatings for improving corrosion resistance and antifriction properties, Eur Polym J 104 (2018) 57–63. https://doi.org/10.1016/J.EURPOLYMJ.2018.04.042.

[63] S.-P. Yu, H.-J. Tai, Sol-gel enhanced polyurethane coating for corrosion protection of 55% Al-Zn alloy-coated steel, 1 (n.d.) 3. https://doi.org/10.1007/s10965-021-02514-0.

[64] Y. Liang, D. Zhang, M. Zhou, Y. Xia, X. Chen, S. Oliver, S. Shi, L. Lei, Bio-based omniphobic polyurethane coating providing anti-smudge and anti-corrosion protection, Prog Org Coat 148 (2020) 105844. https://doi.org/10.1016/J.PORGCOAT.2020.105844.

[65] J. V. Nardeli, C.S. Fugivara, M. Taryba, M.F. Montemor, A. V. Benedetti,

Biobased self-healing polyurethane coating with Zn micro-flakes for corrosion protection of AA7475, Chemical Engineering Journal 404 (2021) 126478. https://doi.org/10.1016/J.CEJ.2020.126478.

[66] A.S. Alshabebi, M.M. Alrashed, L. El Blidi, S. Haider, Preparation of Bio-Based Polyurethane Coating from Citrullus colocynthis Seed Oil: Characterization and Corrosion Performance, Polymers 2024, Vol. 16, Page 214 16 (2024) 214. https://doi.org/10.3390/POLYM16020214.

[67] M. Jones, N. Dhore, E. Prasad, R. Narayan, C.R.K. Rao, A. Palanisamy, Studies on Biobased Non-Isocyanate Polyurethane Coatings with Potential Corrosion Resistance, Sustainable Chemistry 2023, Vol. 4, Pages 95-109 4 (2023) 95–109. https://doi.org/10.3390/SUSCHEM4010008.

[68] A.M. Patil, Synthesis and anticorrosion study of bio-based polyurethane coatings, Bulletin of Pure & Applied Sciences- Chemistry 38c (2019) 33. https://doi.org/10.5958/2320-320X.2019.00004.9.

[69] B. John, P.R. Rajimol, T.P.D. Rajan, S.K. Sahoo, Design and fabrication of nano textured superhydrophobic and anti-corrosive silane-grafted ZnO/bio-based polyurethane bilayer coating, Surf Coat Technol 451 (2022) 129036. https://doi.org/10.1016/J.SURFCOAT.2022.129036.

[70] A.M. Patil, H.D. Jirimali, V. V. Gite, R.N. Jagtap, Synthesis and performance of bio-based hyperbranched polyol in polyurethane coatings, Prog Org Coat 149 (2020) 105895. https://doi.org/10.1016/J.PORGCOAT.2020.105895.

[71] B. Chen, M. Liao, J. Sun, S. Shi, A novel biomass polyurethane-based composite coating with superior radiative cooling, anti-corrosion and recyclability for surface protection, Prog Org Coat 174 (2023) 107250. https://doi.org/10.1016/J.PORGCOAT.2022.107250.

[72] J. Wang, F. Seidi, Y. Huang, H. Xiao, Smart lignin-based polyurethane conjugated with corrosion inhibitor as bio-based anticorrosive sublayer coating, Ind Crops Prod 188 (2022) 115719. https://doi.org/10.1016/J.INDCROP.2022.115719.

[73] P. Alagi, R. Ghorpade, J.H. Jang, C. Patil, H. Jirimali, V. Gite, S.C. Hong, Functional soybean oil-based polyols as sustainable feedstocks for polyurethane coatings, Ind Crops Prod 113 (2018) 249–258. https://doi.org/10.1016/J.INDCROP.2018.01.041.

[74] Y. Liang, D. Zhang, M. Zhou, Y. Xia, X. Chen, S. Oliver, S. Shi, L. Lei, Bio-based omniphobic polyurethane coating providing anti-smudge and anti-corrosion protection, Prog Org Coat 148 (2020) 105844. https://doi.org/10.1016/J.PORGCOAT.2020.105844.

[75] T.H. Mekonnen, T. Haile, M. Ly, Hydrophobic functionalization of cellulose nanocrystals for enhanced corrosion resistance of polyurethane nanocomposite coatings, Appl Surf Sci 540 (2021) 148299. https://doi.org/10.1016/J.APSUSC.2020.148299.

[76] C. Zhang, H. Wang, W. Zeng, Q. Zhou, High Biobased Carbon Content Polyurethane Dispersions Synthesized from Fatty Acid-Based Isocyanate, Ind Eng Chem Res 58 (2019) 5195–5201. https://doi.org/10.1021/ACS.IECR.8B05936/ASSET/IMAGES/LARGE/IE-2018-05936B_0005.JPEG.

[77] S. Ahmad, S. Habib, M. Nawaz, R.A. Shakoor, R. Kahraman, T. Mohammed Al Tahtamouni, The role of polymeric matrices on the performance of smart self-healing coatings: A review, Journal of Industrial and Engineering Chemistry 124 (2023) 40–67. https://doi.org/10.1016/J.JIEC.2023.04.024.

[78] M. Abdolah Zadeh, S. van der Zwaag, S.J. Garcia, Self-healing corrosion-protective sol-gel coatings based on extrinsic and intrinsic healing approaches, Advances in Polymer Science 273 (2016) 185–218. https://doi.org/10.1007/12_2015_339/FIGURES/14.

[79] M. Abdolah Zadeh, S. van der Zwaag, S.J. Garcia, Self-healing corrosion-protective sol-gel coatings based on extrinsic and intrinsic healing approaches, Advances in Polymer Science 273 (2016) 185–218. https://doi.org/10.1007/12_2015_339/FIGURES/14.

[80] P. Panahi, S.N. Khorasani, R.A. Mensah, O. Das, R.E. Neisiany, A review of the characterization methods for self-healing assessment in polymeric coatings, Prog Org Coat 186 (2024) 108055. https://doi.org/10.1016/J.PORGCOAT.2023.108055.

[81] I. Azamian, S.R. Allahkaram, S. Rezaee, Autonomous-healing and smart anti-corrosion mechanism of polyurethane embedded with a novel synthesized microcapsule containing sodium dodecyl sulfate as a corrosion inhibitor, RSC Adv 12 (2022) 14299–14314. https://doi.org/10.1039/D2RA01131J.

[82] C. Xie, Y. Jia, M. Xue, Z. Yin, Y. Luo, Z. Hong, W. Liu, Anti-corrosion and self-healing behaviors of waterborne polyurethane composite coatings enhanced via chitosan-modified graphene oxide and phosphate intercalated hydrotalcite, Prog Org Coat 168 (2022) 106881. https://doi.org/10.1016/J.PORGCOAT.2022.106881.

[83] C. Lin, P. Ying, M. Huang, P. Zhang, T. Yang, G. Liu, T. Wang, J. Wu, V. Levchenko, Synthesis of robust and self-healing polyurethane/halloysite coating via in-situ polymerization, Journal of Polymer Research 28 (2021) 1–9. https://doi.org/10.1007/S10965-021-02742-4/FIGURES/6.

[84] A. Lutz, O. van den Berg, J. Wielant, I. De Graeve, H. Terryn, A multiple-action self-healing coating, Front Mater 2 (2016) 162922. https://doi.org/10.3389/FMATS.2015.00073/BIBTEX.

[85] Z. Wang, H. Liang, H. Yang, L. Xiong, J. Zhou, S. Huang, C. Zhao, J. Zhong, X. Fan, UV-curable self-healing polyurethane coating based on thiol-ene and Diels-Alder double click reactions, Prog Org Coat 137 (2019) 105282. https://doi.org/10.1016/J.PORGCOAT.2019.105282.

[86] M. Mahmoudian, E. Nozad, M.G. Kochameshki, M. Enayati, Preparation and investigation of hybrid self-healing coatings containing linseed oil loaded nanocapsules, potassium ethyl xanthate and benzotriazole on copper surface, Prog Org Coat 120 (2018) 167–178. https://doi.org/10.1016/J.PORGCOAT.2018.03.014.

[87] A. Mirmohseni, M. Akbari, R. Najjar, M. Hosseini, Self-healing waterborne polyurethane coating by pH-dependent triggered-release mechanism, J Appl Polym Sci 136 (2019) 47082. https://doi.org/10.1002/APP.47082.

[88] Y. Liang, D. Zhang, M. Zhou, Y. Xia, X. Chen, S. Oliver, S. Shi, L. Lei, Bio-based omniphobic polyurethane coating providing anti-smudge and anti-corrosion protection, Prog Org Coat 148 (2020) 105844. https://doi.org/10.1016/J.PORGCOAT.2020.105844.

[89] Y. Xu, S. Wang, Z. Liu, S. Lin, X. Cheng, H. Wang, Fabrication of organic/inorganic hybrid waterborne polyurethane coating based on CeNPs @mTi3C2Tx composites for anti-corrosion applications, Prog Org Coat 182 (2023) 107668. https://doi.org/10.1016/J.PORGCOAT.2023.107668.

[90] C. Yu, M. Salzano de Luna, A. Russo, I. Adamiano, F. Scherillo, Z. Wang, X. Zhang, H. Xia, M. Lavorgna, C. Yu, Z. Wang, X. Zhang, H. Xia, M. Salzano de

Luna, A. Russo, I. Adamiano, F. Scherillo, M. Lavorgna, Role of Diisocyanate Structure on Self-Healing and Anticorrosion Properties of Waterborne Polyurethane Coatings, Adv Mater Interfaces 8 (2021) 2100117. https://doi.org/10.1002/ADMI.202100117.

[91] M.M. Alrashed, S. Jana, M.D. Soucek, Corrosion performance of polyurethane hybrid coatings with encapsulated inhibitor, Prog Org Coat 130 (2019) 235–243. https://doi.org/10.1016/J.PORGCOAT.2019.02.005.

[92] Q. Mo, W. Li, H. Yang, F. Gu, Q. Chen, R. Yang, Water resistance and corrosion protection properties of waterborne polyurethane coating enhanced by montmorillonite modified with Ce3+, Prog Org Coat 136 (2019) 105213. https://doi.org/10.1016/J.PORGCOAT.2019.105213.

[93] L. Ni, S. Li, Y. Liu, X. Jiang, P. Cai, L. Feng, S. Zhang, X. Gao, Fabrication of active corrosion protection waterborne polyurethane coatings using cerium modified palygorskite nanocontainers, J Appl Polym Sci 138 (2021) 50899. https://doi.org/10.1002/APP.50899.

[94] S. Li, S. Wang, X. Du, H. Wang, X. Cheng, Z. Du, Waterborne polyurethane coating based on tannic acid functionalized Ce-MMT nanocomposites for the corrosion protection of carbon steel, Prog Org Coat 163 (2022) 106613. https://doi.org/10.1016/J.PORGCOAT.2021.106613.

[95] K.J. Jothi, S. Balachandran, K. Mohanraj, N. Prakash, A. Subhasri, P.S. Gopala Krishnan, K. Palanivelu, Fabrications of hybrid Polyurethane-Pd doped ZrO2 smart carriers for self-healing high corrosion protective coatings, Environ Res 211 (2022) 113095. https://doi.org/10.1016/J.ENVRES.2022.113095.

[96] H. Wang, J. Xu, X. Du, Z. Du, X. Cheng, H. Wang, A self-healing polyurethane-based composite coating with high strength and anti-corrosion properties for

metal protection, Compos B Eng 225 (2021) 109273. https://doi.org/10.1016/J.COMPOSITESB.2021.109273.

[97] H. Wang, J. Xu, H. Wang, X. Cheng, S. Wang, Z. Du, Mechanically robust inorganic/organic hybrid polyurethane films with excellent self-healing and anti-corrosion ability, Prog Org Coat 167 (2022) 106837. https://doi.org/10.1016/J.PORGCOAT.2022.106837.

[98] D. Lou, H. Chen, J. Liu, D. Wang, C. Wang, B.K. Jasthi, Z. Zhu, H. Younes, H. Hong, Improved Anticorrosion Properties of Polyurethane Nanocomposites by Ti 3 C 2 T x MXene/Functionalized Carbon Nanotubes for Corrosion Protection Coatings , ACS Appl Nano Mater 6 (2023) 12515–12525. https://doi.org/10.1021/ACSANM.3C02316/ASSET/IMAGES/LARGE/AN3C02316_0009.JPEG.

[99] S. Li, Y. Xu, F. Xiang, P. Liu, H. Wang, W. Wei, S. Dong, Enhanced corrosion resistance of self-healing waterborne polyurethane coating based on tannic acid modified cerium-montmorillonites composite fillers, Prog Org Coat 178 (2023) 107454. https://doi.org/10.1016/J.PORGCOAT.2023.107454.

[100] S. Liu, Z. Li, Q. Yu, Y. Qi, Z. Peng, J. Liang, Dual self-healing composite coating on magnesium alloys for corrosion protection, Chemical Engineering Journal 424 (2021) 130551. https://doi.org/10.1016/J.CEJ.2021.130551.

[101] J. V. Nardeli, C.S. Fugivara, M. Taryba, M.F. Montemor, A. V. Benedetti, Self-healing ability based on hydrogen bonds in organic coatings for corrosion protection of AA1200, Corros Sci 177 (2020) 108984. https://doi.org/10.1016/J.CORSCI.2020.108984.

[102] J.R. Xavier, Superior corrosion protection performance of polypdopamine-intercalated CeO2/polyurethane nanocomposite coatings on steel in 3.5% NaCl

solution, J Appl Electrochem 51 (2021) 959–975. https://doi.org/10.1007/S10800-021-01547-Z/FIGURES/15.

[103] K.J. Jothi, S. Balachandran, K. Mohanraj, N. Prakash, A. Subhasri, P.S. Gopala Krishnan, K. Palanivelu, Fabrications of hybrid Polyurethane-Pd doped ZrO2 smart carriers for self-healing high corrosion protective coatings, Environ Res 211 (2022) 113095. https://doi.org/10.1016/J.ENVRES.2022.113095.

[104] F. Li, Y. Ma, L. Chen, H. Li, H. Zhou, J. Chen, In-situ polymerization of polyurethane/aniline oligomer functionalized graphene oxide composite coatings with enhanced mechanical, tribological and corrosion protection properties, Chemical Engineering Journal 425 (2021) 130006. https://doi.org/10.1016/J.CEJ.2021.130006.

[105] J. V. Nardeli, C.S. Fugivara, M. Taryba, M.F. Montemor, A. V. Benedetti, Biobased self-healing polyurethane coating with Zn micro-flakes for corrosion protection of AA7475, Chemical Engineering Journal 404 (2021) 126478. https://doi.org/10.1016/J.CEJ.2020.126478.

[106] J. V. Nardeli, C.S. Fugivara, M. Taryba, M.F. Montemor, S.J.L. Ribeiro, A. V. Benedetti, Novel healing coatings based on natural-derived polyurethane modified with tannins for corrosion protection of AA2024-T3, Corros Sci 162 (2020) 108213. https://doi.org/10.1016/J.CORSCI.2019.108213.

[107] M.M. Ariffin, M.M. Aung, L.C. Abdullah, M.Z. Salleh, Assessment of corrosion protection and performance of bio-based polyurethane acrylate incorporated with nano zinc oxide coating, Polym Test 87 (2020) 106526. https://doi.org/10.1016/J.POLYMERTESTING.2020.106526.

[108] X. Li, Z. Xue, W. Sun, J. Chu, Q. Wang, L. Tong, K. Wang, Bio-inspired self-healing MXene/polyurethane coating with superior active/passive anticorrosion

performance for Mg alloy, Chemical Engineering Journal 454 (2023) 140187. https://doi.org/10.1016/J.CEJ.2022.140187.

[109] P. Haghdadeh, M. Ghaffari, B. Ramezanzadeh, G. Bahlakeh, M.R. Saeb, Polyurethane coatings reinforced with 3-(triethoxysilyl)propyl isocyanate functionalized graphene oxide nanosheets: Mechanical and anti-corrosion properties, Prog Org Coat 136 (2019) 105243. https://doi.org/10.1016/J.PORGCOAT.2019.105243.

[110] M.K. Meena, B.K. Tudu, A. Kumar, B. Bhushan, Development of polyurethane-based superhydrophobic coatings on steel surfaces, Philosophical Transactions of the Royal Society A: Mathematical, Physical and Engineering Sciences 378 (2020). https://doi.org/10.1098/RSTA.2019.0446.

[111] H. Wang, H. Hu, C. Zhou, W. Wei, B. Fan, H. Wang, S. Dong, Fabrication of self-healable superhydrophobic polyurethane coating based on functional CeO2 nanoparticles for long-term anti-corrosion application, Prog Org Coat 183 (2023) 107799. https://doi.org/10.1016/J.PORGCOAT.2023.107799.

[112] B. John, P.R. Rajimol, T.P.D. Rajan, S.K. Sahoo, Design and fabrication of nano textured superhydrophobic and anti-corrosive silane-grafted ZnO/bio-based polyurethane bilayer coating, Surf Coat Technol 451 (2022) 129036. https://doi.org/10.1016/J.SURFCOAT.2022.129036.

[113] S. Li, R. Xu, G. Song, B. Li, P. Fang, Q. Fu, C. Pan, Bio-inspired (GO + CNTs)-PU hydrophobic coating via replication of Lotus leaf and its enhanced mechanical and anti-corrosion properties, Prog Org Coat 159 (2021) 106414. https://doi.org/10.1016/J.PORGCOAT.2021.106414.

[114] Á.G. Braz, S.H. Pulcinelli, C. V. Santilli, Glycerol-based polyurethane-silica organic-inorganic hybrid as an anticorrosive coating, Prog Org Coat 169 (2022)

106939. https://doi.org/10.1016/J.PORGCOAT.2022.106939.

[115] H. Wang, J. Xu, X. Du, H. Wang, X. Cheng, Z. Du, Stretchable and self-healing polyurethane coating with synergistic anticorrosion effect for the corrosion protection of stainless steels, Prog Org Coat 164 (2022) 106672. https://doi.org/10.1016/J.PORGCOAT.2021.106672.

[116] M.M. Ariffin, M.M. Aung, L.C. Abdullah, M.Z. Salleh, Assessment of corrosion protection and performance of bio-based polyurethane acrylate incorporated with nano zinc oxide coating, Polym Test 87 (2020) 106526. https://doi.org/10.1016/J.POLYMERTESTING.2020.106526.

[117] T. Allison, Doctor blades, Gravure 21 (2007) 32–35. https://doi.org/10.1007/978-0-387-88953-5_10/COVER.

[118] G.C. Patil, Doctor Blade: A Promising Technique for Thin Film Coating, Simple Chemical Methods for Thin Film Deposition (2023) 509–530. https://doi.org/10.1007/978-981-99-0961-2_12.

[119] K.J. Jothi, S. Balachandran, K. Mohanraj, N. Prakash, A. Subhasri, P.S. Gopala Krishnan, K. Palanivelu, Fabrications of hybrid Polyurethane-Pd doped ZrO2 smart carriers for self-healing high corrosion protective coatings, Environ Res 211 (2022) 113095. https://doi.org/10.1016/J.ENVRES.2022.113095.

[120] A.G. Ulyashin, A. Hadjadj, M.A. Butt, Thin-Film Coating Methods: A Successful Marriage of High-Quality and Cost-Effectiveness—A Brief Exploration, Coatings 2022, Vol. 12, Page 1115 12 (2022) 1115. https://doi.org/10.3390/COATINGS12081115.

[121] S. V. Dorozhkin, There Are over 60 Ways to Produce Biocompatible Calcium Orthophosphate (CaPO4) Deposits on Various Substrates, Journal of Composites Science 2023, Vol. 7, Page 273 7 (2023) 273.

https://doi.org/10.3390/JCS7070273.

[122] H. Wang, H. Hu, C. Zhou, W. Wei, B. Fan, H. Wang, S. Dong, Fabrication of self-healable superhydrophobic polyurethane coating based on functional CeO2 nanoparticles for long-term anti-corrosion application, Prog Org Coat 183 (2023) 107799. https://doi.org/10.1016/J.PORGCOAT.2023.107799.

[123] A.G. Ulyashin, A. Hadjadj, M.A. Butt, Thin-Film Coating Methods: A Successful Marriage of High-Quality and Cost-Effectiveness—A Brief Exploration, Coatings 2022, Vol. 12, Page 1115 12 (2022) 1115. https://doi.org/10.3390/COATINGS12081115.

[124] 4 Types of Coating Techniques - Doxu Chemical, (n.d.). https://doxuchem.com/4-types-of-coating-techniques/ (accessed March 27, 2024).

[125] T. Arunkumar, G. Anand, P. Venkatachalam, M. Anish, J. Jayaprabakar, J.B. Sajin, Effect of Plural Spray Coating Process Parameters on Bonding Strength of Polyurea with Steel and Aluminum for Liquid Storage Applications, J Test Eval 49 (2021) 3319–3332. https://doi.org/10.1520/JTE20200061.

[126] S. Rabbani, E. Bakhshandeh, R. Jafari, G. Momen, Superhydrophobic and icephobic polyurethane coatings: Fundamentals, progress, challenges and opportunities, Prog Org Coat 165 (2022) 106715. https://doi.org/10.1016/J.PORGCOAT.2022.106715.

[127] Y.J. Lee, Y. La, O.S. Jeon, H.J. Lee, M.K. Shin, K.H. Yang, Y.J. You, S.Y. Park, Effects of boron nitride nanotube content on waterborne polyurethane–acrylate composite coating materials, RSC Adv 11 (2021) 12748–12756. https://doi.org/10.1039/D1RA00873K.

[128] S. Ahmad, S. Habib, M. Nawaz, R.A. Shakoor, R. Kahraman, T. Mohammed Al

Tahtamouni, The role of polymeric matrices on the performance of smart self-healing coatings: A review, Journal of Industrial and Engineering Chemistry 124 (2023) 40–67. https://doi.org/10.1016/J.JIEC.2023.04.024.

[129] K.J. Jothi, S. Balachandran, K. Mohanraj, N. Prakash, A. Subhasri, P.S. Gopala Krishnan, K. Palanivelu, Fabrications of hybrid Polyurethane-Pd doped ZrO2 smart carriers for self-healing high corrosion protective coatings, Environ Res 211 (2022) 113095. https://doi.org/10.1016/J.ENVRES.2022.113095.

[130] K. Rajitha, K.N.S. Mohana, M.B. Hegde, S.R. Nayak, N.K. Swamy, Fabrication of ZnO/rGO and ZnO/MWCNT nanohybrids to reinforce the anticorrosion performance of polyurethane coating, FlatChem 24 (2020) 100208. https://doi.org/10.1016/J.FLATC.2020.100208.

[131] D. Xue, Q.B. Meng, Y.X. Lu, L. Liang, Y.H. Wei, X. Bin Liu, Achieving high performance anticorrosive coating via in situ polymerization of polyurethane and poly(propylene oxide) grafted graphene oxide composites, Corros Sci 176 (2020) 109055. https://doi.org/10.1016/J.CORSCI.2020.109055.

[132] L. Benea, N. Simionescu, L. Mardare, The effect of polymeric protective layers and the immersion time on the corrosion behavior of naval steel in natural seawater, Journal of Materials Research and Technology 9 (2020) 13174–13184. https://doi.org/10.1016/J.JMRT.2020.09.059.

[133] H.S. Magar, R.Y.A. Hassan, A. Mulchandani, Electrochemical Impedance Spectroscopy (EIS): Principles, Construction, and Biosensing Applications, Sensors 2021, Vol. 21, Page 6578 21 (2021) 6578. https://doi.org/10.3390/S21196578.

[134] L. Benea, N. Simionescu, L. Mardare, The effect of polymeric protective layers and the immersion time on the corrosion behavior of naval steel in natural

seawater, Journal of Materials Research and Technology 9 (2020) 13174–13184. https://doi.org/10.1016/J.JMRT.2020.09.059.

[135] J.R. Xavier, Electrochemical and dynamic mechanical studies of newly synthesized polyurethane/SiO2-Al2O3 mixed oxide nanocomposite coated steel immersed in 3.5% NaCl solution, Surfaces and Interfaces 22 (2021) 100848. https://doi.org/10.1016/J.SURFIN.2020.100848.

[136] J. V. Nardeli, D. V. Snihirova, C.S. Fugivara, M.F. Montemor, E.R.P. Pinto, Y. Messaddecq, A. V. Benedetti, Localised corrosion assessement of crambe-oil-based polyurethane coatings applied on the ASTM 1200 aluminum alloy, Corros Sci 111 (2016) 422–435. https://doi.org/10.1016/J.CORSCI.2016.05.034.

[137] J. V. Nardeli, C.S. Fugivara, M. Taryba, M.F. Montemor, A. V. Benedetti, Biobased self-healing polyurethane coating with Zn micro-flakes for corrosion protection of AA7475, Chemical Engineering Journal 404 (2021) 126478. https://doi.org/10.1016/J.CEJ.2020.126478.

[138] T. Siva, S.S. Sreeja Kumari, S. Sathiyanarayanan, Dendrimer like mesoporous silica nano container (DMSN) based smart self healing coating for corrosion protection performance, Prog Org Coat 154 (2021) 106201. https://doi.org/10.1016/J.PORGCOAT.2021.106201.

[139] M. Yadav, J.K. Saha, S.K. Ghosh, Surface, Chemical, and Mechanical Properties of Polyurethane-Coated Galvanized Steel Sheets, J Mater Eng Perform (2024) 1–16. https://doi.org/10.1007/S11665-024-09171-6/FIGURES/10.

[140] J. V. Nardeli, C.S. Fugivara, M. Taryba, M.F. Montemor, A. V. Benedetti, Biobased self-healing polyurethane coating with Zn micro-flakes for corrosion protection of AA7475, Chemical Engineering Journal 404 (2021) 126478. https://doi.org/10.1016/J.CEJ.2020.126478.

[141] J. Liu, J. Cao, Z. Zhou, R. Liu, Y. Yuan, X. Liu, Stiff Self-Healing Coating Based on UV-Curable Polyurethane with a “hard Core, Flexible Arm” Structure, ACS Omega 3 (2018) 11128–11135. https://doi.org/10.1021/ACSOMEGA.8B00925/ASSET/IMAGES/LARGE/AO-2018-009253_0011.JPEG.

[142] Y. Sheng, M. Wang, K. Zhang, Z. Wu, Y. Chen, X. Lu, An “inner soft external hard”, scratch-resistant, self-healing waterborne poly(urethane-urea) coating based on gradient metal coordination structure, Chemical Engineering Journal 426 (2021) 131883. https://doi.org/10.1016/J.CEJ.2021.131883.

[143] Q.X. Nguyen, T.T. Nguyen, N.M. Pham, T.T. Khong, T.M. Cao, V. Van Pham, A fabrication of CNTs/TiO2/polyurethane films toward antibacterial and protective coatings, Prog Org Coat 167 (2022) 106838. https://doi.org/10.1016/J.PORGCOAT.2022.106838.

[144] P. Haghdadeh, M. Ghaffari, B. Ramezanzadeh, G. Bahlakeh, M.R. Saeb, Polyurethane coatings reinforced with 3-(triethoxysilyl)propyl isocyanate functionalized graphene oxide nanosheets: Mechanical and anti-corrosion properties, Prog Org Coat 136 (2019) 105243. https://doi.org/10.1016/J.PORGCOAT.2019.105243.

[145] X.F. Zhang, Y.Q. Chen, J.M. Hu, Robust superhydrophobic SiO2/polydimethylsiloxane films coated on mild steel for corrosion protection, Corros Sci 166 (2020) 108452. https://doi.org/10.1016/J.CORSCI.2020.108452.

[146] E. Yousefi, M.R. Ghadimi, S. Amirpoor, A. Dolati, Preparation of new superhydrophobic and highly oleophobic polyurethane coating with enhanced mechanical durability, Appl Surf Sci 454 (2018) 201–209. https://doi.org/10.1016/J.APSUSC.2018.05.125.

[147] S.M. Prasanth, P.S. Kumar, S. Harish, M. Rishikesh, S. Nanda, D.V.N. Vo, Application of biomass derived products in mid-size automotive industries: A review, Chemosphere 280 (2021) 130723. https://doi.org/10.1016/J.CHEMOSPHERE.2021.130723.

[148] F.M. De Souza, P.K. Kahol, R.K. Gupta, Introduction to Polyurethane Chemistry, ACS Symposium Series 1380 (2021) 1–24. https://doi.org/10.1021/BK-2021-1380.CH001/ASSET/IMAGES/LARGE/BK-2020-00517M_G020.JPEG.

[149] M. Fang, T.F. Webster, D. Gooden, E.M. Cooper, M.D. McClean, C. Carignan, C. Makey, H.M. Stapleton, Investigating a novel flame retardant known as V6: Measurements in baby products, house dust, and car dust, Environ Sci Technol 47 (2013) 4449–4454. https://doi.org/10.1021/ES400032V/SUPPL_FILE/ES400032V_SI_001.PDF.

[150] J. Joseph, R.M. Patel, A. Wenham, J.R. Smith, Biomedical applications of polyurethane materials and coatings, Transactions of the IMF 96 (2018) 121–129. https://doi.org/10.1080/00202967.2018.1450209.

[151] M. Shahrousvand, M.S. Hoseinian, M. Ghollasi, A. Karbalaeimahdi, A. Salimi, F.A. Tabar, Flexible magnetic polyurethane/Fe2O3 nanoparticles as organic-inorganic nanocomposites for biomedical applications: Properties and cell behavior, Materials Science and Engineering: C 74 (2017) 556–567. https://doi.org/10.1016/J.MSEC.2016.12.117.

[152] W. Chen, J. Clauser, A.L. Thiebes, D.J. McGrath, N. Kelly, M.J. van Steenbergen, S. Jockenhoevel, U. Steinseifer, P.E. McHugh, W.E. Hennink, R.J. Kok, Gefitinib/gefitinib microspheres loaded polyurethane constructs as drug-eluting stent coating, European Journal of Pharmaceutical Sciences 103 (2017)

94–103. https://doi.org/10.1016/J.EJPS.2017.02.002.

[153] S. Muzaffar, M. Abbas, U.H. Siddiqua, M. Arshad, A. Tufail, M. Ahsan, S.A. Alissa, S.A. Abubshait, H.A. Abubshait, M. Iqbal, Enhanced mechanical, UV protection and antimicrobial properties of cotton fabric employing nanochitosan and polyurethane based finishing, Journal of Materials Research and Technology 11 (2021) 946–956. https://doi.org/10.1016/J.JMRT.2021.01.018.

[154] T.N. Nguyen, H.T. Trinh, L.H. Sam, T.Q. Nguyen, G.T. Le, Halogen-free flame-retardant flexible polyurethane for textile coating: Preparation and characterisation, Fire Mater 44 (2020) 269–282. https://doi.org/10.1002/FAM.2799.

[155] S. Kumar, M.M. Rahman, S. Yoon, S. Kim, N. Oh, K.H. Hong, J. Koh, Synthesis, Characterization, and Functional Properties of ZnO-based Polyurethane Nanocomposite for Textile Applications, Fibers and Polymers 22 (2021) 2227–2237. https://doi.org/10.1007/S12221-021-0815-2/METRICS.

[156] A. Pistone, C. Scolaro, A. Visco, Mechanical Properties of Protective Coatings against Marine Fouling: A Review, Polymers 2021, Vol. 13, Page 173 13 (2021) 173. https://doi.org/10.3390/POLYM13020173.

[157] J. Chungprempree, S. Charoenpongpool, J. Preechawong, N. Atthi, M. Nithitanakul, Simple Preparation of Polydimethylsiloxane and Polyurethane Blend Film for Marine Antibiofouling Application, Polymers 2021, Vol. 13, Page 2242 13 (2021) 2242. https://doi.org/10.3390/POLYM13142242.

[158] M.-G. Kim, K.-I. Jo, E. Kim, J.-H. Park, J.-W. Ko, J.H. Lee, M.-G.; Kim, K.-I.; Jo, E.; Kim, J.-H.; Park, J.-W.; Ko, J.H. Lee, Preparation of Polydimethylsiloxane-Modified Waterborne Polyurethane Coatings for Marine Applications, Polymers 2021, Vol. 13, Page 4283 13 (2021) 4283.

https://doi.org/10.3390/POLYM13244283.

[159] W. Xu, C. Ma, J. Ma, T. Gan, G. Zhang, Marine biofouling resistance of polyurethane with biodegradation and hydrolyzation, ACS Appl Mater Interfaces 6 (2014) 4017–4024. https://doi.org/10.1021/AM4054578/SUPPL_FILE/AM4054578_SI_001.PDF.

[160] Y. Li, B. Li, X. Zhao, N. Tian, J. Zhang, Totally Waterborne, Nonfluorinated, Mechanically Robust, and Self-Healing Superhydrophobic Coatings for Actual Anti-Icing, ACS Appl Mater Interfaces 10 (2018) 39391–39399. https://doi.org/10.1021/ACSAMI.8B15061/SUPPL_FILE/AM8B15061_SI_004.AVI.

[161] W.S.Y. Wong, Z.H. Stachurski, D.R. Nisbet, A. Tricoli, Ultra-Durable and Transparent Self-Cleaning Surfaces by Large-Scale Self-Assembly of Hierarchical Interpenetrated Polymer Networks, ACS Appl Mater Interfaces 8 (2016) 13615–13623. https://doi.org/10.1021/ACSAMI.6B03414/ASSET/IMAGES/LARGE/AM-2016-03414N_0007.JPEG.

[162] K.M. Holder, A.A. Cain, M.G. Plummer, B.E. Stevens, P.K. Odenborg, A.B. Morgan, J.C. Grunlan, K.M. Holder, M.G. Plummer, J.C. Grunlan, A.A. Cain, B.E. Stevens, P.K. Odenborg, A.B. Morgan, Carbon Nanotube Multilayer Nanocoatings Prevent Flame Spread on Flexible Polyurethane Foam, Macromol Mater Eng 301 (2016) 665–673. https://doi.org/10.1002/MAME.201500327.

[163] S. Rabbani, E. Bakhshandeh, R. Jafari, G. Momen, Superhydrophobic and icephobic polyurethane coatings: Fundamentals, progress, challenges and opportunities, Prog Org Coat 165 (2022) 106715. https://doi.org/10.1016/J.PORGCOAT.2022.106715.

[164] S. Jakhmola, S. Das, K. Dutta, Emerging research trends in the field of polyurethane and its nanocomposites: Chemistry, Synthesis, Characterization, Application in coatings and Future perspectives, J Coat Technol Res 21 (2023) 137–172. https://doi.org/10.1007/S11998-023-00841-Z/FIGURES/19.

[165] S.P. Vijayan, B. John, S.K. Sahoo, Modified cardanol based colorless, transparent, hydrophobic and anti-corrosive polyurethane coating, Prog Org Coat 162 (2022) 106586. https://doi.org/10.1016/J.PORGCOAT.2021.106586.

[166] J. Liu, X. Jiao, F. Cheng, Y. Fan, Y. Wu, X. Yang, Fabrication and performance of UV cured transparent silicone modified polyurethane–acrylate coatings with high hardness, good thermal stability and adhesion, Prog Org Coat 144 (2020) 105673. https://doi.org/10.1016/J.PORGCOAT.2020.105673.

[167] S. Habib, A. Qureshi, S. Sajjad, E.M. Ahmed, R.A. Shakoor, TiO2-Mesoporous Ceria Carrier Modified with Sodium Benzoate: An Innovative Polyurethane Matrix for Enhanced Corrosion Protection of steel, Colloids Surf A Physicochem Eng Asp 697 (2024) 134471. https://doi.org/10.1016/J.COLSURFA.2024.134471.

[168] S. Habib, A. Qureshi, M. Faisal, R. Kahraman, E.M. Ahmed, R.A. Shakoor, Advancing steel protection with Ceria@Talc-8-hydroxyquinoline modified Polyurethane coatings, Prog Org Coat 191 (2024) 108446. https://doi.org/10.1016/J.PORGCOAT.2024.108446.

[169] S. Habib, E. Fayyad, M. Nawaz, A. Khan, R.A. Shakoor, R. Kahraman, A. Abdullah, Cerium dioxide nanoparticles as smart carriers for self-healing coatings, Nanomaterials 10 (2020). https://doi.org/10.3390/nano10040791.

[170] S. Habib, E. Fayyed, A. Shakoor, A. Kahraman, Ramazan Abdullah, Improved self-healing performance of polymeric nanocomposites reinforced with talc

nanoparticles (TNPs) and urea-formaldehyde microcapsules (UFMCs), Arabian Journal of Chemistry 14 (2020) 102926. https://doi.org/10.1016/j.arabjc.2020.102926.

[171] S. Habib, A. Qureshi, M. Faisal, R. Kahraman, E.M. Ahmed, R.A. Shakoor, Advancing steel protection with Ceria@Talc-8-hydroxyquinoline modified Polyurethane coatings, Prog Org Coat 191 (2024) 108446. https://doi.org/https://doi.org/10.1016/j.porgcoat.2024.108446.

[172] A.H. Mamaghani, F. Haghighat, C.S. Lee, Role of titanium dioxide (TiO2) structural design/morphology in photocatalytic air purification, Appl Catal B 269 (2020) 118735. https://doi.org/10.1016/J.APCATB.2020.118735.

[173] Q.X. Nguyen, T.T. Nguyen, N.M. Pham, T.T. Khong, T.M. Cao, V. Van Pham, A fabrication of CNTs/TiO2/polyurethane films toward antibacterial and protective coatings, Prog Org Coat 167 (2022) 106838. https://doi.org/10.1016/J.PORGCOAT.2022.106838.

[174] J. Li, H. Zheng, L. Liu, F. Meng, Y. Cui, F. Wang, Modification of graphene and graphene oxide and their applications in anticorrosive coatings, Journal of Coatings Technology and Research 2021 18:2 18 (2021) 311–331. https://doi.org/10.1007/S11998-020-00435-Z.

[175] R.G. Abaszade, Synthesis and analysis of flakes graphene oxide, Journal of Optoelectronic and Biomedical Materials 14 (n.d.) 107–114. https://doi.org/10.15251/JOBM.2022.143.107.

[176] R.G. Abaszade, S.A. Mamedova, F.H. Agayev, S.I. Budzulyak, O.A. Kapush, M.A. Mamedova, A.M. Nabiyev, V.O. Kotsyubynsky, Synthesis and characterization of graphene oxide flakes for transparent thin films, Physics and Chemistry of Solid State 22 (2021) 595–601.

https://doi.org/10.15330/PCSS.22.3.595-601.

[177] W. Li, B. Song, S. Zhang, F. Zhang, C. Liu, N. Zhang, H. Yao, Y. Shi, Using 3-Isocyanatopropyltrimethoxysilane to Decorate Graphene Oxide with Nano-Titanium Dioxide for Enhancing the Anti-Corrosion Properties of Epoxy Coating, Polymers 2020, Vol. 12, Page 837 12 (2020) 837. https://doi.org/10.3390/POLYM12040837.

[178] M. Molaei, A. Fattah-alhosseini, M. Nouri, P. Mahmoodi, A. Nourian, Incorporating TiO2 nanoparticles to enhance corrosion resistance, cytocompatibility, and antibacterial properties of PEO ceramic coatings on titanium, Ceram Int 48 (2022) 21005–21024. https://doi.org/10.1016/J.CERAMINT.2022.04.096.

[179] M.C. Chen, P.W. Koh, V.K. Ponnusamy, S.L. Lee, Titanium dioxide and other nanomaterials based antimicrobial additives in functional paints and coatings: Review, Prog Org Coat 163 (2022) 106660. https://doi.org/10.1016/J.PORGCOAT.2021.106660.

[180] A. Chouhan, H.P. Mungse, O.P. Khatri, Surface chemistry of graphene and graphene oxide: A versatile route for their dispersion and tribological applications, Adv Colloid Interface Sci 283 (2020) 102215. https://doi.org/10.1016/J.CIS.2020.102215.

[181] F.M. Casallas Caicedo, E. Vera López, A. Agarwal, V. Drozd, A. Durygin, A. Franco Hernandez, C. Wang, Synthesis of graphene oxide from graphite by ball milling, Diam Relat Mater 109 (2020) 108064. https://doi.org/10.1016/J.DIAMOND.2020.108064.

[182] M. Muniyalakshmi, K. Sethuraman, D. Silambarasan, Synthesis and characterization of graphene oxide nanosheets, Mater Today Proc 21 (2020)

408–410. https://doi.org/10.1016/J.MATPR.2019.06.375.

[183] N. Sharma, M. Arif, S. Monga, M. Shkir, Y.K. Mishra, A. Singh, Investigation of bandgap alteration in graphene oxide with different reduction routes, Appl Surf Sci 513 (2020) 145396. https://doi.org/10.1016/J.APSUSC.2020.145396.

[184] M. Lal, P. Sharma, C. Ram, Calcination temperature effect on titanium oxide (TiO2) nanoparticles synthesis, Optik (Stuttg) 241 (2021) 166934. https://doi.org/10.1016/J.IJLEO.2021.166934.

[185] S. Mustapha, J.O. Tijani, M.M. Ndamitso, A.S. Abdulkareem, D.T. Shuaib, A.T. Amigun, H.L. Abubakar, Facile synthesis and characterization of TiO2 nanoparticles: X-ray peak profile analysis using Williamson–Hall and Debye–Scherrer methods, Int Nano Lett 11 (2021) 241–261. https://doi.org/10.1007/S40089-021-00338-W/FIGURES/19.

[186] A.Q. Al-Gamal, W.S. Falath, T.A. Saleh, Enhanced efficiency of polyamide membranes by incorporating TiO2-Graphene oxide for water purification, J Mol Liq 323 (2021) 114922. https://doi.org/10.1016/J.MOLLIQ.2020.114922.

[187] K.S. Khashan, G.M. Sulaiman, F.A. Abdulameer, S. Albukhaty, M.A. Ibrahem, T. Al-Muhimeed, A.A. Alobaid, Antibacterial Activity of TiO2 Nanoparticles Prepared by One-Step Laser Ablation in Liquid, Applied Sciences 2021, Vol. 11, Page 4623 11 (2021) 4623. https://doi.org/10.3390/APP11104623.

[188] G. Surekha, V. Krishnaiah, N. Ravi, P. Suvarna, FTIR, Raman and XRD analysis of graphene oxide films prepared by modified Hummers method, J Phys Conf Ser 1495 (2020) 12012. https://doi.org/10.1088/1742-6596/1495/1/012012.

[189] B.Y.S. Chang, N.M. Huang, M.N. An'amt, A.R. Marlinda, Y. Norazriena, M.R. Muhamad, I. Harrison, H.N. Lim, C.H. Chia, Facile hydrothermal preparation of titanium dioxide decorated reduced graphene oxide nanocomposite, Int J

Nanomedicine 7 (2012) 3379–3387. https://doi.org/10.2147/IJN.S28189.

[190] A.S. AlShammari, M.M. Halim, F.K. Yam, N.H.M. Kaus, Synthesis of Titanium Dioxide (TiO2)/Reduced Graphene Oxide (rGO) thin film composite by spray pyrolysis technique and its physical properties, Mater Sci Semicond Process 116 (2020) 105140. https://doi.org/10.1016/J.MSSP.2020.105140.

[191] V.B. Mohan, K. Jayaraman, D. Bhattacharyya, Brunauer–Emmett–Teller (BET) specific surface area analysis of different graphene materials: A comparison to their structural regularity and electrical properties, Solid State Commun 320 (2020) 114004. https://doi.org/10.1016/J.SSC.2020.114004.

[192] S. Habib, A. Hassanein, R. Kahraman, E. Mahdi Ahmed, R.A. Shakoor, Self-healing behavior of epoxy-based double-layer nanocomposite coatings modified with Zirconia nanoparticles, Mater Des 207 (2021) 109839. https://doi.org/10.1016/J.MATDES.2021.109839.

[193] S.S.A. Kumar, S. Bashir, K. Ramesh, S. Ramesh, New perspectives on Graphene/Graphene oxide based polymer nanocomposites for corrosion applications: The relevance of the Graphene/Polymer barrier coatings, Prog Org Coat 154 (2021) 106215. https://doi.org/10.1016/J.PORGCOAT.2021.106215.

[194] Y. Xie, W. Liu, L. Liang, C. Liu, M. Yang, H. Shi, S. Wang, F. Zhang, Incorporation of silica network and modified graphene oxide into epoxy resin for improving thermal and anticorrosion properties, J Appl Polym Sci 137 (2020) 49405. https://doi.org/10.1002/APP.49405.

[195] F. Farivar, P.L. Yap, R.U. Karunagaran, D. Losic, Thermogravimetric Analysis (TGA) of Graphene Materials: Effect of Particle Size of Graphene, Graphene Oxide and Graphite on Thermal Parameters, C 2021, Vol. 7, Page 41 7 (2021) 41. https://doi.org/10.3390/C7020041.

[196] O. Dagdag, A. Berisha, V. Mehmeti, R. Haldhar, E. Berdimurodov, O. Hamed, S. Jodeh, H. Lgaz, E.S.M. Sherif, E.E. Ebenso, Epoxy coating as effective anti-corrosive polymeric material for aluminum alloys: Formulation, electrochemical and computational approaches, J Mol Liq 346 (2022) 117886. https://doi.org/10.1016/J.MOLLIQ.2021.117886.

[197] R. Azari, H.R. Rezaie, A. Khavandi, Effect of titanium dioxide intermediate layer on scratch and corrosion resistance of sol–gel-derived HA coating applied on Ti-6Al-4V substrate, Prog Biomater 10 (2021) 259–269. https://doi.org/10.1007/S40204-021-00169-0/FIGURES/7.

[198] B. Minhas, S. Dino, H. Qian, Y. Zuo, An approach for high stability TiO2 in strong acid environments at high temperature, Surf Coat Technol 395 (2020) 125932. https://doi.org/10.1016/J.SURFCOAT.2020.125932.

[199] C.M. Damian, M.I. Necolau, I. Neblea, E. Vasile, H. Iovu, Synergistic effect of graphene oxide functionalized with SiO2 nanostructures in the epoxy nanocomposites, Appl Surf Sci 507 (2020) 145046. https://doi.org/10.1016/J.APSUSC.2019.145046.

[200] D.S. Chauhan, M.A. Quraishi, K.R. Ansari, T.A. Saleh, Graphene and graphene oxide as new class of materials for corrosion control and protection: Present status and future scenario, Prog Org Coat 147 (2020) 105741. https://doi.org/10.1016/J.PORGCOAT.2020.105741.

[201] N.A. Ismail, R.A. Shakoor, R. Kahraman, Corrosion inhibition performance of developed epoxy coatings containing carbon nanocapsules loaded with diethylenetriamine, Prog Org Coat 183 (2023) 107716. https://doi.org/10.1016/J.PORGCOAT.2023.107716.

[202] A.W. Momber, L. Fröck, T. Marquardt, Effects of accelerated ageing on the

mechanical properties of adhesive joints between stainless steel and polymeric top coat materials for marine applications, Int J Adhes Adhes 103 (2020) 102699. https://doi.org/10.1016/J.IJADHADH.2020.102699.

[203] Y. Ye, H. Chen, Y. Zou, Y. Ye, H. Zhao, Corrosion protective mechanism of smart graphene-based self-healing coating on carbon steel, Corros Sci 174 (2020) 108825. https://doi.org/10.1016/J.CORSCI.2020.108825.

[204] I.A.W. Ma, S. Ammar, S.S.A. Kumar, K. Ramesh, S. Ramesh, A concise review on corrosion inhibitors: types, mechanisms and electrochemical evaluation studies, Journal of Coatings Technology and Research 2021 19:1 19 (2021) 241–268. https://doi.org/10.1007/S11998-021-00547-0.

[205] Y. Tian, Z. Bi, G. Cui, Study on the Corrosion Resistance of Graphene Oxide-Based Epoxy Zinc-Rich Coatings, Polymers 2021, Vol. 13, Page 1657 13 (2021) 1657. https://doi.org/10.3390/POLYM13101657.

[206] K.S. Beenakumari, Electrochemical Deposited Zinc Titanate Film on Mild steel Surface for Enhanced Corrosion Protection Characteristics, (n.d.). www.ijacskros.com (accessed July 2, 2024).

[207] S. Guo, J. Liu, S. Qiu, Y. Wang, X. Yan, N. Wu, S. Wang, Z. Guo, Enhancing Electrochemical Performances of TiO2 Porous Microspheres through Hybridizing with FeTiO3 and Nanocarbon, Electrochim Acta 190 (2016) 556–565. https://doi.org/10.1016/J.ELECTACTA.2015.12.135.

[208] S. Korablov, B. Basavalingu, M. Yoshimura, Wet corrosion of nitride PVD films in supercritical solutions, Corros Sci 47 (2005) 1384–1402. https://doi.org/10.1016/J.CORSCI.2004.07.035.

[209] M.I. Abdou, M.I. Ayad, A.S.M. Diab, I.A. Hassan, A.M. Fadl, Studying the corrosion mitigation behavior and chemical durability of FeTiO3/melamine

formaldehyde epoxy composite coating for steel internal lining applications, Prog Org Coat 133 (2019) 325–339. https://doi.org/10.1016/J.PORGCOAT.2019.04.072.

[210] N. Parhizkar, T. Shahrabi, B. Ramezanzadeh, A new approach for enhancement of the corrosion protection properties and interfacial adhesion bonds between the epoxy coating and steel substrate through surface treatment by covalently modified amino functionalized graphene oxide film, Corros Sci 123 (2017) 55–75. https://doi.org/10.1016/J.CORSCI.2017.04.011.

[211] C.H. Zhou, S. Xu, Y. Yang, B.C. Yang, H. Hu, Z.C. Quan, B. Sebo, B.L. Chen, Q.D. Tai, Z.H. Sun, X.Z. Zhao, Titanium dioxide sols synthesized by hydrothermal methods using tetrabutyl titanate as starting material and the application in dye sensitized solar cells, Electrochim Acta 56 (2011) 4308–4314. https://doi.org/10.1016/j.electacta.2011.01.054.

[212] M. Farahmandjou, Self-cleaning Measurement of Nano-Sized Photoactive TiO2 Self-Cleaning Measurement of Nano-Sized Photoactive TiO 2, Journal of Computer & Robotics 5 (2014) 15–19.

[213] M.B. Suwarnkar, G. V. Khade, S.B. Babar, K.M. Garadkar, Microwave synthesis of In-doped TiO2 nanoparticles for photocatalytic application, Journal of Materials Science: Materials in Electronics 28 (2017) 17140–17147. https://doi.org/10.1007/s10854-017-7641-8.

[214] M. Ahamed, M.A.M. Khan, M.J. Akhtar, H.A. Alhadlaq, A. Alshamsan, Ag-doping regulates the cytotoxicity of TiO2 nanoparticles via oxidative stress in human cancer cells, Sci Rep 7 (2017) 17662. https://doi.org/10.1038/s41598-017-17559-9.

[215] N. Ali, A. Said, F. Ali, M. Khan, Z.A. Sheikh, M. Bilal, Development and

Characterization of Functionalized Titanium Dioxide-Reinforced Sulfonated Copolyimide (SPI/TiO2) Nanocomposite Membranes with Improved Mechanical, Thermal, and Electrochemical Properties, J Inorg Organomet Polym Mater 30 (2020) 4585–4596. https://doi.org/10.1007/s10904-020-01636-0.

[216] S. Hosseini, H. Jahangirian, T.J. Webster, S. Masoudi Soltani, M.K. Arou, Synthesis, characterization, and performance evaluation of multilayered photoanodes by introducing mesoporous carbon and TiO2for humic acid adsorption, Int J Nanomedicine 11 (2016) 3969–3978. https://doi.org/10.2147/IJN.S96558.

[217] M. Thommes, K. Kaneko, A. V Neimark, J.P. Olivier, F. Rodriguez-Reinoso, J. Rouquerol, K.S.W. Sing, Physisorption of gases, with special reference to the evaluation of surface area and pore size distribution (IUPAC Technical Report), 87 (2015) 1051–1069. https://doi.org/doi:10.1515/pac-2014-1117.

[218] S. Habib, A. Qureshi, R.A. Shakoor, R. Kahraman, N.H. Al-Qahtani, E.M. Ahmed, Corrosion inhibition performance of polyolefin smart self-healing composite coatings modified with ZnO@β-Cyclodextrin hybrid particles, Journal of Materials Research and Technology 21 (2022) 3371–3385. https://doi.org/https://doi.org/10.1016/j.jmrt.2022.10.148.

[219] P. Praveen, G. Viruthagiri, S. Mugundan, N. Shanmugam, Structural, optical and morphological analyses of pristine titanium di-oxide nanoparticles - Synthesized via sol-gel route, Spectrochim Acta A Mol Biomol Spectrosc 117 (2014) 622–629. https://doi.org/10.1016/j.saa.2013.09.037.

[220] L.S. Chougala, M.S. Yatnatti, R.K. Linganagoudar, R.R. Kamble, J.S. Kadadevarmath, A simple approach on synthesis of TiO2 nanoparticles and its

application in dye sensitized solar cells, Journal of Nano- and Electronic Physics 9 (2017). https://doi.org/10.21272/jnep.9(4).04005.

[221] M. Manivannan, S. Rajendran, A.A. Nagar, Investigation of inhibitive action of urea - ZN 2 + sytem in the corrosion control of carbon steel in sea water, Journal of Engineering Science and Techology 3 (2015) 8048–8060.

[222] E. Magovac, B. Vončina, A. Budimir, I. Jordanov, J.C. Grunlan, S. Bischof, Environmentally benign phytic acid-based nanocoating for multifunctional flame-retardant/antibacterial cotton, Fibers 9 (2021). https://doi.org/10.3390/fib9110069.

[223] E.D. Mekeridis, I.A. Kartsonakis, G.S. Pappas, G.C. Kordas, Release studies of corrosion inhibitors from cerium titanium oxide nanocontainers, Journal of Nanoparticle Research 13 (2011) 541–554. https://doi.org/10.1007/s11051-010-0044-x.

[224] S. Habib, E. Fayyed, R.A. Shakoor, R. Kahraman, A. Abdullah, Improved self-healing performance of polymeric nanocomposites reinforced with talc nanoparticles (TNPs) and urea-formaldehyde microcapsules (UFMCs), Arabian Journal of Chemistry 14 (2021) 102926. https://doi.org/https://doi.org/10.1016/j.arabjc.2020.102926.

[225] M.S. Sepehri Sadeghian, A. Raisi, A thermodynamic study on relationship between gas separation properties and microstructure of polyurethane membranes, Sci Rep 13 (2023) 1–17. https://doi.org/10.1038/s41598-023-32908-7.

[226] G.G. Silva, H.D.R. Calado, A.W. Musumeci, W. Martens, E.R. Waclawik, R.L. Frost, G.A. George, Polymer nanocomposites based on P3OT, TPU and SWNT: Preparation and characterization, Proceedings of the 2006 International

Conference on Nanoscience and Nanotechnology, ICONN (2006) 182–185. https://doi.org/10.1109/ICONN.2006.340581.

[227] M.S. Prabhudesai, P.M. Paraskar, R. Kedar, R.D. Kulkarni, Sea Buckthorn Oil Tocopherol Extraction's By-Product Utilization in Green Synthesis of Polyurethane Coating, European Journal of Lipid Science and Technology 122 (2020) 1–9. https://doi.org/10.1002/ejlt.201900387.

[228] D. Jero, N. Caussé, O. Marsan, T. Buffeteau, F. Chaussec, A. Buvignier, M. Roy, N. Pébère, Film-forming amines adsorption and corrosion kinetics on carbon steel surface in neutral solution investigated by EIS and PM-IRRAS analysis, Electrochim Acta 443 (2023). https://doi.org/10.1016/j.electacta.2023.141925.

[229] P. Cao, R. Gu, Z. Tian, Electrochemical and Surface-Enhanced Raman, (2002) 7609–7615.

[230] W.W. So, S. Bin Park, K.J. Kim, C.H. Shin, S.J. Moon, The crystalline phase stability of titania particles prepared at room temperature by the sol-gel method, J Mater Sci 36 (2001) 4299–4305. https://doi.org/10.1023/A:1017955408308.

[231] M.H. Sliem, M. Afifi, A. Bahgat Radwan, E.M. Fayyad, M.F. Shibl, F.E.T. Heakal, A.M. Abdullah, AEO7 Surfactant as an Eco-Friendly Corrosion Inhibitor for Carbon Steel in HCl solution, Sci Rep 9 (2019) 1–16. https://doi.org/10.1038/s41598-018-37254-7.

[232] T. Luttrell, S. Halpegamage, J. Tao, A. Kramer, E. Sutter, M. Batzill, Why is anatase a better photocatalyst than rutile? - Model studies on epitaxial TiO2 films, Sci Rep 4 (2014) 4043. https://doi.org/10.1038/srep04043.

Appendix A: Supplementary Data

Figure 41 shows the EDX mapping images of the fGO coating. It shows a uniform distribution of oxygen (O), carbon (C), silicon (Si), nitrogen (N), and titanium (Ti) across the sample. This confirms the successful functionalization and incorporation of these elements into the fGO structure. These images provide comprehensive evidence supporting the composition distribution of fGO.

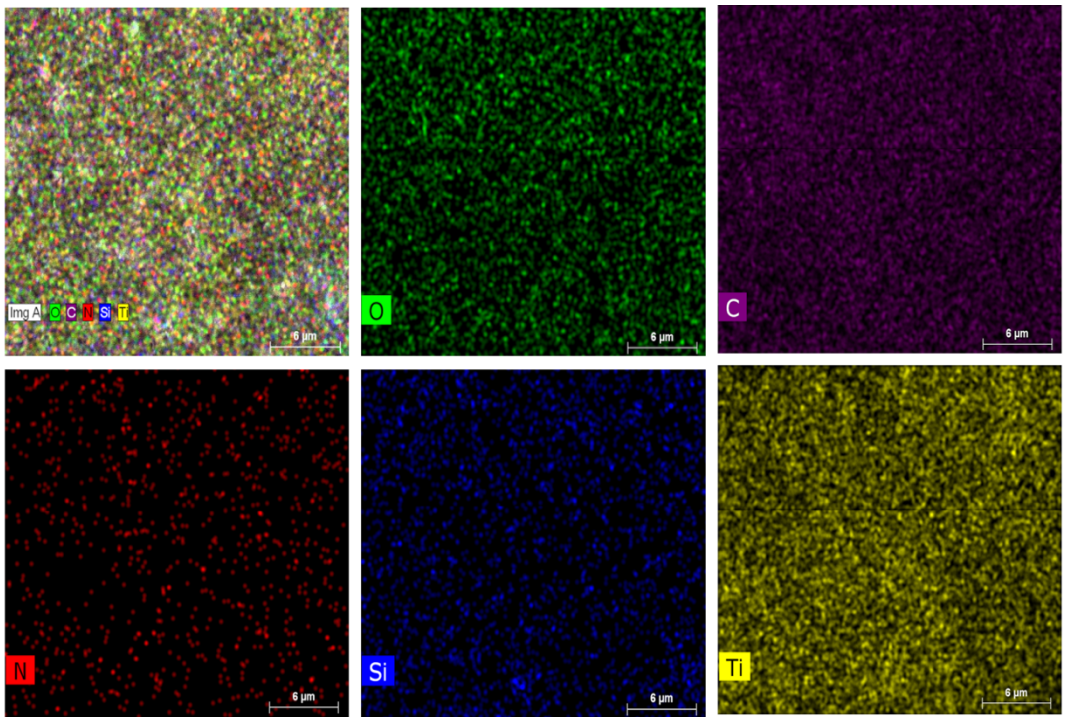

Figure 41: EDX mapping images of fGO.

Figure 42 and Figure 43 show the electron microscopy images and elemental analysis of unmodified TiO_2 and DAMO-modified TiO_2. The SEM images and corresponding elemental analysis of the unmodified TiO_2 clearly show the presence of only titanium (Ti) and oxygen (O), which is consistent with the expected elemental composition of pure TiO_2.

Furthermore, additional SEM images and elemental mapping of DAMO-modified TiO_2

(fTiO₂) confirm the successful modification. The presence of nitrogen (N), carbon (C), oxygen (O), and silicon (Si) elements in the modified samples, which were not present in the unmodified TiO₂, clearly indicates the attachment of the DAMO silane groups to the TiO₂ surface.

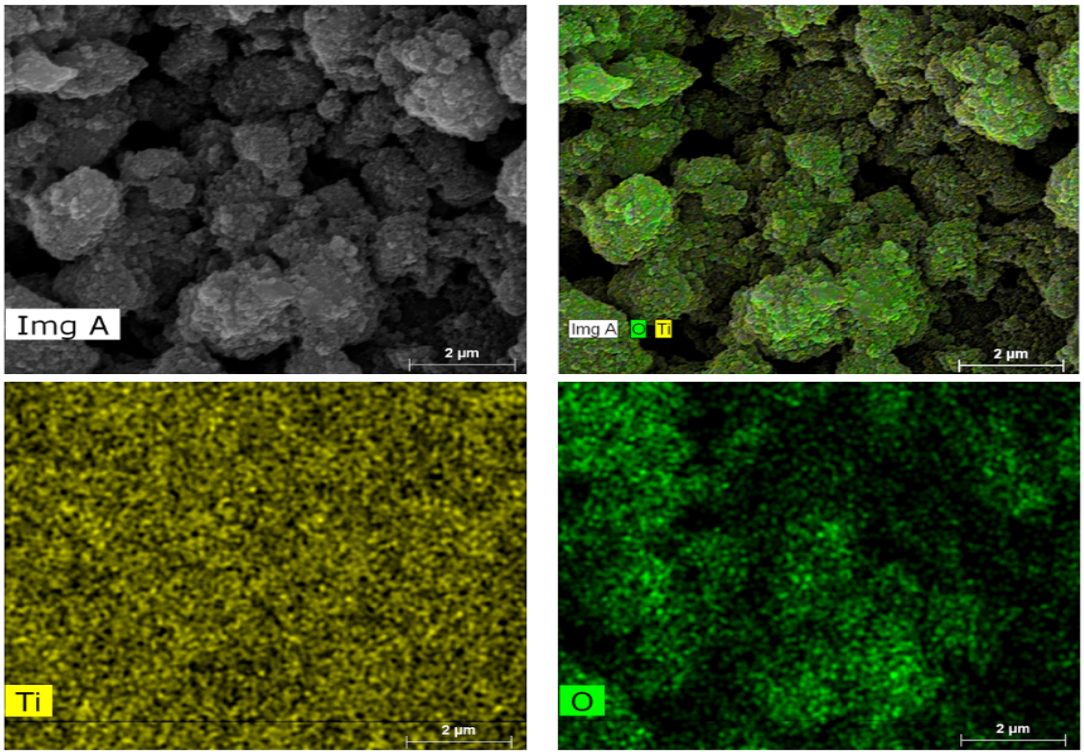

Figure 42: Electron microscopy images and Elemental mapping of TiO₂.

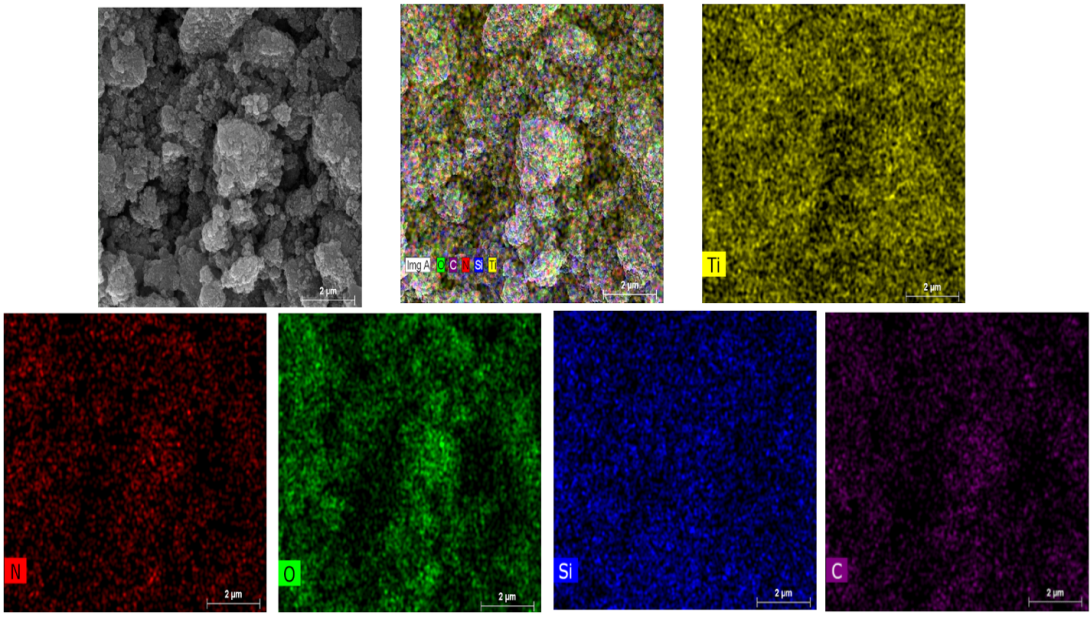

Figure 43: Electron microscopy images and elemental mapping of $fTiO_2$.

Figure 44 shows the FTIR spectra of TiO_2 before and after modification with DAMO. The peak at 2200–2300 cm^{-1} corresponds to the C≡N stretching, indicating the presence of nitrile groups formed during the DAMO modification. The peak at 1089 cm^{-1} represents the Ti-O-Ti stretching, showing that the TiO_2 structure remains intact after modification. Additionally, the new peak at 800 cm^{-1} confirms the formation of Si-O-Ti bonds, indicating the silane group's successful attachment to the TiO_2 surface. These spectral changes confirm the successful modification of TiO_2 with DAMO.

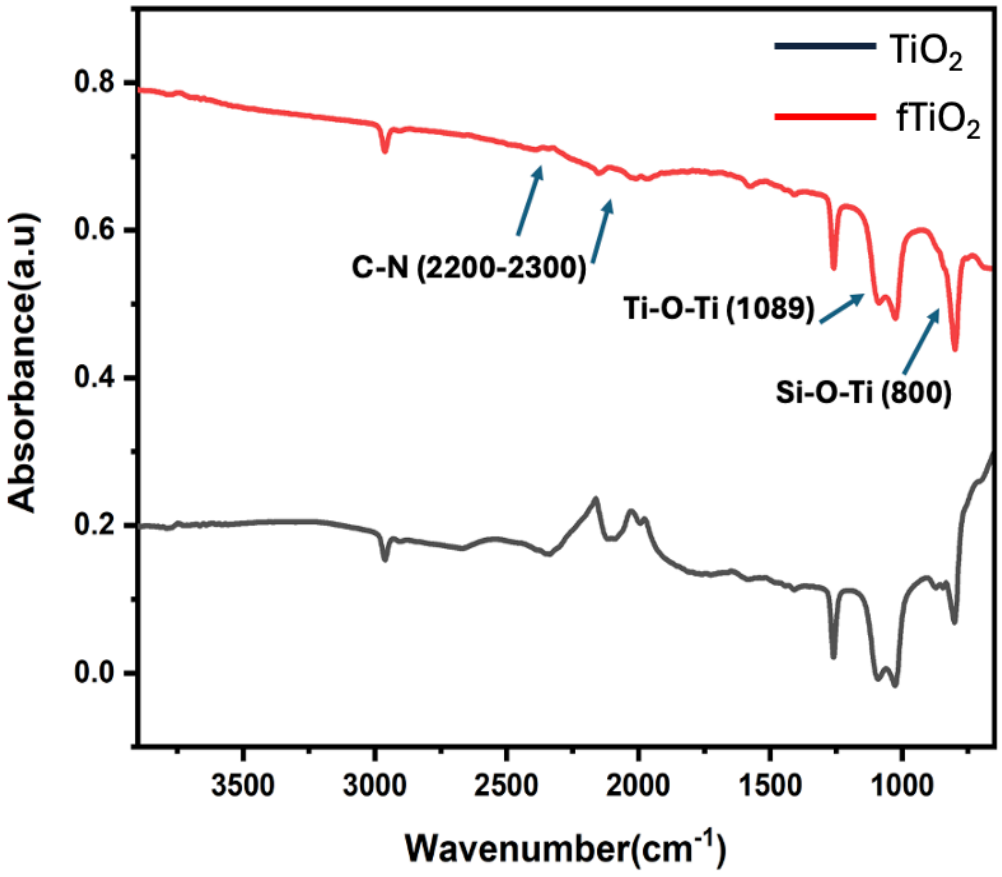

Figure 44: FTIR of TiO_2 and $fTiO_2$.

Appendix B: Supplementary Data

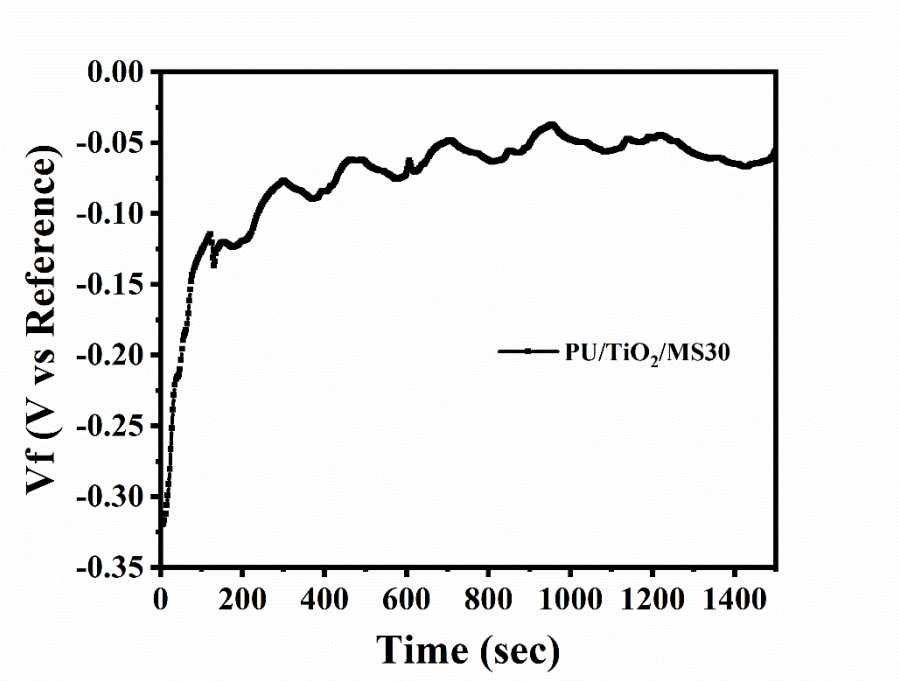

Figure 45: OCP plot of the PU/TiO_2/MS30 coatings immersed in 3.5 wt. % NaCl solution after 7 weeks of immersion over the time of 1500 seconds.